Synthesis, Characterisation and Property Evaluation of Excess and Deficient MgO in $MgO.Al_2O_3$ spinel

Thesis Submitted By

Srinath Ranjan Ghosh

Registration no: 1021712003, Dated: 30/03/2017

Index no.-143/17/E

DOCTOR OF PHILOSOPHY (ENGINEERING)

Department of Metallurgical and Material Engineering

Faculty of Engineering and Technology

Jadavpur University

Kolkata: 700032, INDIA

2024

INDEX NO.- 143/17/E

1. **Title of the thesis:**

Synthesis, Characterisation and Property Evaluation of Excess and Deficient MgO in MgO.Al2O3 spinel

2. **Name, Designation & Institution of the Supervisor/s :**

i) Name: (Dr.) Sathi Banerjee

Designation: Associate Professor

Department: Metallurgical and Material Engineering Department

Institution of the Supervisor: Jadavpur University

ii) Name: (Dr.) Soumya Mukherjee

Designation: Assistant Professor

Department: Metallurgical Engineering Department

Institution of the Supervisor: Kazi Nazrul University

3. List of Publication

I. Solution Combustion Synthesis of Alumina Spinel and Its Characterization, S.R. Ghosh, S. Mukherjee, S. Banerjee, Interceram 1-2, 67th Volume, 1-2

II. Development Of Spinel Magnesium Aluminate by Solution Combustion Route Using Thiourea and Urea as Fuel, Srinath Ranjan Ghosh, Soumya Mukherjee, Sathi Banerjee, The Journal of Engineering Research (TJER), Vol. 17, No. 2, (2020) 135-141

III. Evaluation Of Properties of Non-Stoichiometric Alumina Magnesia Spinel Using Thiourea as Fuel by Varying Soaking Time, Sathi Banerjee, Soumya Mukherjee, and Srinath Ranjan Ghosh, The Journal of Engineering Research (TJER), Vol. 17, No. 2, (2020) 135-14

IV. List of Patents: NIL

V. List of Presentations in National/ International/ Conferences/ Workshops

I. Comparative Study Between Stoichiometric and Non-Stoichiometric Magnesium Aluminate Spinel Prepared by Solution Combustion Route, S R Ghosh, S Banerjee, S Mukherjee, Proceedings of International Conference on Energy and Sustainable Development Jointly organized by Jadavpur University and The Institution of Engineers, India, February 14-15, 2020.

"Statement of Originality"

I, **Srinath Ranjan Ghosh**, registered on **30th March, 2017** do hereby declare that this thesis entitled "**Synthesis, Characterisation and Property Evaluation of Excess and Deficient MgO in $MgO.Al_2O_3$ spinel**" contains literature survey and original research work done by the undersigned candidate as part of Doctoral studies.

All information in this thesis have been obtained and presented in accordance with existing academic rules and ethical conduct. I declare that, as required by these rules and conduct, I have fully cited and referred all materials and results that are not original to this work.

I also declare that I have checked this thesis as per the "Policy on Anti Plagiarism, Jadavpur University, 2019", and the level of similarity as checked by iThenticate software is 9 %.

Srinath Ranjan Ghosh.

Signature of Candidate:

Date: 18.06.25

Banerjee 18/06/25

Certified by Supervisor(s)

Date:

HEAD OF THE DEPARTMENT
Metallurgical & Material Engineering Deptt.
Jadavpur University, Kolkata-700 032

Soumya Mukherjee
18/06/2025

Assistant Professor
Department of Metallurgical Engineering
School of Mines & Metallurgy
JADAVPUR UNIVERSITY
KOLKATA-700 032

CERTIFICATE FROM THE SUPERVISOR/S

This is to certify that the thesis entitled "**Synthesis, Characterisation and Property Evaluation of Excess and Deficient MgO in MgO.Al2O3 spinel**" submitted by Shri **Srinath Ranjan Ghosh**, who got his/her name registered on **30th March, 2017** for the award of Ph.D. (Engineering) degree of Jadavpur University is absolutely based upon his/her own work under the supervision of **(Dr.) Sathi Banerjee** and **(Dr.) Soumya Mukherjee** and that neither their thesis nor any part of the thesis has been submitted for any degree/diploma or any other academic award anywhere before.

Banerjee 18/06/25

HEAD OF THE DEPARTMENT
Metallurgical & Material Engineering Deptt.
Jadavpur University, Kolkata-700 032

Signature of the Supervisor
and date with Office Seal

Soumya Mukherjee
18/06/2025

Signature of the Supervisor
and date with Office Seal

Assistant Professor
Department of Metallurgical Engineering
School of Mines & Metallurgy
KAZI NAZRUL UNIVERSITY
Asansol, W.B.-713340

ACKNOWLEDGEMENT

Completing this PhD thesis has been a profound journey, and I am deeply indebted to the individuals and institutions whose support has been fundamental to this accomplishment.

Foremost, my sincere appreciation goes to (Dr.) Sathi Banerjee and (Dr.) Soumya Mukherjee, my supervisors, for their unwavering support, scholarly guidance, and mentorship throughout this research endeavor. I extend my profound gratitude to Prof. (Dr.) Siddhartha Mukherjee, the pivotal figure in this research, whose invaluable guidance and wisdom has been the cornerstone of my academic journey. His insights have been instrumental in shaping the trajectory of this work.

I extend my gratitude to Prof. (Dr.) Pravash Chandra Chakraborty, Metallurgical and Materials Engineering Department at Jadavpur University, for fostering an academic environment conducive to research and innovation.

I appreciate the camaraderie and support from my friends in various capacities – Chirantan Mukherjee (Scholar, Jadavpur University), Ambikesh Kr. Srivastwa (Assistant Engineer, WB Govt), Soumyajit Roy (Scholar, Jadavpur University), Dr. Subhasish Sarkar (Assistant Engineer, WB Govt.), Priyankari Bhattacharya (Post Doctoral Fellow, Jadavpur University) and Rupam Mandal (Scholar, Jadavpur University). Your friendship has been a source of strength.

I extend my thanks to the laboratories at Jadavpur University (Materials Lab of Met. and mat. Engg. Dept., Metrology Lab and Metallography Lab of Mechanical Engg. Dept.) and IIEST Shibpur (Metallography Lab, Met. and mat. Engg. Dept.) for providing essential facilities for my research.

I express my gratitude to all the colleagues and staff of the Metallurgical and Material Engineering Department at Jadavpur University for their support. My heartfelt thanks go to my family for their unwavering encouragement and understanding throughout this academic journey.

Finally, I acknowledge the financial support from TEQIP through the scholarship, which has played a pivotal role in enabling my research endeavors.

Thank you all for being integral parts of this academic odyssey.

Srinath Ranjan Ghosh.
18.06.25

Contents

List of Figures

List of Tables

Chapter-1

INTRODUCTION

1.1 Introduction Hardened glass, like bulletproof glass, and high-strength ceramics both use magnesium aluminate spinel as a matrix. Aluminates are substances utilised in the water treatment and ceramics industries, consisting of a negatively charged alumina ion and a metallic oxide. Spinel is a type of oxide mineral with crystal structure. The general formula for this material is $\mathbf{AB_2X_4}$ where, divalent ions such as **A**= Mg ion, Cr ion, trivalent ions such as **B** = Al ion, Ga ion, **X** = O ion, Si ion etc. Alumina rich spinels possess good thermal characteristics, high hot strength, thermal shock resistance, corrosion resistant, dielectric , mechanical and optical properties.

High processing cost restricts use of magnesium aluminate spinel for use in major applications. In this present work main emphasis has been made to synthesize low temperature spinel as an effective tool for possible industrial applications.

1.2 Types of Spinel Group

There are basically 4 types of spinel group:

Aluminium spinel group: The spinel group is classified into three immiscible series: the spinel (aluminium-spinel) series, in which B is aluminium. Example: $MgAl_2O_4$, $BeAl_2O_4$, $ZnAl_2O_4$, $FeAl_2O_4$, $MnAl_2O_4$ etc.

Iron spinel group: In this group B represent iron. Example: $CuFe_2O_4$, $MnFe_2O_4$, $MgFe_2O_4$, $NiFe_2O_4$etc.

Chrome spinel group: Chrome spinels are frequent accessory minerals in a variety of ultrabasic rocks that form over a wide P-T range and exist in a variety of geological environments. Kimberlites, lamproites, and peridotites from orogenic massifs are among these rocks, which belong to the ophiolitic association. Example: $FeCr_2O_4$, $MgCr_2O_4$, $ZnCr_2O_4$ etc.

Other spinel groups: FeV_2O_4, MgV_2O_4 etc.

Spinel unit cell consists of eight FCC cells. Anions (usually oxide ions: O_2) Occupy the FCC grid (18). There are two types of voids are present in spinel structure.

- Tetrahedral voids
- Octahedral voids

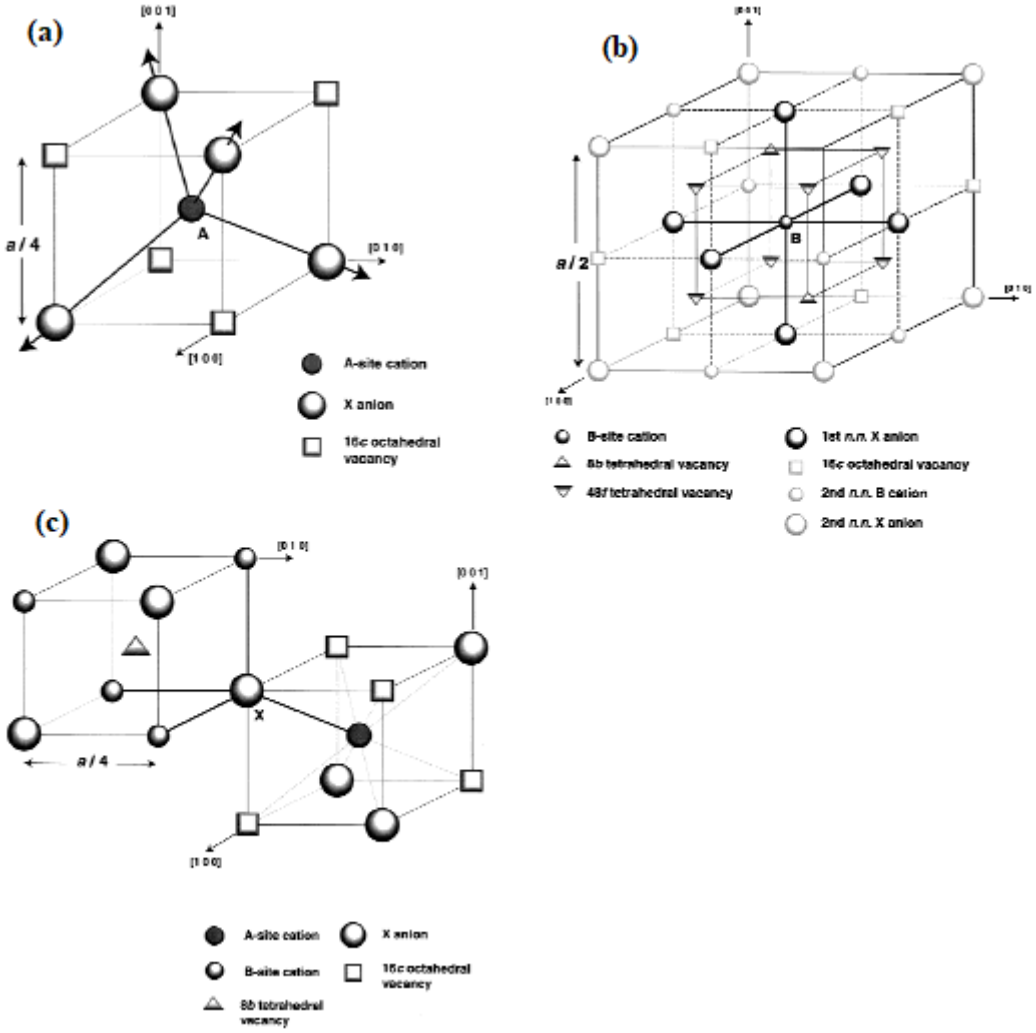

Figure : 1.1 Schematic diagrams of lattice arrangement and nearest neighbours for tetrahedral (a) octahedral (b) anion dilations has been indicated in by arrows(c)[ref -1]

There are four types based on the structure of spinel:

- Normal spinel
- Inverse spinel Post spinel
- Intermediate or defective spinel

Normal Spinel: Basically, Spinel structures exhibit a cubic close-packed arrangement of oxides, featuring eight tetrahedral and four octahedral sites per unit cell. Notably, the tetrahedral sites are smaller in size compared to the octahedral spaces. Within the structure, half of the octahedral sites are filled by B ions, while only one-eighth of the tetrahedral voids are occupied by A ions.". General chemical formula of normal spinel is $(A^{2+})(B^{3+})_2O_4$. Among all natural as well as artificial spinel found in earth till now, maximum of them are aluminates, such as $MgAl_2O_4$, $FeAl_2O_4$, $CoAl_2O_4$, and a few are ferrites, such as $ZnFe_2O_4$.

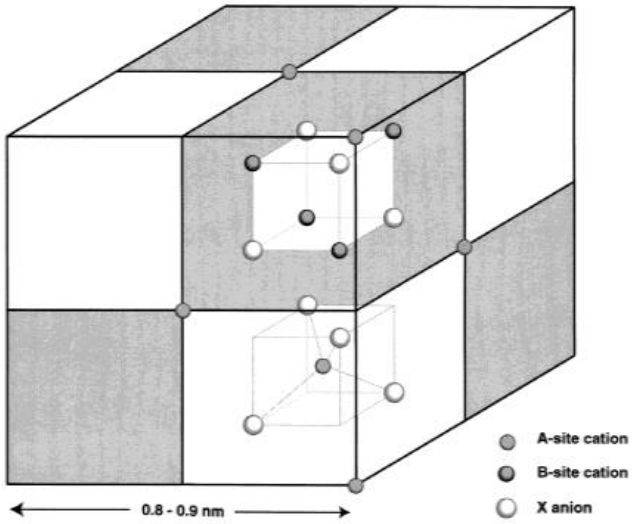

Figure :1.2 Schematic diagram of normal spinel [ref 1]

Two types of cations are present in the spinel crystal structure. One is A^{+2} and B^{+3} and all A ions captures tetrahedral sites where as all B^{3+} ions capture octahedral sites in the spinel structure. Stoichiometry of normal spinel can be verified using the bond strength rule. The stoichiometric ratio of A^{+2}: B^{+3}: O^{-2} = 8 : 16 : 32 = 1 : 2 : 4 [1].

Inverse Spinel: The A-site ions and half of the B-site ions trade places in inverse spinel, which have a similar structure (with the same huge unit cell). $B(AB)O_4$ is the formula for inverse spinel, with the AB ions in parenthesis occupying octahedral sites and the other B ions occupying tetrahedral sites [2].

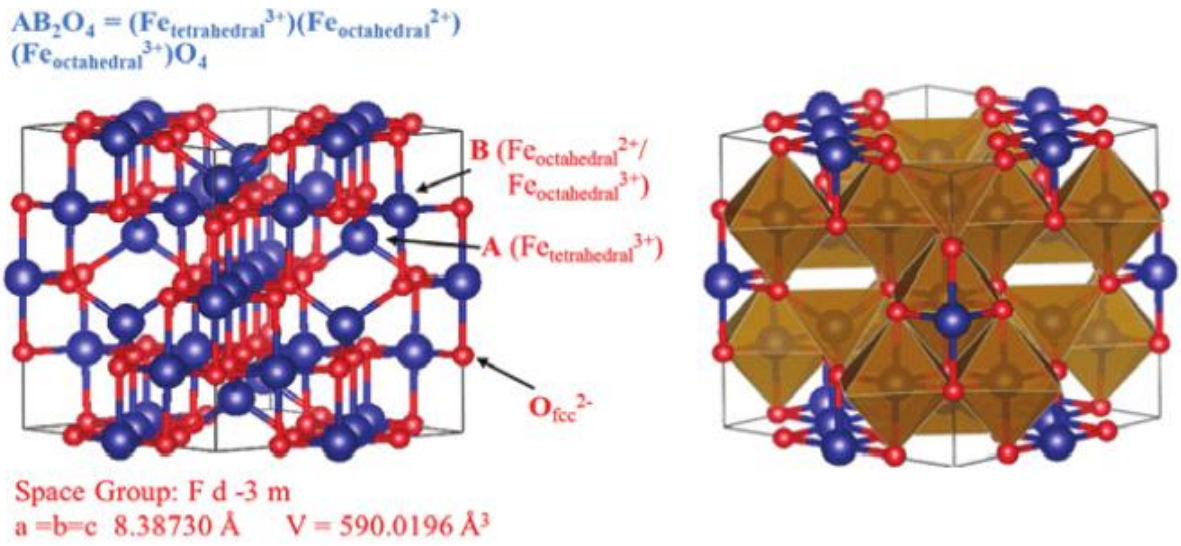

Figure :1.3 Schematic diagram of inverse spinel [ref. 2].

Chemical formula of inverse spinel can be written as $(A^{2+}).(B^{3+})_2O_4$, however it is easier to remember as $B(AB)O_4$. Most of them are ferrites, such as Fe_3O_4 (or $FeO.Fe_2O_3$), $NiFe_2O_4$, $CoFe_2O_4$, and others, have this the octahedral voids. B^{+3} ions are divided into two halves that reside in octahedral sites and tetrahedral vacancies. The tetrahedral sites are occupied by half of the B^{3+} ions, whereas the remaining half of the B^{3+} ions and all A^{2+} ions occupy the octahedral sites.".

- Examples: $Fe_3O_4 = Fe^{+3}(Fe^{+2}Fe^{+3})O^{-4}$ (Magnetite) structure.

Post spinel: The structural chemistry of oxometallates with the composition AM_2O_4 is summarised in this paper, which shows that there are more than 30 different structures for the formulae AM_2O_4 and A_2MO_4. Spinel, spineloid, closed octahedra layers compound, tunnel structures, square polygons, and dumb-bells are among the formations documented [3].

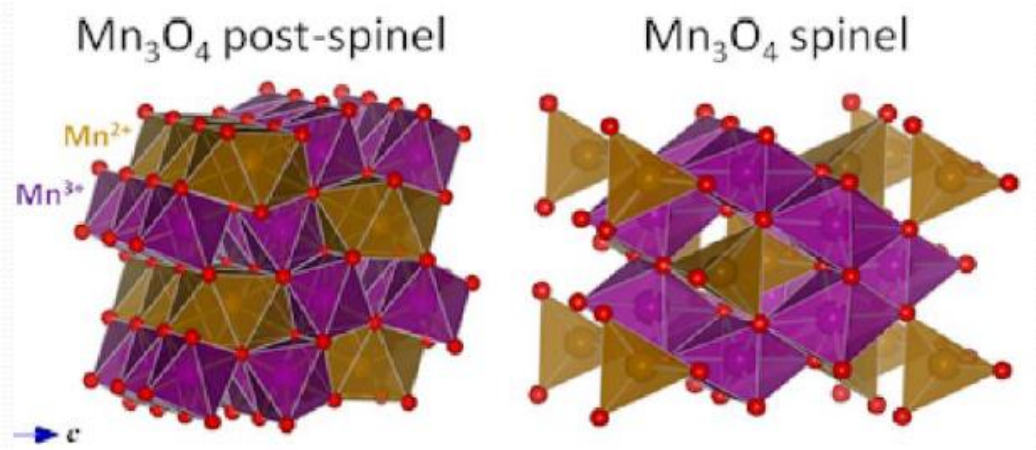

Figure :1.4 Schematic diagram of post spinel and spinel [ref-3]

Some spinels undergo in structural phase transition at high pressure. The structures formation of post-spinel AM_2O_4 are similar with MO_6 octahedral forming so-called "double-rutile chains". The mobility of cations is high through the lattice so it is useful in rechargeable Li-ion batteries.

- Example of post spinel: Mn_3O_4 (Orthorhombic symmetry)

Intermediate or Defected spinel: The cation or anion distribution is described by the formula (A1−xBx)[Ax⁄2B1−x⁄2]2O4 in intermediate scenarios, where the parentheses () and brackets [] represent tetrahedral and octahedral positions, respectively. In cases of perfect randomness, the inversion degree (x) varies between 0 (for a normal structure) and 1 (for an inverse structure), with an ideal value of 2/3. The general formula for an intermediate or defective spinel remains (A1−xBx)[Ax⁄2B1−x⁄2]2O4. The occupancy of octahedral sites may exhibit ordered or random arrangements, with disordered occupation leading to spinel defects. The value of x ranges from 0 to 1, where 0 represents a normal spinel, 1 signifies an inverse spinel, and a value of 2/3 indicates complete random distribution.

- Example: $NiAl_2O_4$= $(A_{l0.75}Ni_{0.25})[Ni_{0.75}Al_{1.25}]_2O_4$.

The magnesium aluminate spinel is a mineral that belongs to the broader spinel family. In the cubic crystal structure, it has the formula $MgAl_2O_4$. The category of minerals known as spinel compounds includes oxides of magnesium, iron, manganese, and aluminium. Spinel gets its name from the Latin word "spina", which means "thorn" referring to its pointed octahedral crystal habit. Spinel minerals can be found on the surface of the planet, in meteorites, and in lunar rock. Spinel, Magnetite, and Chromite are the three minerals that

make up the spinel series. These are extremely hard, multicoloured minerals with octahedral crystals that are found in ignition and carbonates rocks. Spinels are a popular subject for material science and engineering research. Aluminium spinels are highly refractory, ranging in colour from colourless to green, blue, brown, and black and varying in transparency from translucent to transparent [4]**.**

1.3 Structure, property, and phase of magnesium aluminate spinel:

The general formulae for magnesium aluminate spinel can be expressed as $(A^{2+})(B^{3+})_2O_4$, AB_2O_4, or $AO{\cdot}B_2O_3$. Typically, spinel structures exhibit a cubic close-packed oxide arrangement, featuring eight occupied tetrahedral and four occupied octahedral sites per unit. It is worth noting that the tetrahedral voids are smaller than the octahedral spaces. Within the structure, half of the octahedral sites are filled by B ions, while A ions occupy one-eighth of the tetrahedral voids [**5].** A unit-cell of spinel is made up of eight FCC cells created by oxygen ions resulting in a structure with 32 oxygen atoms, 8 divalent atoms, and 16 trivalent atoms. Spinel structure can be Normal or Inverse according to the arrangement of cations in different interstices.

Physical characteristics:

- Density (gram per cubic centimetre): 3.58
- Thermal conductivity (W/mK): 5.9
- Thermal expansion coefficient (K^{-1}): 7.6
- Common crystal shapes are octahedrons, usually twins.
- There is no actual split, but you can see the octahedral split and the shell destruction.
- Transparent to opaque, glass to matte lustre.
- It can be colourless, but usually comes in a variety of shades.
- Spinels are one of the most eminent gems. The Black Prince's Ruby among them is classified as British Crown Jewels, and the former French Crown Jewels.
- Magnesium aluminate spinel ($MgAl_2O_4$) has high-temperature features, including a high melting point, great chemical resistance, potential for high strength even at high temperatures, and outstanding thermal properties.

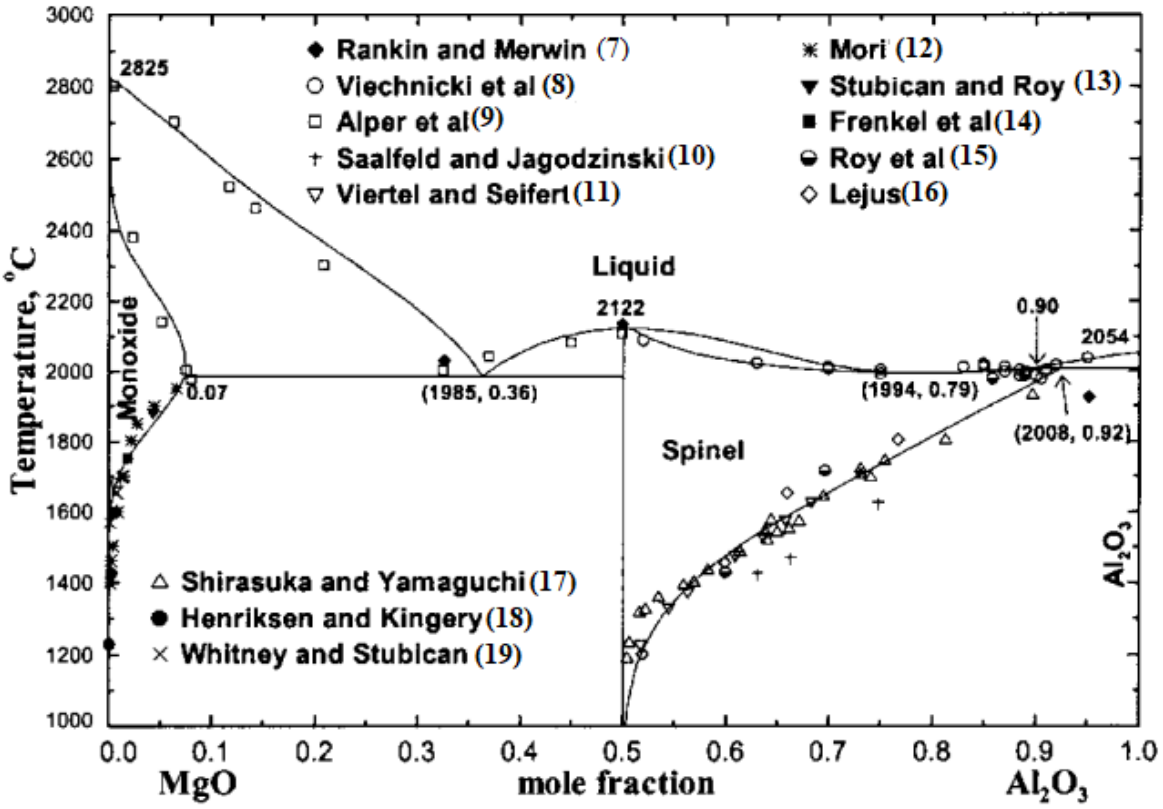

Figure :1.5 Calculated phase diagram of the MgO-Al2O3 binary system [ref-6]

1.4 $MgO-Al_2O_3$ System:

The phase diagram of the $MgO-Al_2O_3$ system is illustrated in the above figure. Rankin and Merwin [6-7] previously determined the equivalent melting temperature of $MgAl_2O_4$ in preliminary investigations. Alper et al. [9] utilized a quenching procedure followed by X-ray diffraction (XRD) or optical phase identification to elucidate the phase diagram of the $MgO-MgAl_2O_3$ system. Employing the collapsing cone approach, Viechnicki et al. [8] investigated the solidus and liquidus under Argon atmospheres. Their findings revealed a eutectic reaction between spinel and Al2O3 at 1975°C, slightly higher than Rankin and Merwin's temperature of 1925°C [7]. Numerous experiments have been conducted to ascertain the solubility of Al_2O_3 in MgO (periclase) [22,24-28] and in the spinel solution [7] across a temperature range spanning from 1230°C to 1975°C. XRD measurements, taken for the change in lattice parameters of quenched materials, were commonly employed to determine solubilities. While the measured Al_2O_3 solubilities in periclase exhibit close agreement among authors, the reported solubilities in the spinel phase display significant variation. Shirasuka and Yamaguchi [21] investigated solubility at temperatures ranging from 1327°C to 1927°C.

Utilizing a homogenization technique, Viertel et al. [10-17] assessed solubility with discernible accuracy at 1 kbar total pressure within the temperature range of 1125°C to 1625°C. Lejus et al. [22] and Lejus et al. [16] reported MgO to be insoluble in $MgAl_2O_4$, whereas Alper et al. [9], Chiang et al. [23], and Fujii et al. [24] observed a low solubility of MgO in $MgAl_2O_4$ (less than 3 mol percent). Generally, MO solubility in MAl_2O_4 spinels is quite unusual. In this study, the solubility of MgO in $MgAl_2O_4$ spinel is deemed insignificant.

1.5 Various applications of Magnesium Aluminate Spinel

Industrial sector:

Electro Ceramic Materials: Recent research has focused on exploring dielectric materials with low dielectric constants, high quality factors, and near-zero temperature coefficients of resonant frequency in the microwave domain, as they hold promise for applications in high-frequency wireless communication systems. Among these materials, $MgAl_2O_4$, a spinel-structured ceramic, has garnered significant attention [25-29]. Investigating the electronic state and microwave dielectric characteristics of $MgAl_2O_4$ (MA-S) and Mg0.4Al2.4O4 (M04A24), researchers utilized solid-state (MA-S) and molten salt (MA-M) methods [30].

Porous Materials: Porous $MgAl_2O_4$ spinel ceramics have garnered increasing attention across industries due to their exceptional properties, including a high melting point temperature (2135°C), excellent shock resistance in thermal atmospheres, and remarkable chemical inertness. Moreover, these spinel materials exhibit low thermal conductivity and thermal expansion coefficients. Widely utilized for diverse applications worldwide, such as gas filtration, thermal insulation, wastewater filtration, and separation membranes, they offer versatile solutions. In recent years, various accessible technologies, including gel casting, the addition of pore-forming agents, sacrificial templating, in-situ synthesis, and combustion synthesis, have been employed to tailor the porosity of $MgAl_2O_4$ spinel ceramics to meet specific requirements for a range of purposes [31-35].

Sensors: The transparency property of spinel ($MgAl_2O_4$) ceramics finds application in laser windows, particularly for high-energy applications, owing to its exceptional transmission capabilities across visible wavelengths and mid-wavelength infrared (0.2–5.0 μm). Additionally, porous magnesium aluminate ($MgAl_2O_4$) semi-thick films serve as capacitive

sensors, demonstrating excellent humidity detection characteristics within the range of 2% to 98% relative humidity (RH). A straightforward solid-state process was employed to synthesize MgAl2O4 nanoparticles, facilitating the fabrication of porous semi-thick films through a screen-printing technique [36].

Refractory Material: In the $MgO\text{-}Al_2O_3$ system the sole chemical with a high melting point (2135 °C) is $MgAl_2O_4$ spinel. The spinel shows a good refractoriness, very low thermal expansion, stability in chemical, thermal shock resistance, and resistance in corrosion atmosphere. It's become a popular ingredient in refractory. Magnesium aluminate ($MgAl_2O_4$) spinel is an engineered material renowned for its favourable chemical, mechanical, thermal, optical, and dielectric properties. Because of such qualities, MAS became a very important material for optically transparent windows, armours and domes as well as some refractory applications [37].

Cement Kilns: $MgAl_2O_4$ shows lack of toxicity, and resistance to basic slags due its high melting point property. Magnesium-based refractories have been widely utilised in cement rotary kilns and steel ladles.

Glass lining: Transparent magnesium-aluminate spinel has been investigated for a variety of transmission applications, including domes and armour windows, throughout a broad transmission spectrum. Current commercial approaches to successfully creating large specimens with high transparency demand the employment of aggressive densification procedures, which result in very coarse microstructures (average grain sizes up to 500 m, with some grains nearing 1 mm in size). Commercial spinels have a lesser strength than traditional fine-grained spinel due to their coarse microstructure. Swab et al. observed that the coarse-grained spinel was roughly 75 MPa when it is measured for flexural strength under the identical loading circumstances. The strength of fine-grained sintered spinel was close to 200 MPa [38].Because of the coarse-grained material's low strength, transparent spinel's feasibility in demanding applications requiring high area sizes are limited.

Defence sector:

Armor and domes materials: The thermal, chemical, dielectric, optical, mechanical, and characteristics of magnesium aluminate ($MgAl_2O_4$) spinel (MAS) are pretty good to use in defense sector. Because of the aforesaid characteristics, MAS is suitable for windows which are optically transparent, domes, and armors, as well as some refractory applications. Efforts have been undertaken to create efficient manufacturing procedures for polycrystalline spinel

which is transparent, a material utilized in rather large dome-shaped sections with very uniform optical characteristics [39].

Medical sector:

Humidity sensor: The porous semi-thick film capacitive sensor based on magnesium aluminate ($MgAl_2O_4$) demonstrates reliable humidity detection across a broad range from 2% to 98% relative humidity (RH). Tea and coffee industry poses great demand as a humidity sensor, medical industry, textile industry, etc. [40-44]. Inexpensive polymer moisture sensors are extensively studied and available in commercial market [45-46].

Photo catalytic materials: Pressure is increasing as the global economy develops at a rapid speed. It is unique in the environment, especially when it comes to printing dye factories, textile factories, and food processing plants, to name a few. The river's banks are filled with water-dependent enterprises. The direct release of dye effluent pollutes the river [47-48].To alleviate the environmental pollution caused by dye wastewater, semiconductor photocatalytic technology has been created as a green method to breakdown organic dyes [49-50].

1.6 Various synthesis procedures of Magnesium aluminate spinel:

Freeze-drying: Freeze drying involves placing a fully frozen sample in vacuum atmosphere to eliminate any water or other solvents, allowing the ice for transition directly from a solid to a vapour without passing through a liquid phase [51].

Sol-gel condensation: The sol–gel process is a wet chemical procedure that requires numerous processes, which are listed below in chronological order: gelation, ageing, drying, densification, and crystallisation are all examples of hydrolysis and polycondensation [52].

Co-precipitation: Co-precipitation is similar to the sol–gel technique. This technique helps to keep the needed cations close together in the medium where reaction will take place and decreases the temperature of decomposition. Metal salts that dissolve very easily in water or other solvents which is suitable for this technique can be used as starting materials [53].

Mechanochemical activation: A technique capable of inducing structural disorder through extensive grinding is known as mechanochemical activation. It has the potential to boost the chemical reactivity of the treated substance under specific circumstances. The method is widely used in extractive metallurgy, nanocomposites synthesis, and pharmaceuticals [54].

Solid state reaction: Through solid-state diffusion, the solid-state reaction method is a well-known processing way for generating thermodynamically stable phases even at high temperatures. To make mgal2o4 from binary oxides, for example, a local 1:2 stoichiometry of Al_2O_3 to MgO is required [55].

Soft resolution chemistry routes: Soft chemistry (also known as chimiedouce) is a form of chemistry that uses reactions in open reaction vessels at room temperature with reactions that are comparable to those seen in biological systems [56].

Thick/thin films of MAS: A thin film is a material layer that ranges in thickness from fractions of a nano meter (monolayer) to several micrometres. In many applications, the controlled synthesis of materials as thin films (a process known as deposition) is a crucial step [57].

Fibres and single crystals synthesis:A monocrystalline solid exhibits a continuous crystal lattice throughout the entire sample, devoid of any grain boundaries [58].

References:

1. Sickafus, K. E., Wills, J. M., & Grimes, N. W. (1999). Structure of spinel. Journal of the American Ceramic Society, 82(12), 3279–3292.

2. Von Hippel A.R. Dielectrics and Waves,John Wiley & Sons, New York, 1954.

3. Kingery W.D., Bowen H.K., Uhlmann D.R. John Wiley & Sons,p-64, 1975.

4. Reimanis, I., &Kleebe, H. J. (2009). A review on the sintering and microstructure development of transparent spinel (MgAl 2O 4). Journal of the American Ceramic Society, 92(7), 1472–1480.

5. I. Ganesh, B. Srinivas, R. Johnson, B. P. Saha and Y. R. Mahajan: Br. Ceram. Trans., 2002, 101, (6), 1–8.

6. I.-H. Jung, S. A. Decterov, and A. D. Pelton, "Critical Thermodynamic Evaluation and Optimization of the $MgO-Al_2O_3$, $CaO-MgO-Al_2O_3$ and $MgO-Al_2O_3-SiO_2$ Systems," *J. Phase Equilibria Diffus.*, vol. 25, no. 4, pp. 329–345, 2004, doi: 10.1361/15477030420106.

7. A. Rankin and H.E. Merwin: "The Ternary System CaOAl2O3-MgO," J. Am. Chem. Soc., 1916, 38, pp. 568-88.

8. Viechnicki, F. Schmid, and J.W. Mccauley: "Liquidus Solidus Determinations in the System MgAl2O4-Al2O3," J. Am. Ceram. Soc., 1974, 57, pp. 47-48.

9. A.M. Alper, R.N. McNally, P.H. Ribbe, and R.C. Doman: "The System MgO-MgAl2O4," J. Am. Ceram. Soc., 1962, 45, pp. 263-68.

10. H. Saalfeld and H. Jagodzinski: "Segregation of Mg-Al SpinelsWith an Excess of Al2O3," Z. Krist., 1957, 109, pp. 87-109.

11. H.U.B. Viertel and F.K. Seifert: "Thermal Stability of Defect Spinels in the System MgAl2O4-Al2O3," N. Jb. Miner. Abh., 1980, 140, pp. 89-101.

12. T. Mori: "Solubility of Aluminum Oxide in Magnesium Oxide," YogyoKyokaishi, 1982, 90, pp. 551-52.

13. V.S. Stubican and R. Roy: "Mechanism of the Precipitation of the Spinel from MgO-Al2O3 Solid Solutions," J. Phys. Chem. Solids, 1965, 26, pp. 1293-97.

14. A.S. Frenkel, K.M. Shmukler, D.Ya. Sukharevskij, and N.V. Gul'ko: Dokl. Akad. Nauk SSSR, 1960, 130, pp. 1095-98.

15. D.M. Roy, R. Roy, and E.F. Osborn: “The System MgOAl2O3-H2O and Influence of Carbonate and Nitrate Ions on the Phase Equilibria,” Am. J. Sci., 1953, 251, pp. 337-61

16. A.M. Lejus: “Sur la Formation à Haute Température de Spinelles non Stoechiométriques et de Phases Dérivées,” Revue Int. Haut. Temp. Refract., 1964, 1, pp. 53-95 (in French)

17. K. Shirasuka and G. Yamaguchi: “Precise Measurement of the Crystal Data and the Solid Solution Range of the Defective Spinel Magnesium Oxide.n (Aluminum Oxide),” YogyoKyokaishi, 1974, 82, pp. 34-37

18. A.F. Henriksen and W.D. Kingery: “The Solid Solubility of Sc2O3, Al2O3, Cr2O3, SiO2 and ZrO2 in MgO,” Ceramurgia Int., 1979, 5, pp. 11-17.

19. W.P. Whitney and V.S. Stubican: “Interdiffusion in the System MgO-MgAl2O4,” J. Am. Ceram. Soc., 1971, 54, pp. 349- 52

20. Navrotsky, A., Wechsler, B. A., Geisinger, K., & Seifert, F. (1986). Thermochemistry of MgA1204-A18 , 304 Defect Spinels AR , IK ! NG. 22, 418–422.

21. K. Shirasuka and G. Yamaguchi, “Precise measurement of the crystal data and the solid solution range of the defective spinel, MgO nAl2O3.,” J. Ceram. Assoc. Japan, vol. 82, no. 952, pp. 650–653, 1974.

22. Lejus, A. M., And R. Collongues. "Chimie Minerale-Sur La Formation A Haute Temperature De Phases Type Alumine Delta Dans Plusieurs Systemes A Base Dalumine." Comptes Rendus Hebdomadaires Des Seances De L Academie Des Sciences 254.15 (1962): 2780.

23. Y. M Chiang and W. D. Kingery, “Grain-Boundary Migration in Nonstoichiometric Solid Solutions of Magnesium Aluminate Spinel: II, Effects of Grain-Boundary Nonstoichiometry,” J. Am. Ceram. Soc., vol. 73, no. 5, pp. 1153–1158, 1990

24. J. T. Young, “Faith, medical alchemy and natural philosophy: Johann moriaen, reformed intelligencer, and the hartlib circle,” Faith, Med. Alchemy Nat. Philos. Johann Moriaen, Reform. Intell. Hartlib Circ., vol. 40, no. 11, pp. 1–278, 2018

25. Search, H., Journals, C., Contact, A., Iopscience, M., & Address, I. P. (n.d.). Quality Factor of Forsterite for Ultrahigh Frequency Dielectrics Depending on Synthesis Process Quality Factor of Forsterite for Ultrahigh Frequency Dielectrics Depending on Synthesis Process. 7729.

26. Taylor, P., Kagomiya, I., Matsuda, Y., Kakimoto, K., & Ohsato, H. (2010). Ferroelectrics Microwave Dielectric Properties of YAG Ceramics. October 2014, 37–41.

27. Guo, Y., Ohsato, H., & Kakimoto, K. (2006). Characterization and dielectric behavior of willemite and TiO 2 -doped willemite ceramics at millimeter-wave frequency. 26, 1827–1830.

28. Wu, S., Jiang, C., Mei, Y., & Tu, W. (2012). Synthesis and Microwave Dielectric Properties of Sm 2 SiO 5 Ceramics. 40(30230), 37–40.

29. Ogawa, H., Kan, A., Ishihara, S., & Higashida, Y. (2003). Crystal structure of corundum type Mg 4 (Nb 2 À x Ta x) O 9 microwave dielectric ceramics with low dielectric loss. 23, 2485–2488.

30. Takahashi, S., Ogawa, H., & Kan, A. (2018). Electronic states and cation distributions of MgAl2O4 and Mg0.4Al2.4O4 microwave dielectric ceramics. *Journal of the European Ceramic Society*, *38*(2), 593–598.

31. Shahbazi, H., Shokrollahi, H., & Alhaji, A. (2017). Optimizing the gel-casting parameters in synthesis of MgAl2O4 spinel. In *Journal of Alloys and Compounds*. Elsevier B.V.

32. Honda, S., Hashimoto, S., Yase, S., Daiko, Y., & Iwamoto, Y. (2016). Fabrication and thermal conductivity of highly porous alumina body from platelets with yeast fungi as a pore forming agent. *Ceramics International*, *42*(12), 13882–13887.

33. Hashimoto, S., Honda, S., Hiramatsu, T., & Iwamoto, Y. (2013). Fabrication of porous spinel (MgAl2O4) from porous alumina using a template method. *Ceramics International*, *39*(2), 2077–2081.

34. Yan, W., Chen, J., Li, N., Qiu, W., Wei, Y., & Han, B. (2015). Preparation and characterization of porous MgO-Al2O3 refractory aggregates using an in-situ decomposition pore-forming technique. *Ceramics International*, *41*(1), 515–520.

35. Bai, J., Wei, C., Meng, F., Liu, J., Wang, P., Du, Q., & Tang, Z. (2011). Fabrication of porous Al2O3-MgAl2O 4 ceramics using combustion-synthesized powders containing in situ produced pore-forming agents. *Materials Letters*, *65*(11), 1559–1561.

36. Das, S., Rahman, M. L., Mondal, P. P., Mahapatra, P. L., & Saha, D. (2021). Screen-printed MgAl2O4 semi-thick film based highly sensitive and stable capacitive humidity sensor. *Ceramics International*, *47*(23), 33515–33524.

37. Ganesh, I. (2013). A review on magnesium aluminate (MgAl2O4) spinel: Synthesis, processing and applications. *International Materials Reviews*, *58*(2), 63–112.

38. Swab, J. J., Pavlacka, R., Gilde, G., Kilczewski, S., Wright, J., & Harris, D. (2014). Determining the strength of coarse-grained AlON and Spinel. *Journal of the American Ceramic Society*, *97*(2), 592–600.

39. Goldstein, A. (2012). Correlation between MgAl 2O 4-spinel structure, processing factors and functional properties of transparent parts (progress review). *Journal of the European Ceramic Society*, *32*(11), 2869–2886.

40. Dijkink, B. H., Tomassen, M. M., Willemsen, J. H. A., & Van Doorn, W. G. (2004). Humidity control during bell pepper storage, using a hollow fiber membrane contactor system. *Postharvest Biology and Technology*, *32*(3), 311–320.

41. Blanco, M., Coello, J., Iturriaga, H., Maspoch, S., & Rovira, E. (1997). Determination of water in ferrous lactate by near infrared reflectance spectroscopy with a fibre-optic probe. *Journal of Pharmaceutical and Biomedical Analysis*, *16*(2), 255–262.

42. Fujita, A., Kurose, R., & Komori, S. (2010). Experimental study on effect of relative humidity on heat transfer of an evaporating water droplet in air flow. *International Journal of Multiphase Flow*, *36*(3), 244–247.

43. Previati, M., Canone, D., Bevilacqua, I., Boetto, G., Pognant, D., & Ferraris, S. (2012). Evaluation of wood degradation for timber check dams using time domain reflectometry water content measurements. *Ecological Engineering*, *44*, 259–268.

44. Green, J., & Dyer, I. (2009). Measurement of humidity. *Anaesthesia and Intensive Care Medicine*, *10*(1), 45–47.

45. Gusmano, G., Montesperelli, G., Traversa, E., & Mattogno, G. (1993). Microstructure and Electrical Properties of MgAl2O4 Thin Films for Humidity Sensing. *Journal of the American Ceramic Society*, *76*(3), 743–750.

46. Buvailo, A., Xing, Y., Hines, J., & Borguet, E. (2011). Thin polymer film based rapid surface acoustic wave humidity sensors. *Sensors and Actuators, B: Chemical*, *156*(1), 444–449.

47. He, Q., Peng, S., Zhai, J., & Xiao, H. (2011). Development and application of a water pollution emergency response system for the Three Gorges Reservoir in the Yangtze River, China. *Journal of Environmental Sciences*, *23*(4), 595–600.

48. Shen, Z., Qiu, J., Hong, Q., & Chen, L. (2014). Simulation of spatial and temporal distributions of non-point source pollution load in the Three Gorges Reservoir Region. *Science of the Total Environment*, *493*, 138–146.

49. Mills, A., Davies, R. H., & Worsley, D. (1993). Water purification by semiconductor photocatalysis. *Chemical Society Reviews*, *22*(6), 417–425.

50. Hoffmann, M. R., Martin, S. T., Choi, W., & Bahnemann, D. W. (1995).

Environmental Applications of Semiconductor Photocatalysis. *Chemical Reviews*, *95*(1), 69–96.

51. Wang, C. -T, Lin, L. -S, & Yang, S. -J. (1992). Preparation of MgAl2O4 Spinel Powders via Freeze-Drying of Alkoxide Precursors. *Journal of the American Ceramic Society*, *75*(8), 2240–2243.

52. Parmentier, J., Richard-Plouet, M., & Vilminot, S. (1998). Influence of the sol-gel synthesis on the formation of spinel MgAl2O4. *Materials Research Bulletin*, *33*(11), 1717–1724.

53. Rashad, M. M., Zaki, Z. I., & El-Shall, H. (2009). A novel approach for synthesis of nanocrystalline MgAl2O 4 powders by co-precipitation method. *Journal of Materials Science*, *44*(11), 2992–2998.

54. Abdi, M. S., Ebadzadeh, T., Ghaffari, A., & Feli, M. (2015). Synthesis of nano-sized spinel (MgAl2O4) from short mechanochemically activated chloride precursors and its sintering behavior. *Advanced Powder Technology*, *26*(1), 175–179.

55. Parvarinezhad, S., Salehi, M., & Khademinia, S. (2018). Solid state synthesis of MgAl2O4 nanomaterials and solar light-induced photocatalytic removal of Malachite Green. *International Journal of Nano Dimension*, *10*(1), 89–104.

56. Kong, L., Wei, T., Zhang, Y., Karatchevtseva, I., & Chironi, I. (2020). One-pot synthesis of Ln2Sn2O7 pyrochlore and MgAl2O4 spinel by soft chemistry route as potential inert matrix fuel system, and the microstructural analysis. *Journal of Nuclear Materials*, *531*, 152037.

57. Gusmano, G., Montesperelli, G., Nunziante, P., & Traversa, E. (1993). Study of the conduction mechanism of MgAl2O4 at different environmental humidities. *Electrochimica Acta*, *38*(17), 2617–2621.

58. Kawakami, S., Yamada, T., Sakakibara, S., & Tabata, H. (1995). Preparation of spinel fibers by directional solidification of MgA1204-MgzSiO 4 eutectic. *Journal of Crystal Growth*, *154*, 193–196.

Chapter-2

LITERATURE REVIEW

The magnesium aluminate (MgAl2O4) mineral boasts an array of captivating properties, including a lofty melting point (2135°C), exceptional chemical resilience, and robust mechanical strength across both low and high temperatures [1]. Synthesizing $MgAl_2O_4$ mineral involves solid-state reactions of metals at elevated temperatures (1600°C), presenting challenges in organizing powders with particle sizes around 0.5 mm. To address this, various non-conventional methods such as sol-gel, co-precipitation, spray-drying, freezing, and mechanical activation have been explored to yield $MgAl_2O_4$ mineral powders of high purity [4], [5-10]. The oxidation temperature significantly influences the reactivity of calcined powder, affecting agglomeration and grain development [11]. Efforts to attain pure mineral formation at lower oxidation temperatures have utilized co-precipitation, freeze-drying, and sol-gel techniques, observing an oxidation temperature of 1100°C [12], [13]. Additionally, a mechanochemical approach has been proposed for synthesizing monolithic minerals at 900°C [14].

$MgAl_2O_4$ spinel, a solid crystal substance derived from a metal chemical combination, exhibits exceptional chemical, thermal, dielectric, mechanical, and optical characteristics, rendering it indispensable in various industrial applications, notably in the iron and steel industries [15–17]. However, the dense nature of MAS ceramics has limited their utility, necessitating multi-stage firing approaches to produce dense bodies. Yet, the processing value of dense MAS mineral can be significantly reduced by employing appropriate precursors, powder processing methods, and understanding the mechanisms of MAS production and compression [15–17]. Recently, the magnesium aluminate ($MgAl_2O_4$) mineral has garnered substantial attention from both the scientific and business communities due to its multitude of attractive properties, including its elevated freezing point, high mechanical strength, and resistance to chemical environments [15–17].

Furthermore, the unique properties of magnesium aluminate spinel make it highly versatile in a range of applications, including as a reactor power core insulator in electronic devices and as a catalyst for various reactions [15–17]. Its utilization extends to thermal barrier coatings for turbine blades, metallic element electrolytic cells, and catalytic roles in environmental and chemical manufacturing processes [18]. Despite the wealth of literature on MAS, there remains a need for comprehensive information on its fundamental properties, crystal structure, and processing techniques to address volume enlargement issues and reduce processing costs effectively.

2.1 Synthesis routes of magnesium aluminate spinel (MAS):

Jianjun Guo *et. al.* explores An innovative synthesis approach for producing high surface area MgAl2O4 spinel, pivotal as a catalyst substrate. It introduces a modified sol-gel route which combines gelation and coprecipitation processes to synthesize precursors. These were calcined at varying temperatures, and resulting phases were analyzed using XRD, TGA, and FTIR. Spinel powder with uniform porosity formed at low temperatures (600°C), exhibiting higher thermal stability compared to conventional methods. The specific surface area increased with the M/PVA ratio, indicating PVA's significant impact. Highlighting $MgAl_2O_4$'s wide applications as a ceramic material and catalyst support, the study stresses the importance of surface area and active sites in spinels. Experimental procedures detail preparation using metal nitrates, PVA, and ammonia, with analysis via XRD, FTIR, and surface area measurements. The findings underscore the efficiency and cost-effectiveness of the modified sol-gel process, offering insights for industrial catalyst support applications[19].

C. Pacurariu *et. al.* investigates various synthesis methods and precursors for magnesium aluminate ($MgAl_2O_4$) spinel, focusing on their effects on synthesis temperature, particle size, and morphology. Three methods - thermal conversion, combustion, and sol-gel - are compared to understand their advantages and disadvantages in synthesizing $MgAl_2O_4$ spinel. Using X-ray diffraction and scanning electron microscopy, the research aims to characterize the synthesized samples, with the objective of identifying variations in properties. It underscores $MgAl_2O_4$'s industrial significance due to its desirable properties and challenges conventional synthesis methods face. Emphasizing unconventional methods and organic precursors, the study seeks to address these limitations. Experimental procedures detail synthesis approaches, while results highlight low-temperature spinel formation and the impact of synthesis methods on crystallite size and morphology. Additionally, it discusses the effect of combustion fuel on crystallite size and compares $MgAl_2O_4$ phase parameters among different methods. The conclusion summarizes findings, noting differences in crystallite size and highlighting the study's contributions to ceramic synthesis knowledge [20].

I. Ganesh *et. al*examines the fabrication of nanocrystalline magnesium aluminate spinel utilizing both microwave-assisted combustion synthesis and conventional combustion synthesis (CCS) techniques, evaluating their impact on specific surface area, crystallite size, compositional consistency, and phase purity. It reveals that increasing batch size results in decreased surface area and increased crystallite size, especially in MWCS powders. MWCS yields materials with larger crystallite sizes and higher stability compared to CCS. MWCS

powders have 20–50 nm crystals, while CCS powders have aggregates of 100–250 nm crystals. The study highlights the influence of treatment temperature on crystallite sizes and the superior properties of MWCS powders. Overall, it suggests MWCS as a promising technique for high-quality nanocrystalline spinel powder production, offering valuable insights into materials synthesis and contributing significantly to the field [21].

Guotian Ye *et. al.* discusses a novel method for synthesizing $MgAl_2O_4$ spinel through a combination route of sol-gel and precipitation processes. It investigates the thermal decomposition as well as phase growth of the precursor, as well as agglomeration of the heat-treated powder based on particle and crystal size. The study determines 900°C as the optimum calcination temperature for obtaining completely crystallized ultrafine spinel powder. The experimental methodologies, encompassing synthesis, calcination, and characterization procedures such as X-ray diffraction and transmission electron microscopy, are meticulously outlined. Emphasizing $MgAl_2O_4$ spinel's desirable properties and conventional synthesis methods, the study underscores the importance of calcination temperature in controlling powder reactivity and specific surface area. Results highlight thermal analysis findings, phase development, and the influence of calcination temperature on spinel powder properties. The research concludes that the novel synthesis route enhances precursor homogeneity which enables the production of pure nano-particulate spinel at lower heating temperature. Overall, the study offers insights into spinel powder synthesis and characterization, with potential applications in refractory materials and ceramics [22].

E. N. Alvar*et. al* explores the synthesis of mesoporous nanocrystalline $MgAl_2O_4$ spinel powders using the route of co-precipitation method. It examines the molar ratio of surfactant to metaleffects on structural properties. Characterization techniques including XRD, N_2 adsorption, TGA, DTA, FTIR, and TEM analyze the samples. Results show that a CTAB to metal ratio of 0.3 yields the highest specific surface area as well as smallest size of crystallite, while higher ratios decrease surface area due to pore wall destruction. CTAB addition decreases crystallite size, increases surface area, and improves thermal stability. However, higher ratios reduce surface area and increase pore size due to pore wall destruction. The study demonstrates a straightforward method for synthesizing mesoporous nanocrystalline MgAl2O4 spinel powders and underscores the surfactant ratio's critical role in structural properties, offering insights for spinel synthesis with enhanced surface area and thermal stability. This contributes to understanding nanocrystalline material synthesis, holding

relevance for industries needing specific material properties. The research provides a comprehensive synthesis overview and characterization techniques discussion [23].

V.N Singh *et. al* discovers low-temperature synthesis of spinel ($MgAl_2O_4$) via a gelation-precipitation process using aluminum and magnesium sulfates. XRD shows spinel-like phase formation at 600°C, complete at 1000°C in 1 hour. Calcined powder has 0.2 µm average particle size, sintering well, reaching 95% density within 3 hours at 1450°C. SEM reveals faceted grains, suggesting high-temperature application potential. The introduction highlights spinel ceramics' suitability for high temperatures. Various chemical techniques for spinel synthesis, especially the sol-gel process, are discussed. The presented method combines precipitation and gelation for spinel preparation. Experimental procedures cover solution prep, gel formation, thermal analysis, XRD, particle size, and sintering. Results analyze gel's thermal decomposition, spinel formation, and powder densification. Conclusively, spinel can be synthesized simply, yielding materials sinterable at low temperatures. This process, compared favourably to costly methods, holds potential for practical spinel ceramic applications, offering valuable insights for materials science and engineering researchers and practitioners [24].

S. Zhang, *et. al* investigates magnesium aluminate ($MgAl_2O_4$) spinel powder synthesis using molten salt synthesis (MSS) as an alternative to conventional mixed oxide synthesis (CMOS). MSS's feasibility for complex oxide synthesis, particularly MA powder, is investigated. CMOS, involving high-temperature solid–solid reactions, often results in impurities and agglomeration. MSS significantly reduces synthesis temperature, retaining the original Al_2O_3 raw material's size and morphology, indicating a "template formation mechanism." Experimental procedures mix equimolar MgO and Al_2O_3 with different salts, heating in the 800-1150°C range. XRD analysis shows earlier MA spinel peak formation using MSS compared to CMOS. Despite minor salt impurities after washing, MSS effectively decreases synthesis temperature, especially with LiCl. MSS's "template formation mechanism" suggests potential for synthesizing other high melting complex oxides. Overall, the study underscores MSS's potential as an efficient, low-temperature alternative for complex oxide synthesis, offering valuable insights for materials science researchers [25].

Li-Zhai *et. al.* explores low-temperature synthesis route of magnesium oxide (MgO) and magnesium aluminate powder via a sol-gel route, offering a simple, efficient, and cost-effective methodThe study delves into the decomposition of the citrate precursor derived

from magnesium chloride, aluminum nitrate, and citric acid. Analytical techniques including X-ray diffraction (XRD), scanning electron microscopy (SEM), thermogravimetric analysis coupled with differential scanning calorimetry (TGA-DSC), and Fourier transform infrared spectroscopy (FTIR) were employed to investigate the formation of cubic MgO and magnesium aluminate spinel (MAS). The findings reveal the successful synthesis of single-phase cubic MgO at 800°C and MAS at 1200°C, respectively.. Ball milling reduces powder conglomeration and size. The study underscores practical significance for applications like refractories, paints, and catalysts. It addresses challenges in MgO synthesis, introducing sol-gel as an effective method and discussing MAS purity challenges. Potential commercial production from inexpensive precursors is highlighted, addressing industry needs for cost-effective synthesis methods. Overall, the document contributes valuable insights into low-temperature MgO and MAS synthesis, advancing materials science and industrial applications [26].

2.2 Characterisation techniques of magnesium aluminate spinel (MAS):

V. Montouillout*et. al.* investigates $MgAl_2O_4$ spinel precursor synthesis via aqueous routes like spray drying and citrate complexing, examining morphology, crystallization behaviour, and aluminum local structures. Characterization methods include high-resolution solid-state NMR, notably 27Al MAS NMR and double-resonance experiments. Results reveal synthesis route-dependent variations in precursor properties, particularly in crystallization behaviour and aluminium local structures. NMR techniques probe aluminum coordination states and spatial proximity to residual protons, offering insights into precursor structural features. Experimental procedures detail sample preparation for atomization and complexation, highlighting morphological and thermal differences. The study emphasizes precursor synthesis route impact on MgAl2O4 spinel precursor structure and properties. Variations in morphology, crystallization, and aluminum structures stem from synthesis methods, informing on precursor synthesis's role in ceramic powder property tailoring. In conclusion, the study underscores precursor synthesis route significance, with advanced NMR techniques providing crucial insights into spinel precursor structural details [27].

S. S. Milani *et. al.* focuses on preparing and characterizing a magnesium aluminate spinel using inorganic salts. The sol is synthesized through the route of high-speed stirring of inorganic precursors, resulting in a stable, nearly translucent sol with pH 3-4 and picnometric density of 1.19 g/cm^3. Kept for a month at 25°C due to small size of particle, the sol prevents

particle precipitation by Brownian motion overcoming gravitational forces. Physical, thermal, and microstructural characterization involves TGA/DSC, FTIR, XRD, and FESEM techniques. Results show single-phase $MgAl_2O_4$ formation up to 600°C, with 50 nm grain size at 1000°C calcination. EDS spectra reveal Al, Mg, O, and N peaks, detailing sol chemical composition. The study advances understanding of sol-gel synthesis methods and suggests potential industrial applications for the resulting spinel sol, contributing valuable insights to materials science and engineering. No competing financial interests or personal relationships influencing the work are declared, ensuring research integrity [28].

M.F. Zawrah*et. al.* explores the influence of sintering aids, namely ZnO and MnO_2, to densify magnesium aluminate spinel. Various experimental procedures involved spinel powder preparation, characterization via various analytical techniques, ceramic body processing, and spinel body densification. Results cover phase composition, infrared spectroscopy, morphology, densification, phase composition, microstructure, and mechanical properties. Nanocrystalline magnesium aluminate spinels were successfully prepared using traditional co-precipitation with cost-effective chemicals. Effect of ZnO/MnO_2 addition as sintering aids significantly affected the ability of spinel to sinter and mechanical properties, with optimal density and strength achieved at specific additive concentrations. The findings have implications for cost-effective nano $MgAl_2O_4$ spinel synthesis. Overall, the study offers valuable insights into synthesis, characterization, and properties of nano $MgAl_2O_4$ spinel, elucidating the impact of sintering aids on densification and mechanical properties. Detailed experimental procedures and thorough analysis contribute to ceramic materials synthesis and processing knowledge [29].

M. F. M. Zawrah*et. al.*underscores the advantages of nanocrystalline materials, particularly $MgAl_2O_4$ ceramic spinel, over conventional alternatives, highlighting their physical, thermal properties, and mechanical strength. It outlines challenges associated with conventional sintering processes, including reduced reactivity, surface area, and strength. To address these issues, low-temperature spinel formation methods are explored, encompassing various techniques like solid-state reactions, sol-gel methods, and plasma spray decomposition. The co-melting method emerges as promising, yielding nanocrystalline $MgAl_2O_4$ powders with over 98% spinel content at temperatures up to 1000°C. Detailed experimental procedures for powder preparation, including co-melting, are provided, with characterization via XRD, TEM, and IR spectroscopy. Results demonstrate successful synthesis of nanocrystalline spinel with high purity and small particle sizes. Conclusions highlight technical advantages

and potential industrial applications, offering valuable insights into nanocrystalline $MgAl_2O_4$ synthesis using molten salts, aiding cost-effective and energy-efficient production. The study contributes to nanomaterial synthesis advancement and provides groundwork for further research in the field [30].

M Wang *et. al.* discusses the synthesis and properties of mechanically alloyed and nanocrystalline materials. It explores the impact of mechanically alloying on material properties, particularly in the context of nanocrystalline structures. Additionally, the document discusses the synthesis and characterization of $MgAl_2O_4$ spinel ceramic precursor, providing insights into the methods and techniques used in creating this ceramic material. The research contributes to the understanding of advanced materials and their potential applications in various fields, offering valuable insights into material synthesis and characterization. It serves as a valuable resource for researchers and professionals in the materials science domain, providing comprehensive information on the synthesis and properties of advanced materials [31].

H. Li *et. al.*aimed to produce high-quality $MgAl_2O_4$ spinel nano-powders for potential use in porous ceramic materials. Preparation involved various techniques including thermal analyses, XRD, FTIR, SEM, and TEM. Results indicated pure spinel phase, nano meter-sized particles, high specific surface area, and mesoporous structure. Sintering behaviour revealed formation of small open pores. The study emphasized potential applications of the synthesized nano-powders in porous ceramics, discussing phase evolution, gel formation process, and particle size distribution. Comprehensive analysis covered chemical and physical properties including specific surface area, pore size distribution, and morphology. Overall, the research successfully synthesized fine $MgAl_2O_4$ spinel nano-powders via non-hydrolytic sol-gel method, showcasing their potential for porous ceramic materials. The findings offer valuable insights into advanced material development, hinting at further research and applications in ceramic materials field [32].

Alinejad *et. al.*shown In his research, magnesium aluminate spinel was synthesized utilizing metal nitrates and a polymer matrix precursor. Characterization techniques including STA, XRD, FT-IR, FE-SEM, and TEM were employed. Spinel formation commenced between 600 and 700°C, with synthesized temperature at 800°C for 2 hours resulting in 8–12 nm crystallite size. The polymer-to-metal ions ratio significantly affected crystallite size. Experimental steps included sol preparation, heating, dehydration, and calcination. Results

covered STA curves, FTIR spectra, XRD patterns, and polymer matrix effects on crystallite size. The method yielded nanocrystalline $MgAl_2O_4$ spinel powder at low temperatures, with crystallite size influenced by gas and heat. The study offered insights into synthesis, crystallite size variation, and polymer matrix influence, suggesting cost-effective and efficient ceramic powder synthesis for diverse applications [33].

A. K. ADAK *et. al.* presents a pioneering chemical approach entailing rapid vaporization of polyvinyl alcohol introduced into the mixed metal nitrate solution, succeeded by pyrolysis. This method offers simplicity, cost-effectiveness, and energy efficiency in material synthesis. Detailed analyses, including TGA, DTA, XRD patterns, and infrared spectra of original material and heat-treated powders, provide insights into synthesized materials' characteristics. X-ray of amorphous powders urges even after calcination at 600°C for 2 hours, with crystallization beginning at 650°C. Crystallite size increases with higher calcination temperatures, and IR spectra depict band disappearance with increased heat treatment. The research findings suggest that this approach to synthesizing magnesium aluminate spinel offers technical simplicity, cost-effectiveness, and energy efficiency, effectively addressing affordability and versatility challenges within the field of materials science. Its implications extend to material science and industrial applications, contributing to cost-effective and efficient synthetic routes for refractory oxide materials [34].

2.3 Property evaluation of magnesium aluminate spinel (MAS):

Y. Akimun *et. al.* discusses Knoop microhardness anisotropy profiles for single-crystal stoichiometric $MgAl_2O_4$ spinel, revealing maximum microhardness in the [001] direction for the (100) plane, suggesting {111} as the primary slip system. Conversely, microhardness for the (111) plane remains independent of indenter orientation, supporting a {111} primary slip system. It notes microhardness anisotropy alone may be unreliable due to secondary slip systems. Additionally, the outgassing behaviour of ZrF_4-based glasses, particularly ZBLAN and ZBL glasses, is investigated, unveiling evaporation of ZrF_2, ZrF_4, ZrF_6, HF, HCl, O_2, CO_2, and atomic fluorine. Weight loss and white film formation during melting, primarily composed of ZrO_2, are observed. Experimental procedures detail Knoop microhardness measurement and outgassing analysis. The study aims to understand ZrF_4-based glasses' behaviour under heating conditions, offering insights into material properties and behaviour. It contributes to understanding microhardness anisotropy and outgassing behaviour, enriching knowledge of material properties under specific conditions [35].

S. A. Zaidan *et. al.* investigates the impact of incorporating spinel ($MgAl_2O_4$) particles into Y_2O_3–ZrO_2 composite material, varying the $MgAl_2O_4$ percentages. Tests measure density, porosity, mechanical properties, and microstructure. Results show $MgAl_2O_4$ affects physical and mechanical properties, altering density, porosity, Vickers hardness, and fracture toughness. X-ray diffraction and scanning electron microscopy are employed to analyze the phase composition and microstructure, shedding light on the influence of MgAl2O4. Bulk density and apparent porosity vary with $MgAl_2O_4$ percentage. Vickers hardness and fracture toughness peak at 15% $MgAl_2O_4$. Microstructure analysis confirms $MgAl_2O_4$'s impact on grain boundaries and porosity. The study provides insights into enhancing Y_2O_3–ZrO_2 composites with $MgAl_2O_4$, offering a comprehensive understanding of their behaviour. These findings could optimize ceramic materials for applications requiring high mechanical performance and tailored microstructures [36].

Oleg Khasanov *et. al.* discusses the synthesis and characterization of transparent polycrystalline $MgAl_2O_4$ spinel using Spark Plasma Sintering (SPS) and its impact on optical and mechanical properties. The study aims to achieve high transparency while maintaining strong mechanical properties for applications like armour and IR-windows. Analytical techniques such as SEM, XRD, nano-indentation, and optical property studies are employed. Results show under optimal SPS conditions, ceramics exhibit submicron grains, dense boundaries, and high strength, with no impurities. Transparency reaches 72.6% at 555 nm, showing fracture toughness of 2.4 MPa × $m^{1/2}$ and microhardness of 18.52 GPa. The study determines optimal SPS conditions for synthesizing polycrystalline $MgAl_2O_4$ spinel, highlighting its effectiveness in achieving high transparency and excellent mechanical properties. It also discusses spinel behaviour concerning heating duration and pressure force, offering insights into material characteristics under different synthesis conditions [37].

C.A. Black *et. al.* explores the effect of neutron irradiation (highly dose) at 385 and 750°C onto the microhardness of stoichiometric $MgAl_2O_4$ spinel powder, a material considered for fusion reactors due to its neutron resistance. Hot-pressed polycrystalline specimens were irradiated, and their microhardness and crystallographic orientation dependence were analyzed. Results showed initial hardening followed by slight recovery, indicating activation of a secondary slip system. At 750°C, orientation dependence persisted, suggesting a stronger secondary slip system. The material exhibited minor hardening, peaking early and relaxing at higher exposure levels, maintaining suitability for fusion applications, hinting at an efficient self-healing process. The study sheds light on $MgAl_2O_4$ spinel's radiation response,

supporting its use in fusion reactors and elucidating factors influencing microhardness under neutron irradiation. It underscores crystal orientation and mechanical stability's role in microhardness response [38].

S. Benaissa *et. al.* studies investigate nanostructured $MgAl_2O_4$ ceramics fabricated via Spark Plasma Sintering (SPS) at different temperatures, evaluating their properties. Samples sintered at 1300°C exhibited finer microstructures, higher density, and superior mechanical properties (Hv 18 GPa, E 228 GPa, m 0.06), alongside improved optical transmittance (70% at 550 nm, 78% at 1100 nm). Microstructural analysis revealed uniformity and densification at 1300°C, correlating with enhanced properties. Optical features were influenced by sintering temperature, with higher temperatures reducing transmittance. Mechanical traits like hardness, modulus, and toughness were temperature-dependent, with finer microstructures enhancing performance. Tribological studies showed sintering temperature's role in wear resistance. The research underscores sintering's critical role in shaping microstructure, density, and subsequent properties of $MgAl_2O_4$ ceramics, offering insights for tailored ceramic development [39].

A.R. Molla *et. al.* explores the fabrication and characterization of Cr3+-doped $MgAl_2O_4$ spinel glass-ceramic nanocomposites. Glasses were prepared via melt-quenching, followed by heat treatment to form glass-ceramics. Extensive characterization included DSC, XRD, FE-SEM, TEM, FT-IR, PL, optical absorbance, and EPR analyses. Properties such as microstructure, mechanical, thermal, and optical features were assessed. Results highlighted thermal, physical, microstructural, and mechanical properties of the ceramic glass, detailing with the influence of Cr^{+3} ion doping. References for further research were provided [40].

References:

1. Z. E. Nakagawa, N. Enomoto, I. S. Yi and K. Asano: Proc. UNITECER ’95 Cong., Tokyo, Japan, November 1995, Technical Association of Refractories, 379–386.
2. Book: S. Zhang and W. E. Lee: ‘Spinel-containing refractories’, in ‘Refractories handbook’, (ed. C. Schacht), 215–257; 2004, New York, Marcel Dekker.
3. J. G. Li, T. Ikegami, J. H. Lee and T. Mori: J. Am. Ceram. Soc., 2000, 83, (11), 2866–2868.
4. S. Sharafat, N. M. Ghoniem, P. I. H. Cooke, R. C. Martin, F.Najmabadi, K. R. Schultz and C. P. C. Wong: Fusion Eng. Des., 1993, 23, 99–113.
5. S. Mathur, M. Veith, T. Ruegamer, E. Hemmer and H. Shen: Chem. Mater., 2004, 16, 1304–1312.
6. R. J. Bratton and S. M. Ho: J. Am. Ceram. Soc., 1968, 51, (1), 56–57.
7. R. H. Arlett and M. Robbins: J. Am. Ceram. Soc., 1967, 50, (5), 273–274.
8. Book: W. D. Kingery, H. K. Bowen and D. R. Uhlmann: ‘Introduction to ceramics’, 656–667; 1976, New York, John Wiley & Sons.
9. Book: D. C. Cranmer: ‘Introduction to glasses and ceramics’, Vol. 4, 18; 1991, Materials Park, OH, ASM International.
10. G. Ye, G. Oprea, and T. Troczynski: J. Am. Ceram. Soc., 2005, 88, (11), 3241–3244.
11. P. Duran, J. Tartaj, J. F. Fernandez, M. Villegas, and C. Moure, ‘‘Crystallisation and Sintering Behaviour of Nanocrystalline Y-TZP Powders Obtained by Seeding-Assisted Chemical Coprecipitation,’’ Ceram. Int., 25, 125–35 (1999).
12. R. J. Bratton, ‘‘Coprecipitates Yielding MgAl2O4 Spinel Powders,’’ Am. Ceram. Soc. Bull., 48 [10] 759–62 (1968).
13. W. Kim and F. Saito, ‘‘Effect of Grinding on Synthesis of MgAl2O4 Spinel from a Powder Mixture of Mg(OH)2 and Al(OH)3,’’ Powder Technol., 113, 109–13 (2000).
14. J. H. Belding and E. A. Letzgus: US Patent 3 950 504, 13 April 1976.
15. P. Magne and U. Belser: Int. J. Prosthodont., 1997, 10, (5), 459– 466.
16. G. Gusmano, G. Montesperelli, E. Traversa and A. Bearzotti: Sens. Actuators B, 1993, 14B, (1–3), 525–527.
17. H. S. Tripathi, B. Mukherjee, S. Das, M. K. Haldar, S. K. Das and A. Ghosh: Ceram. Int., 2003, 29, 915–918.
18. W. Kim and F. Saito: Powder. Technol., 2000, 113, 109–113.

19. J. Guo, H. Lou, H. Zhao, X. Wang, and X. Zheng, “Novel synthesis of high surface area MgAl2O4 spinel as catalyst support,” *Mater Lett*, vol. 58, no. 12–13, pp. 1920–1923, May 2004.
20. C. Păcurariu, I. Lazău, Z. Ecsedi, R. Lazău, P. Barvinschi, and G. Mărginean, “New synthesis methods of MgAl2O4 spinel,” *J Eur Ceram Soc*, vol. 27, no. 2–3, pp. 707–710, 2007.
21. I. Ganesh, R. Johnson, G. V. N. Rao, Y. R. Mahajan, S. S. Madavendra, and B. M. Reddy, “Microwave-assisted combustion synthesis of nanocrystalline MgAl 2O4 spinel powder,” *Ceram Int*, vol. 31, no. 1, pp. 67–74, 2005.
22. G. Ye, G. Oprea, and T. Troczynski, “Synthesis of MgAl2O4 spinel powder by combination of sol-gel and precipitation processes,” *Journal of the American Ceramic Society*, vol. 88, no. 11, pp. 3241–3244, Nov. 2005.
23. E. N. Alvar, M. Rezaei, and H. N. Alvar, “Synthesis of mesoporous nanocrystalline MgAl2O4 spinel via surfactant assisted precipitation route,” *Powder Technol*, vol. 198, no. 2, pp. 275–278, Mar. 2010.
24. V. K. Singh and R. K. Sinha, “Low temperature synthesis of spine1 (MgA1,04),” 1997.
25. S. Zhang, D. D. Jayaseelan, G. Bhattacharya, and W. E. Lee, “Molten salt synthesis of magnesium aluminate (MgAl 2O 4) spinel powder,” *Journal of the American Ceramic Society*, vol. 89, no. 5, pp. 1724–1726, May 2006.
26. L.-Z. Pei, W.-Y. Yin, J.-F. Wang, J. Chen, C.-G. Fan, and Q.-F. Zhang, “Low Temperature Synthesis of Magnesium Oxide and Spinel Powders by a Sol-Gel Process,” 2010.
27. V. Montouillout, D. Massiot, A. Douy, and J. P. Coutures, “Characterization of MgAl 2 O 4 Precursor Powders Prepared by Aqueous Route.”
28. S. S. Milani, M. G. Kakroudi, N. P. Vafa, S. Rahro, and F. Behboudi, “Synthesis and characterization of MgAl2O4 spinel precursor sol prepared by inorganic salts,” *Ceram Int*, vol. 47, no. 4, pp. 4813–4819, Feb. 2021.
29. M. F. Zawrah, H. Hamaad, and S. Meky, “Synthesis and characterization of nano MgAl2O4 spinel by the co-precipitated method,” *Ceram Int*, vol. 33, no. 6, pp. 969–978, Aug. 2007.
30. M. F. M. Zawrah and A. A. El Kheshen, “Synthesis and characterisation of nanocrystalline MgAl2O4 ceramic powders by use of molten salts,” *British Ceramic Transactions*, vol. 101, no. 2, pp. 71–74, 2002.
31. M. S. Wang and M. Muhammed, “Synthesis and Characterisation of $MgAl_2O_4$ Spinel Ceramic Precursor,” *Materials Science Forum*, vol. 235–238, pp. 241–248, Oct. 1996.

32. H. Li *et al.*, “Synthesis and characterisation of MgAl2O4 spinel nanopowders via nonhydrolytic sol-gel route,” *Journal of the Ceramic Society of Japan*, vol. 125, no. 3, pp. 100–104, Mar. 2017.
33. B. Alinejad, H. Sarpoolaky, A. Beitollahi, A. Saberi, and S. Afshar, “Synthesis and characterization of nanocrystalline MgAl2O4 spinel via sucrose process,” *Mater Res Bull*, vol. 43, no. 5, pp. 1188–1194, May 2008.
34. A. K. Adak, S. K. Saha, and P. Pramanik, “Synthesis and characterization of MgAl2O4 spinel by PVA evaporation technique,” *J Mater Sci Lett*, vol. 16, no. 3, pp. 234–235, 1997.
35. R. C. Bradt, “Knoop Microhardness Anisotropy of Single-Cry stal S toichiometric MgA1204 Spinel,” 1987.
36. S. A. Zaidan and S. M. Majeed, “Effect of MgAl 2 O 4 Particles on Characterization of Y 2 O 3-ZrO 2 System,” 2015.
37. O. Khasanov, E. Dvilis, A. Khasanov, E. Polisadova, and A. Kachaev, “Optical and mechanical properties of transparent polycrystalline MgAl2O4 spinel depending on SPS conditions,” *Physica Status Solidi (C) Current Topics in Solid State Physics*, vol. 10, no. 6, pp. 918–920, Jun. 2013.
38. C. A. Black, F. A. Garner, and R. C. Bradt, “Influence of high dose neutron irradiation at 385 and 750°C on the microhardness of MgAl2O3 spine1 *,” 1994.
39. S. Benaissa, M. Hamidouche, M. Kolli, G. Bonnefont, and G. Fantozzi, “Characterization of nanostructured MgAl2O4 ceramics fabricated by spark plasma sintering,” *Ceram Int*, vol. 42, no. 7, pp. 8839–8846, May 2016.
40. A. R. Molla *et al.*, “Microstructure, mechanical, thermal, EPR, and optical properties of MgAl2O4:Cr3+ spinel glass-ceramic nanocomposites,” *J Alloys Compd*, vol. 583, pp. 498–509, 2014.

Chapter-3

EXPERIMENTAL PROCEDURE

In the previous chapter overviews of a few synthesis processes of magnesium aluminate spinel have been discussed. With the help of technological evolvement many new synthesis procedures have been discovered day by day. From various literature survey and detailed analysis, we came to a conclusion that sol-gel process is the best route for the production of $MgAl_2O_4$.

3.1 Selection of precursors:

Alumina precursor: Because of their great mechanical strength, thermal stability across a wide temperature range, and high specific surface, aluminium oxides are commonly used in catalytic processes. The goal of this investigation was to see how the process conditions in the hydrolysis of hydrous aluminium nitrate (especially the temperature and digesting time) affected the thermal stability of the aluminium oxides formed by thermal decomposition of the hydroxides formed during the hydrolysis.[1]

Magnesia precursor: The formula $Mg(NO_3)_2(H_2O)_x$, here x = 6, 2, and 0, are referred to as magnesium nitrate. They're all white solids. Because the anhydrous substance is hygroscopic, it forms the hexahydrate fast when exposed to air. In both water and ethanol, all of the salts are extremely soluble. Magnesium nitrate has very high attraction for water, heating the hexahydrate causes it to decompose into magnesium oxide, oxygen, and nitrogen oxides rather than dehydration**.**

Various catalytic agents or fuels: In chemistry, a catalyst is any substance that speeds up a reaction without being consumed. Various catalytic action, in general, is a reaction of chemical between a catalyst and a reactant. The reaction produces chemical intermediates that can react more easily amongst each other or with another reactant to produce the desired product. We have used various catalyst or we can say fuel in our project such as thiourea, glycine, citric acid, urea etc. and compared their catalytic efficiency in producing better spinel.

Physical Properties and Applications of Magnesium Nitrate and Aluminum Nitrate

Magnesium Nitrate

- Density: 2.3 g/cm³ (anhydrous)
- Melting Point: 129°C

- Boiling Point: 330°C
- Solubility: Soluble in water; moderately soluble in ammonia and ethanol
- Nature: Hygroscopic

Applications:
Magnesium nitrate is utilized across various industries, including food, pharmaceuticals, air conditioning, and oil and gas. Additionally, it plays a role in wastewater and industrial effluent treatment. Magnesium nitrate is a key source of magnesium, an essential element for chlorophyll production, photosynthesis, and carbohydrate formation.

Aluminum Nitrate

- Density: 1.72 g/cm³ (nonahydrate)
- Melting Point: 66°C (anhydrous); 73.9°C (nonahydrate)
- Appearance: White crystals, solid, hygroscopic
- Odor: Odorless

Applications:
Aluminum nitrate is primarily used in the preparation of magnesium aluminate spinel (MA). This note outlines the key properties and industrial applications of magnesium nitrate and aluminum nitrate. Both compounds have significant roles in various processes and products. Magnesium nitrate $Mg(NO_3)_2$ and aluminum nitrate are both important in materials science, each exhibiting a wide range of chemical properties.

Magnesium Nitrate

- Solubility: Highly soluble in water; moderately soluble in ammonia and ethanol
- Thermal Stability: Decomposes at elevated temperatures, releasing nitrogen dioxide and oxygen gas
- Acid-Base Reactions: Reacts with acids to form magnesium salts, and with bases to form magnesium hydroxide and nitrate salts
- Redox Reactions: Reacts with sodium hydroxide and hydrogen peroxide, producing magnesium oxide, water, and oxygen gas
- Uses: Employed as a desiccant, a component of fertilizers, and in the preparation of magnesium hydroxide

Aluminum Nitrate: Utilized in tanning leather, in antiperspirants, as a corrosion inhibitor, in uranium extraction, petroleum refining, and as a nitrating agent.Applications: Used in the production of alumina for insulating papers, cathode ray tube heating elements, and transformer core laminates

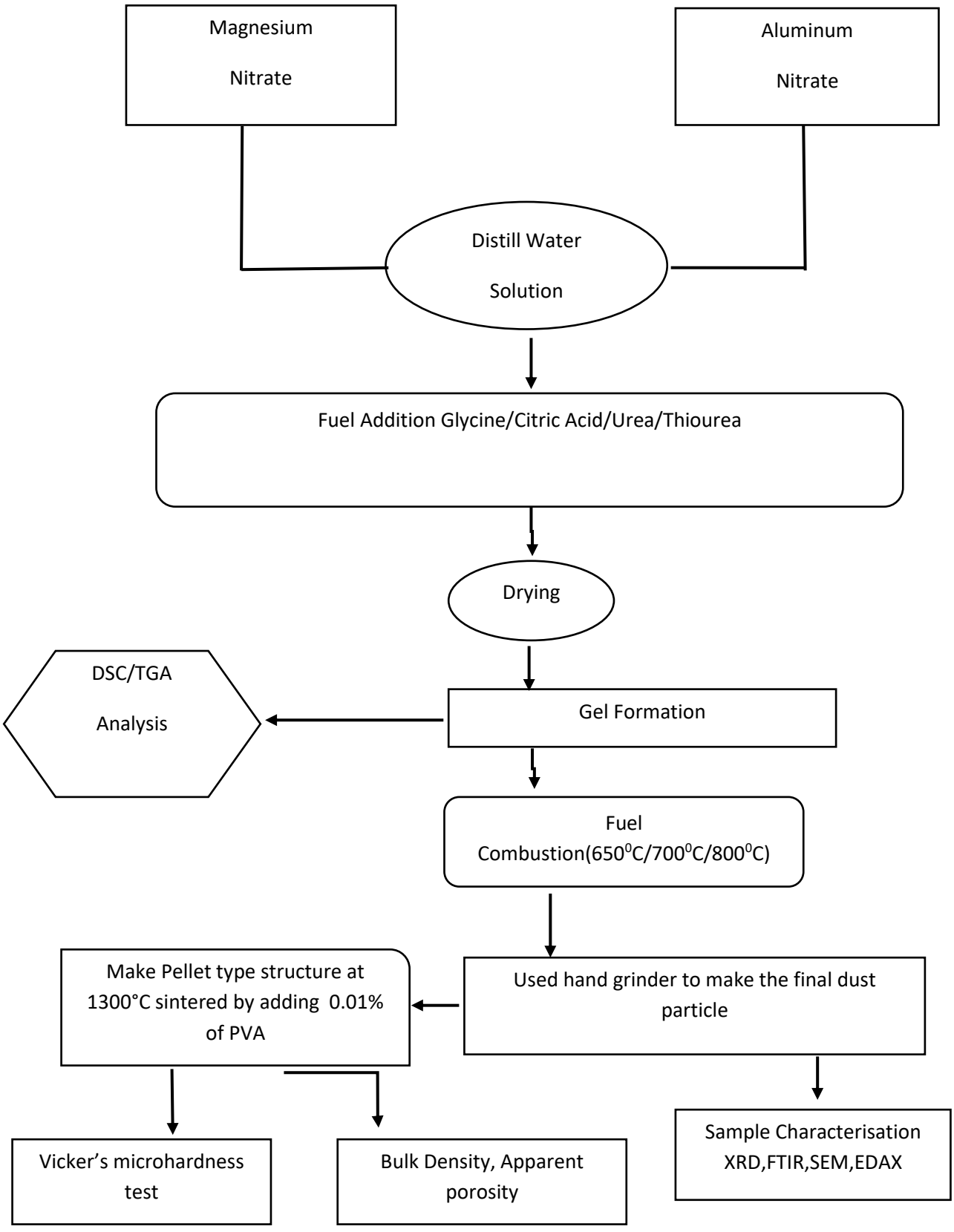

Figure : 3.1a) Flow Chart

3.2 Preamble:

The details of the experimental procedure for evaluating $MgAl_2O_4$ production are explained in this section using the sol-combustion method see Figure 3.1 a. To determine the molar ratios of aluminium oxide, magnesium oxide, and fuel, a review of the literature was conducted. We'll compare the properties of alumina and spinel at various treatment temperatures. The basic supplies for this study were provided by an analytical supply store, which comprised aluminium nitrate, magnesium nitrate, and fuels as needed.

3.3 Material Preparation:

Preparation of spinel:

The magnesium-to-aluminium stoichiometric ratio in $MgAl_2O_4$ spinel was 1:2. Our goal was to see if we can employ surplus alumina in the experiment and, if so, at what ratio. We have also experimented with excess magnesium. Magnesium nitrate and Aluminium nitrate was taken with stoichiometric mole ratio 1:2, and non-stoichiometric mole ratio 1:1.75, 1:2.25. Four different batches are done where catalytic agents like thiourea, glycine, citric acid, urea are used respectively by mixing in bowl figure 3.1b. A small amount of water was then added to the mixture. Water was uniformly mixed with the material. The mixture was then dried at 80°C for 3-4 hours see figure 3.2. After the drying process was done, the mixture was turned into gel like mixture. The gel was then gone through various heating treatment. Following that, each part was given a 2-hour heat treatment at a specific temperature. Processing temperatures of 650°C, 700°C, and 800°C were employed.

Figure: 3.1b) Ceramic powder mixing bowl and mixing hammer

Figure : 3.2 –Control temperature magnetic Stirrer cum Heater

Pressing/Compaction for Micro Hardness Test:

In a die system consisting of two punches (a stationary lower punch / base and a moveable higher punch) and the middle block consisting of the cylindrical mould cavity, the powder mixtures were poured into a 12 mm diameter mould cavity. The entire die system was placed in a hydraulic pressing machine that was operated manually. The pressing was done with a uniaxial pressure of 1500 kg/cm^2 (figure 3.3 and 3.4). As a result, cylindrical alumina and spinel pellets of various heat treated powders were obtained.

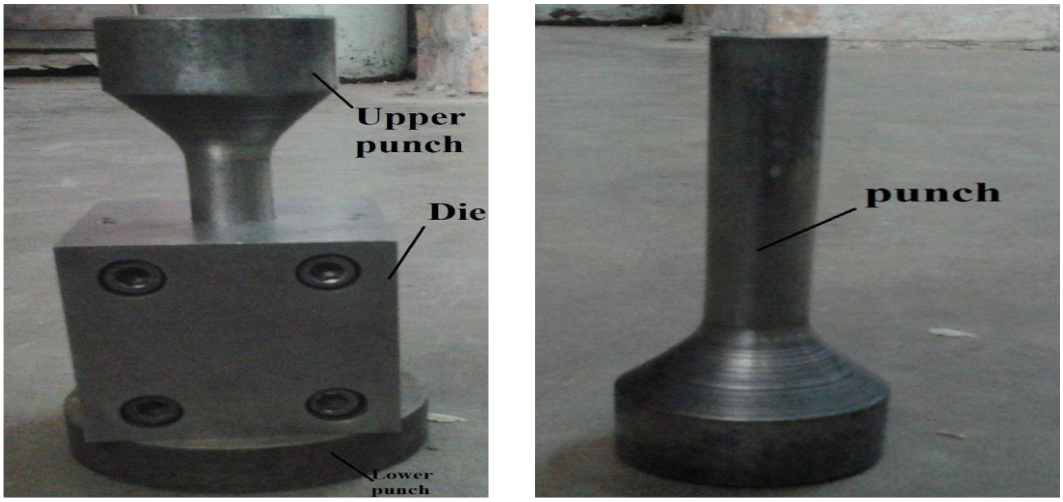

Figure : 3.3- Die and Punch System

Figure3.4: Hydraulically controlled high-pressure pressing machine

Curing

The compacted samples were subjected to curing at various temperature like 650^0C, 700^0C, 800^0C for about 1 hours as per the requirement of experiment (figure 3.5). This was done in order to facilitate the following

- Elimination of residual water, volatile matters and phenols if present in sample.

- Development of sufficient strength and proper binding of the constituents so that tablets can be used as micro hardness test.

Figure 3.5: Pot furnace

3.5 CHARACTERISATIONS /TESTS:

Differential Scanning Calorimetry &Thermo gravimetric Analysis:

Differential Thermal &Thermo gravimetric Analysis is very important characterization tool for characterization. In DSC-TGA we can identify any phase change or any chemical/physical change in the system where enthalpy changes occurs are measured by controlling temperature at particular rate of heating or cooling. Diamond DT-TGA can also analyze DSC by suitable software to measure heat flow Vs temperature plot and change in weight Vs Temperature see figure 3.6. This system can measure simultaneously both weight change and heat flow and accordingly any phase change can be identified precisely as most of the phase change occurs without change in weight. Below, schematic view and the image of DSC-TGA instrument is given below-

Figure 3.6: DSC-TGA instrument

DSC-TGA analysis was gone through machine with following specifications:

Model No. : Pyris Diamond (TG/DSC)

MAKE :PerkinElmer

Nitrogen Atmosphere kept at the rate of 150ml/min

Platinum crucible has been used with alpha alumina powder as reference sample.

Figure 3.7: X-ray diffraction machine

Using Bruker D8 Advance, X-ray diffraction analysis (figure 3.7) was performed on all materials in the same conditions using Cu Kα radiation. whose-

- Tube voltage: 40 kV
- Tube current: 40 mA.
- Scan Range: 10º-90º
- Scan Mode: Continuous
- Speed: 1º/min

These settings were used throughout the entire XRD analysis. The XRD spectrum gives us the diffraction intensity Vs 2θ plot, where θ is the Bragg's angle in degrees. The XRD plot gives the d-values of the samples along with the values of flex width, 2θ and intensity of the respective peaks. The calculated d-values for the respective peaks in the XRD plot of $MgAl_2O_4$ (spinel), pure Al_2O_3, and were matched with the standard JCPDS data and all the phases corresponding to each of these peaks were identified.

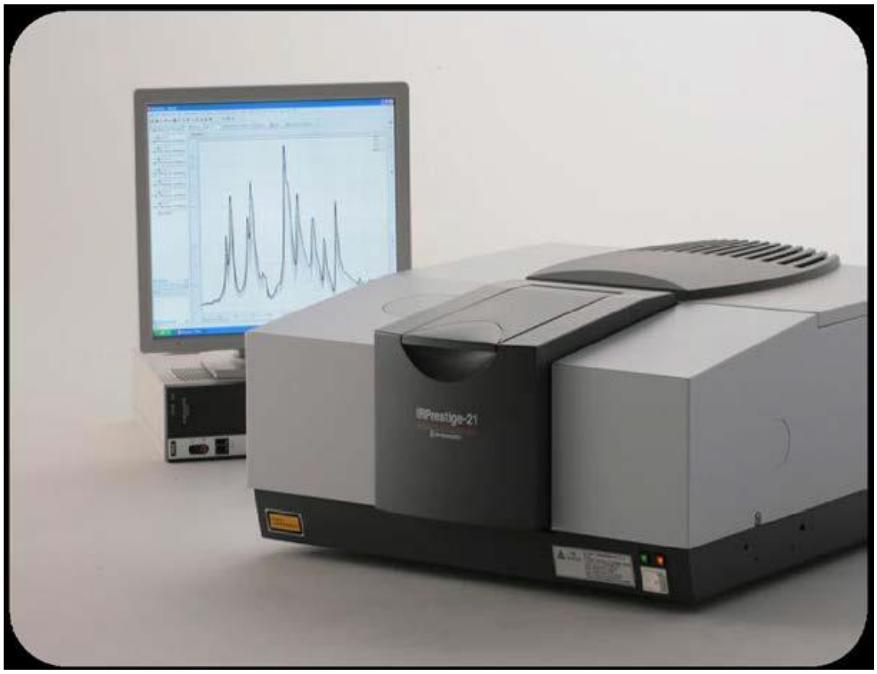

Figure 3.8: Shimadzu IRPrestige-21 FTIR spectrometer

Fourier Transform Infrared Spectroscopy (FTIR) spectroscopy of different batches:

The resulting FTIR spectrum provides a molecular fingerprint of the sample by illustrating the molecule absorption and transmission. No two distinct molecule configurations produce the same infrared spectrum, similar to fingerprints. From this analysis we can identify

- Unknown material in the sample.
- Determine the quality of sample.
- Determine the amount of the components in a mixture.

The peaks in the spectrum is an indication of the amount of material present and the position indicates typical bonds (figure 3.8). The sample was prepared for FTIR spectroscopy by adding KBr and using hydraulic pressure to form a pellet. For the reference material, a single KBr pellet was also created.

Figure3.9: Scanning Electron Microscope

The examination of samples at a microscopic level was conducted using a Scanning Electron Microscope (SEM) with a high depth of field capability see figure 3.9. This allowed for a substantial portion of the sample to remain in focus simultaneously, resulting in the generation of precise three-dimensional images. Through SEM analysis, a wealth of topographical and elemental information such as grain size, surface roughness, porosity, particle size distributions, and material homogeneity can be obtained. The samples utilized directly in the SEM included alumina and MgAl2O4 (spinel), which had been subjected to various heat treatment temperatures.

The primary objective of employing SEM was to investigate the morphology and particle size distributions of both alumina and MgAl2O4 (spinel) samples.

Theory:

Within an SEM, electrons are accelerated to carry significant kinetic energy. Upon interaction with the solid sample, this energy is dissipated, giving rise to a range of signals. These signals encompass secondary electrons (used for SEM imaging), backscattered electrons (BSE), diffracted backscattered electrons (EBSD, employed for determining crystal structures and mineral orientations), photons (characteristic X-rays, utilized for elemental analysis), visible light (cathodoluminescence-CL), and heat.

Of these signals, secondary electrons are particularly valuable for revealing sample morphology and topography, while backscattered electrons excel at illustrating composition contrasts in multiphase samples, aiding in rapid phase discrimination. X-ray generation occurs due to inelastic collisions between incident electrons and electrons within the sample's atomic orbitals. As excited electrons transition back to lower energy states, characteristic X-rays are emitted at fixed wavelengths, corresponding to the energy level differences of electrons in different atomic shells of a given element.

Consequently, each mineral element excited by the electron beam produces characteristic X-rays. Notably, SEM analysis is non-destructive, as X-rays generated during electron interactions do not result in sample volume loss, permitting repeated material analyses.

Key Elements of Every Scanning Electron Microscope (SEM):

Instrument Components:

- Electron Emitter ("Gun")
- Electron Optics System
- Sample Manipulation Stage
- Signal Detection Systems
- Display and Data Output Interfaces
- Necessary Infrastructure:
- Reliable Power Supply
- Vacuum Chamber and Pumping System
- Effective Cooling Mechanism
- Stable, Vibration-Damped Flooring
- Shielded Environment from Magnetic and Electric Interference

References:

1. Barbara Pacewska, M. Keshr and O. Kluk, “Aluminium nitrate as a precursor of mesoporous aluminium oxides”, Journal of Thermal Analysis and Calorimetry, Vol. 74 (2003) 595–603.

Chapter -4

RESULTS AND DISCUSSIONS

4.1 AIM OF CHARACTERISATION:

The present aim of study is to synthesize spinel optimising the molar weight of the precursors as well as obtaining best fuel used in the reaction and also to find out the lower processing temperature used in the reaction. Best fuel / catalyst have been selected for the experiment by selecting various fuels in the reaction and observing their effect in the reaction by changing their concentrations and temperature in the process of making spinel. With the help of best fuel selected, a mixture has been prepared by changing the concentration of magnesium nitrate in the process of making spinel. The synthesis materials are gone through various physical and chemical characterisation techniques like DSC/TGA, XRD, FTIR, SEM, EDAX, micro hardness, bulk density, apparent porosity etc. to identify how the properties could be achieved after low temperature synthesis.

Differential Scanning Calorimetry (DSC) / Thermogravimetric Analysis (TGA):

4.1.1 DSC/TGA Analysis of various compositions:

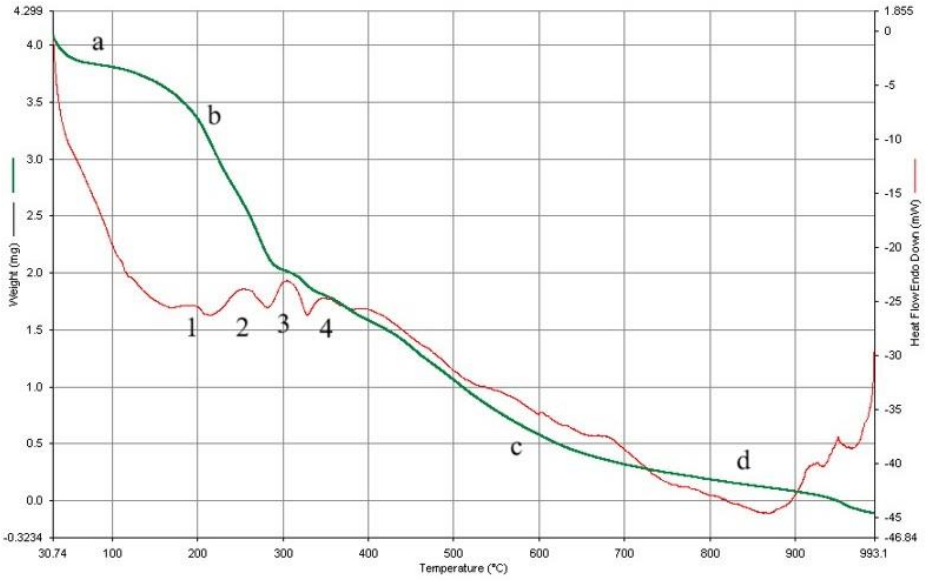

Figure 4.1: DSC/TGA graph of precursors mixtures with fuel: citric acid and heating rate of 10ºC/min

Thermal analysis of precursors material of alumina and MgO has been studied at the heating rate of 10ºC/ min from room temperature to 1000ºC (fig. 4.1) using citric acid as fuel. TG (green colour) plot indicates a steady constant weight loss from room temperature to 1000ºC with three steps. Initial drop of weight is due to removal of moisture and physically held volatile content up to the 150ºC (point a to b). After 150ºC onwards (point b to c) there is a

drastic drop of weight due to dissociation of chemically held moisture content. From 350ºC onwards (point c to d) the change in weight has been observed almost at a constant rate nearly upto the 1000ºC. For DSC plot there are three drops followed by small peaks of curve at 220ºC (point 1), 280ºC (point 2), 340ºC (point 3). All these changes are due to fuel reaction and peaks are indication of initial crystallization. Release of chemically held moisture occurs in these regions. At the range between 600ºC (point 4) to 850ºC and onwards initiation of crystallization of spinel $MgAl_2O_4$ occurs which is indicated by exothermic trends at 900°C. Thus, onset of crystallisation is indicated at about 670°C onwards coupled with exothermic peak.

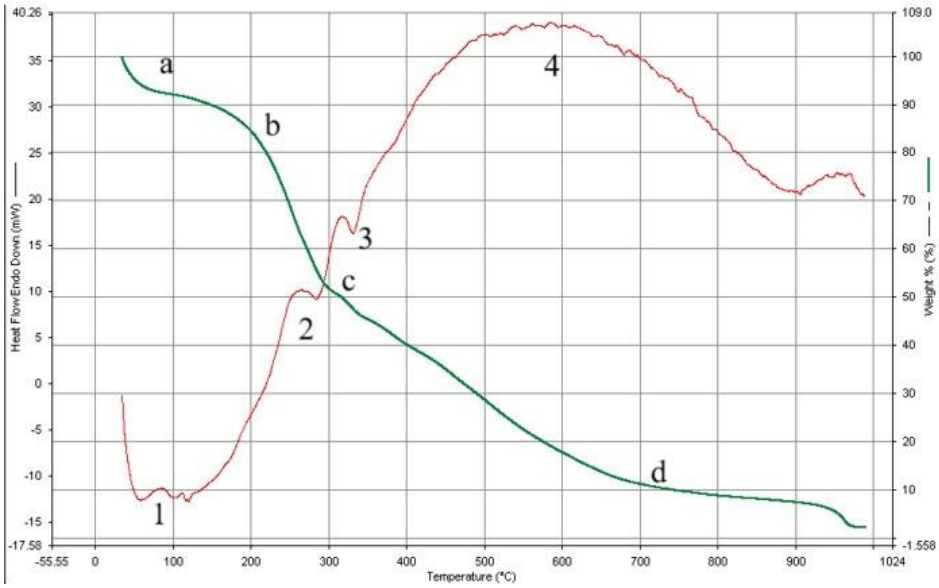

Figure 4.2: DSC/TGA of mixture magnesium nitrate and aluminium nitrate using glycine as a fuel at the heating rate of 10ºC/min

Thermal analysis of gel produced using glycine as a fuel from precursors materials of alumina and MgO has been studied at the heating rate of 10ºC/ min from room temperature to 1000ºC (fig. 4.2). TG (green coloured) for the current plot indicates almost similar loss pattern from room temperature to 1000ºC with three steps. Initial weight loss corresponds to moisture removal, physically held volatile content up to the 150ºC (point a to b) while from 150ºC (point b to c) onwards, drastic drop of weight is due to dissociation of chemically held moisture content with initial combustion reaction. Form 350ºC (c to d) onwards the change in weight has been observed almost at a constant rate nearly till 700^0 C with minor change upto

the temperature 1000ºC. DSC plot indicates rapid endothermic reaction at 100^0C coupled with three inflection point on curve at 280ºC (point 2), 320ºC (point 3), 600ºC (point 4) respectively. All the changes are due to glycine reactions with precursors. Exothermic peak is observed to be about 600°C with hump initiating from 500°C till 800°C corresponding to zone of crystallization for spinel $MgAl_2O_4$. An exothermic peak is also noted at about at 950^0 C indicating full phase formation at higher temperature for shorter duration of soaking while onset of crystallization is about 600/700°C.

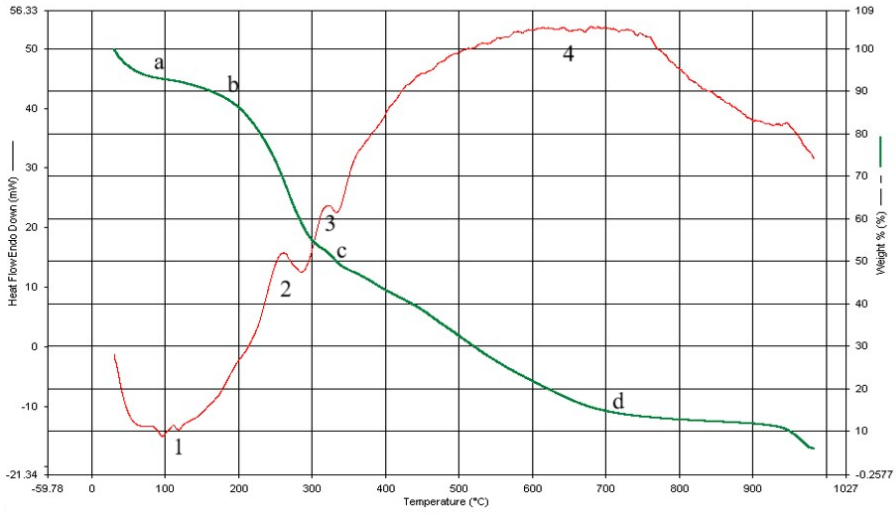

Figure 4.3: DSC/TGA of mixture with magnesium nitrate and aluminium nitrate using thiourea as a fuel at heating rate of 10ºC/min

Figure 4.3 representing DSC/TGA plot of 10 ºC/min using thiourea as fuel with precursors. It shows close similar behaviour with glycine as fuel in comparing with the previous graph. Initial weight change is upto 150°C(point a-b) which is possibly due to loss of water of crystallization along with loss of volatile matter from fuel as noted from DSC analysis. The change in nature of peak is also observed in DSC plot at 280ºC and 340ºC (point 3) due to chemical reaction with fuel. The exothermic nature is observed subsequently due to formation of crystallized phase of alumina at about 600ºC (point 4). Near about 800ºC almost constant weight is observed showing complete spinel formation during solution combustion process. Using thiourea as fuel, onset of crystallization for spinel is noted to be prominent at about 700°C onwards.

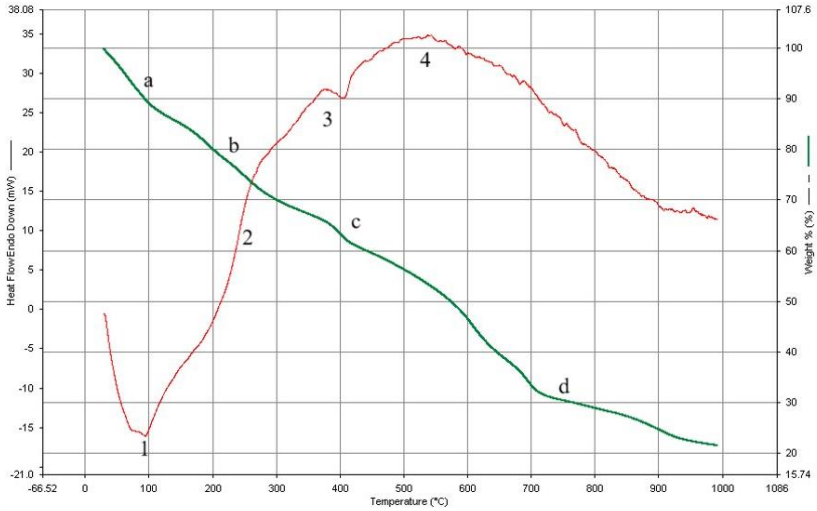

Figure 4.4: DSC/TGA of mixture of magnesium nitrate and aluminium nitrate using urea as a fuel at heating rate of 10ºC/min

Figure 4.4 shows the plot of DSC/TGA of spinel precursors with the heating rate of 10ºC/min using urea as fuel. An endothermic peak is observed initially at upto 100ºC indicating loss of physically held volatile content. From 1-2 region of DSC exothermic reaction happens due to fuel interaction with precursors. Another change in the DSC plot is observed around 400 ºC (point 3) reflecting massive chemical reaction of fuel. The above observation also confirmed from TG curve showing constant steady state weight loss. The crystallisation of spinel formation is observed at around 550 ºC (point 4) in the heating rate of 10ºC/min. The completion of spinelisation is observed at about 950ºC. The onset of crystallization is noted to be about 500°C using urea as fuel.

From these above four graphs it can be observe that citric acid is acting as a best fuel in the reaction. As such, citric acid has been taken as a major fuel for further investigations to assess the structural aspect and other various properties for low temperature spinel formation. This is reflected from low temperature crystallisation formation as discussed from XRD results.

In the next step of the experiments molar concentrations of two precursors have been varied keeping the fuel ratio constant to determine the best suited molar ratio of the precursors.

4.1.2 XRD (X ray Diffraction) Characterization of synthesized materials:

XRD (X ray diffraction) is a non-destructive characterisation process. It gives specific information about the phase formations, structure of crystallite, structural behaviour as well as physical characteristics of materials.

XRD Analysis of non-stoichiometric spinel(Mg precursors: Al precursor = 1:1.75) with Fuel- Citric Acid: Spectra shows the planes corresponding to the peaks which have been indexed with the help of the standard JCPDS(card number: 77-1193) library. The presence of peaks of $MgAl_2O_4$ is the sign of formation of non-stoichiometric spinel at 800ºC (The angle values are specified in degrees). The result gives mixed phase formation of alumina and spinel with good crystallinity. Analysis of data is provided below-

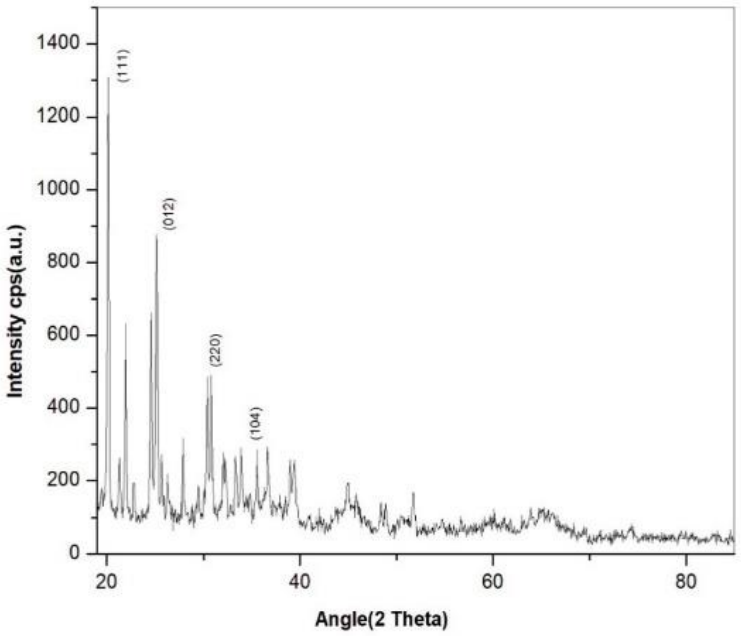

Figure 4.5:XRD plot of non-stoichiometric spinel with Mg precursors: Al precursor = 1:1.75 using Fuel- Citric Acid, Heat Treated at 800ºC

Planes (111), (220), are shown in figure 4.5 as $MgAl_2O_4$ spinel at the 2θ values of 19.80, 30.85 respectively obtained from the above diffractogram. Planes indexed along (012),(104), are noted as Alpha-Al_2O_3 and Gamma-Al_2O_3 powder at the 2θ values of 25.14,34.37 respectively. Crystallite size of spinel powder is measured using Scherrer equation;

$D = \frac{K.\lambda}{\beta.\cos\theta}$, (XRD patterns with Cu Kα radiation) here λ is denoted as wavelength (=0.15406 nm), θ is denoted as Bragg angle, k is denoted as constant (=0.9), and D is denoted as the crystallite size. Two peaks (111) and (220) are taken for measuring the size of crystallites. Average crystallite size is found using Scherrer's equation to be 17.24 nm. Presence of alpha Al_2O_3 and gamma Al_2O_3 is noted in optimum in compare to major spinel phase formation.

XRD analysis of stoichiometric spinel (Mg precursors: Al precursor = 1:2) with Fuel-Citric Acid: Spectra from XRD exhibit the planes corresponding to the peaks which have been indexed with standard JCPDS (card number: 77-1193) library. The presence of $MgAl_2O_4$ peak from spectral analysis as per JCPDS correlates with stoichiometric spinel at 800ºC (The angle values are specified in degrees). Limited minor phase of alumina is observed along with major spinel phase with good crystallinity. Detailed spectra is given below in figure 4.6.

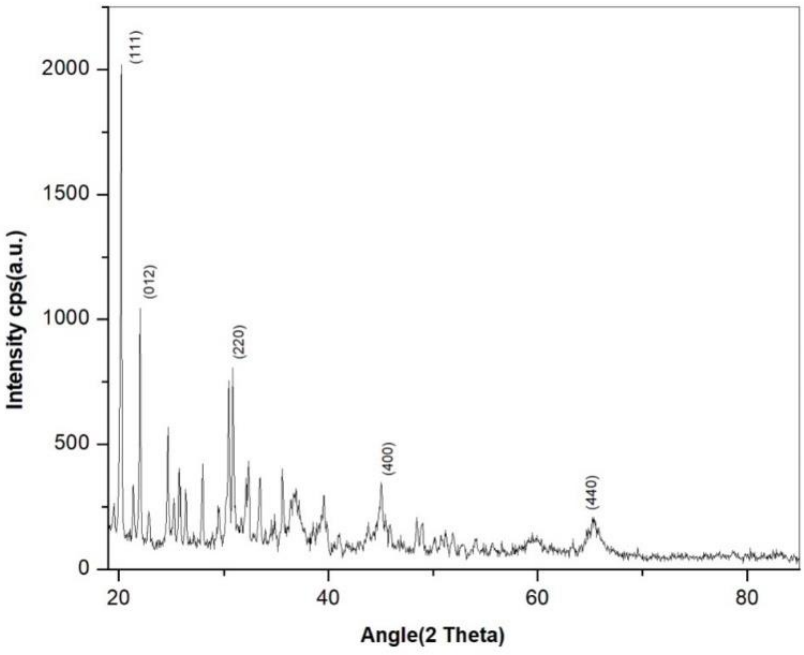

Figure 4.6: XRD Analysis of stoichiometric spinel with Mg precursors: Al precursor = 1:2 using fuel Citric Acid, Heat Treated at 800ºC

Planes indexed along (111), (220), (400), (440) are shown as $MgAl_2O_4$ spinel corresponding to 2θ values of 19.80, 30.62, 44.35, 64.78 respectively obtained from the above diffractogram. Presence of α-alumina, γ powder of Alumina at the 2θ values of 25.14 obtained from the above plot along (012) plane. Experimental parameters for XRD remain the same as reported previous result. The Scherrer equation; $D = \frac{K.\lambda}{\beta.\cos\theta}$, is used for crystallite size calculation which is noted to be about 25.23nm where λ is denoted as wavelength (=0.15406 nm), θ is denoted as Bragg angle, k is denoted as constant (=0.9), and D is denoted as the crystallite size. Four diffraction peaks (111),(220), (400), (440) are taken for measuring the size of spinel crystallites.

XRD Analysis of non-stoichiometric spinel (Mg precursors: Al precursor = 1:2.25) with Fuel- Citric Acid: Similar to the above, spectral analysis shows the indexed planes corresponding to the peaks-with the help of the standard JCPDS(card number: 77-1193) library. XRD spectral analysis indicate-formation of non-stoichiometric spinel at 800ºC (The angle values are specified in degrees) along with alumina phase with good crystallinity. The result is given below in figure 4,7.

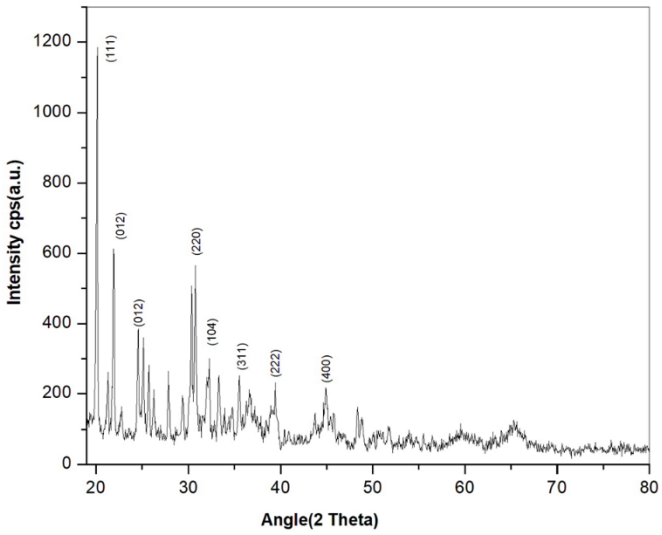

Figure 4.7: XRD Analysis of non-stoichiometric spinel with Mg precursors: Al precursor (1:2.25) using Fuel- Citric Acid, Heat Treated at 800ºC

From the figure 4.7 planes (111), (220), (311), (222), (400) are shown as $MgAl_2O_4$ spinel at the 2θ values of 19.58, 31.62, 36.23, 38.13, 44.35 respectively. Planes (012), (104) are shown as Alpha $Al_2O_3$and Gamma Al_2O_3 powder respectively at the 2θ values of 25.14, 34.37. Crystallite size is estimated using Scherrer's equation to be 28.52nm considering four diffraction planes of (111), (220), (400), (440) only.

XRD Analysis of non-stoichiometric spinel (Mg precursors: Al precursor = 1:1.75) with Fuel- Thiourea: Spectra shows the planes corresponding to these peaks have been indexed with the help of the standard JCPDS (card number: 77-1193) library. Peak spectral position from XRD exhibits non-stoichiometric spinel at 800ºC (The angle values are specified in degrees) along with minor alumina phase. The result is provided below in figure-4.8.

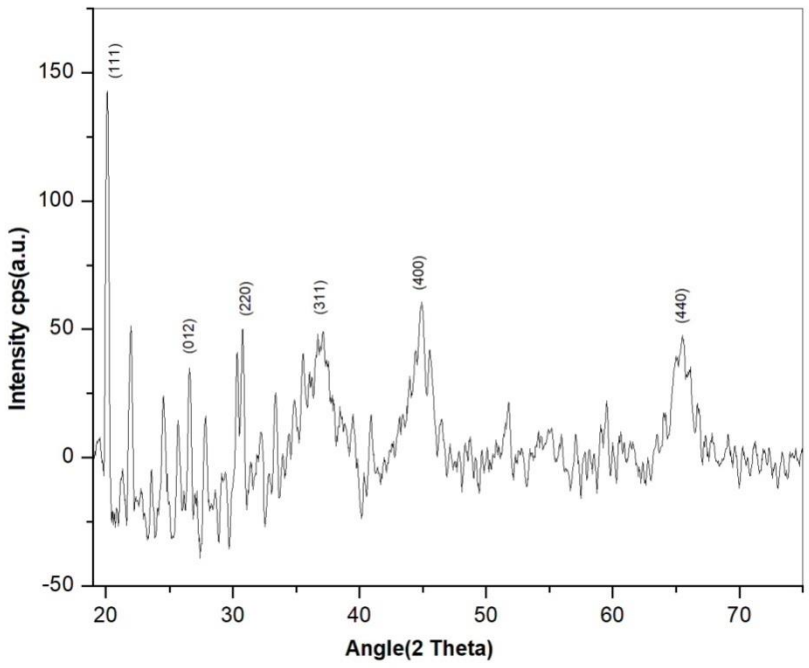

Figure 4.8: XRD Analysis of non-stoichiometric spinel with Mg precursors: Al precursor = 1:2.25 using fuel Thiourea, Heat Treated at 800ºC

Planes (111), (220), (311), (440), (400) are identified as $MgAl_2O_4$ spinel at the 2θ values of 19.48, 31.42, 36.23, 64.78, 44.76 respectively obtained from the above result. Planes (012), is shown as Alpha alumina powder at the 2θ values of 25.43 is obtained from the above graph.

. Crystallite size of spinel powder was measured using Scherrer equation; $D = \frac{K.\lambda}{\beta.\cos\theta}$, here λ is denoted as wavelength (=0.15406 nm), θ is denoted as Bragg angle, k is denoted as constant (=0.9), and D is denoted as the crystallite size. Four diffraction peaks at (111),(220), (311), (400), (440) planes were taken for measuring the size of crystallites. Average crystallite size is found from the Scherrer equation is 56.23 nm.

XRD Analysis of stoichiometric spinel (Mg precursors: Al precursor = 1:2) with Fuel-Thiourea: Spectra shows the planes corresponding to these peaks have been indexed with the help of the standard JCPDS (card number: 77-1193) library. The presence of peaks of $MgAl_2O_4$ aligns it with the formation of stoichiometric spinel at 800ºC (The angle values are specified in degrees). The result yields in major spinel phase with average crystallinity. A detail spectrum is shown in figure-4.9.

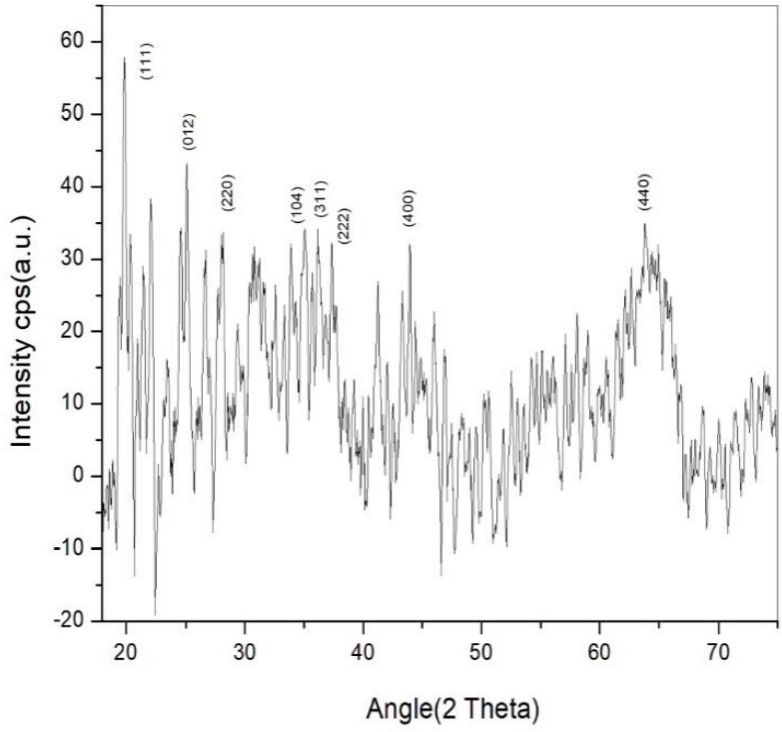

Figure 4.9: XRD Analysis of stoichiometric spinel with Mg precursors: Al precursor = 1:2 using Fuel Thiourea, Heat Treated at 800ºC

From the JCPDS data the Planes (111), (220), (311), (222) (400), (440) are identified as $MgAl_2O_4$ spinel at the 2θ values of 19.56, 31.69, 36.47, 38.13, 44.43, 64.78 respectively. The Planes at (012), (104) are of Alpha and Gamma powder at the 2θ values of 25.14, 34.37 obtained from the above graph. Crystallite size is estimated to be about 45.73nm using Scherrer's equation.

XRD Analysis of non-stoichiometric spinel (Mg precursors: Al precursor = 1:2.25) with Fuel- Thiourea: Spectra in the figure 4.10 shows the planes corresponding to the $MgAl_2O_4$, alpha and gamma powder (Al_2O_3). The peaks have been indexed with the help of the standard JCPDS (card number: 77-1193) library. The presence of peaks of $MgAl_2O_4$ is the sign of formation of non-stoichiometric spinel at 800ºC (The angle values are specified in degrees). The result gives mixed phase formation of alumina and spinel with average crystallinity. The analysis of results are given below-

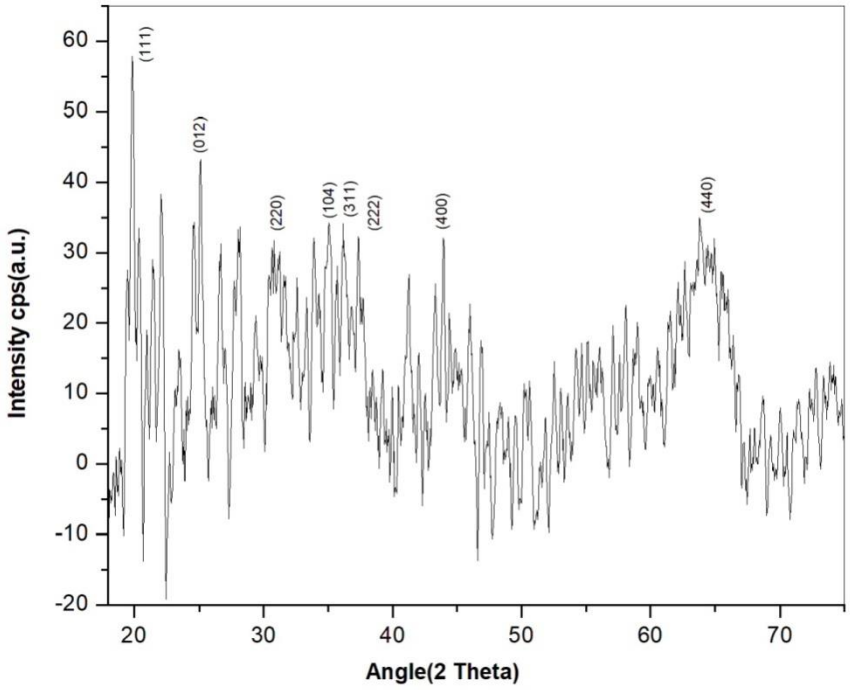

Figure 4.10: XRD Analysis of non-stoichiometric spinel with Magnesium Nitrate: Aluminium Nitrate = 1:2.25 using Fuel Thiourea, Heat Treated at 800ºC

The diffractogram indicate peaks at planes (111), (220), (311), (222) (400), (440) which indexed to be $MgAl_2O_4$ spinel at the 2θ values of 19.45, 31.57, 36.23, 38.53, 44.35, 64.78 respectively. Further, Planes(012), (104) exhibits Alpha and Gamma powder at the 2θ values of 25.35, 34.54 respectively with average crystallite size using Scherrer's equation to be 67.85nm.

XRD Analysis of non-stoichiometric spinel (Magnesium Nitrate: Aluminium = 1:1.75) with Fuel- Urea: Spectra in the graph given below shows the planes corresponding to the $MgAl_2O_4$ and alpha and gamma powder (Al_2O_3). The peaks have been indexed with the help of the standard JCPDS (card number: 77-1193) library. The presence of $MgAl_2O_4$ is the sign of formation of non-stoichiometric spinel at 800ºC (The angle values are specified in degrees). The result gives mixed phase formation of alumina and spinel with average crystallinity. The analysis report is given below in figure-4.11.

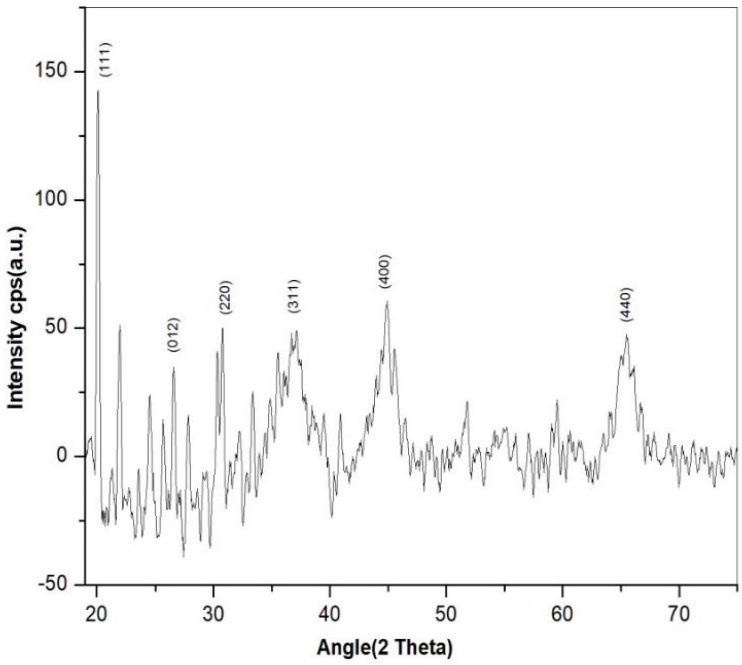

Figure 4.11: XRD Analysis of non-stoichiometric spinel with Magnesium Nitrate: Aluminium Nitrate = 1:1.75 using Fuel Urea, Heat Treated at 800ºC

From the JCPDS data $MgAl_2O_4$ spinel formation identified at the 2θ values of 19.986, 31.79, 36.87, 44.58, 64.92 respectively obtained from the planes (111), (220), (311), (400) and (440). Alpha phase powder at the 2θ values of 25.73 is indexed along plane (012) while average crystallite size is estimated to be 71.35nm using Scherrer's equation.

XRD Analysis of stoichiometric spinel (Magnesium Nitrate: Aluminium Nitrate = 1:2) with Fuel- Urea: Spectra in the graph given in figure 4.12 shows the planes corresponding to the $MgAl_2O_4$ spinalization, alpha and gamma powder of Al_2O_3. The peaks have been indexed with the help of the standard JCPDS (card number: 77-1193) library. The presence of peaks of $MgAl_2O_4$ is the signature for stoichiometric spinel at 800ºC (The angle values are specified in degrees). The result gives majorly spinel phase with average crystallinity. Detailed analysis is provided in diffractogram below-

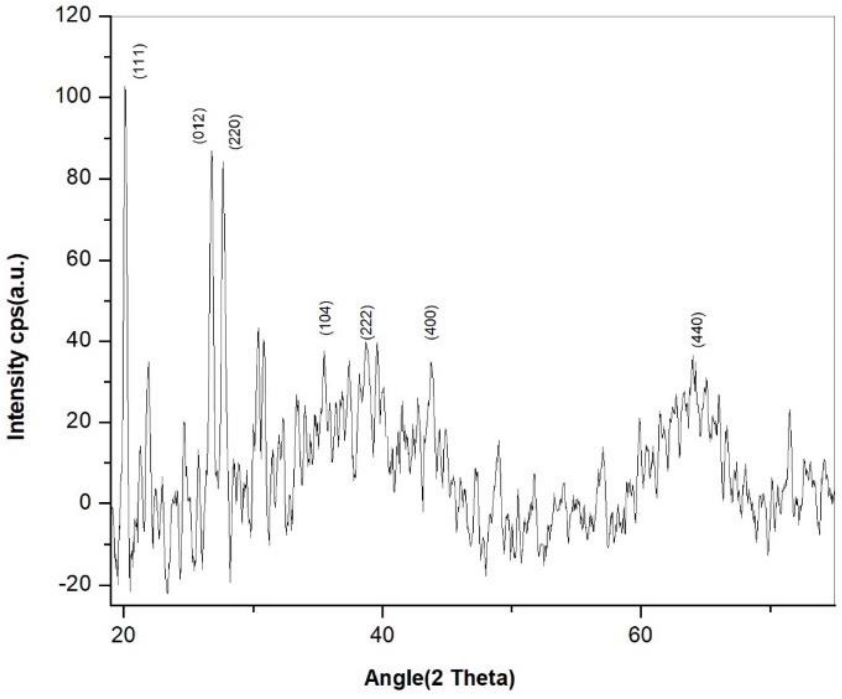

Figure 4.12: XRD plot of stoichiometric spinel with Magnesium Nitrate: Aluminium Nitrate = 1:2 using Fuel Urea, Heat Treated at 800ºC

As per previous trends the major indexed planes (111), (220), (222), (400), (440) of $MgAl_2O_4$ spinel formation at the 2θ values of 19.36, 31.37, 38.25, 44.93, 64.63 is noted. Planes (012), (104) are shown as Alpha and Gamma powder at the 2θ values of 25.84, 34.98 are obtained. The size of spinel powder is measured using Scherrer equation; $D = \frac{K.\lambda}{\beta.\cos\theta}$, here λ is denoted as wavelength (=0.15406 nm), θ is denoted as Bragg angle, k is denoted as constant (=0.9), and D is denoted as the crystallite size. Five diffraction peaks (111), (220), (222), (400), (440) were taken for measuring the size of crystallites. Average crystallite size is 77.95nm using the Scherrer's equation.

XRD Analysis of non-stoichiometric spinel (MagnesiumNitrate: Aluminium Nitrate = 1:2.25) with Fuel- Urea: XRD Spectra in figure 4.13 gives the planes corresponding to the $MgAl_2O_4$ along with minor alpha and gamma powder of Al_2O_3 formation. The peaks have been indexed with the help of the standard JCPDS (card number: 77-1193) library. Detailed analysis is given below-

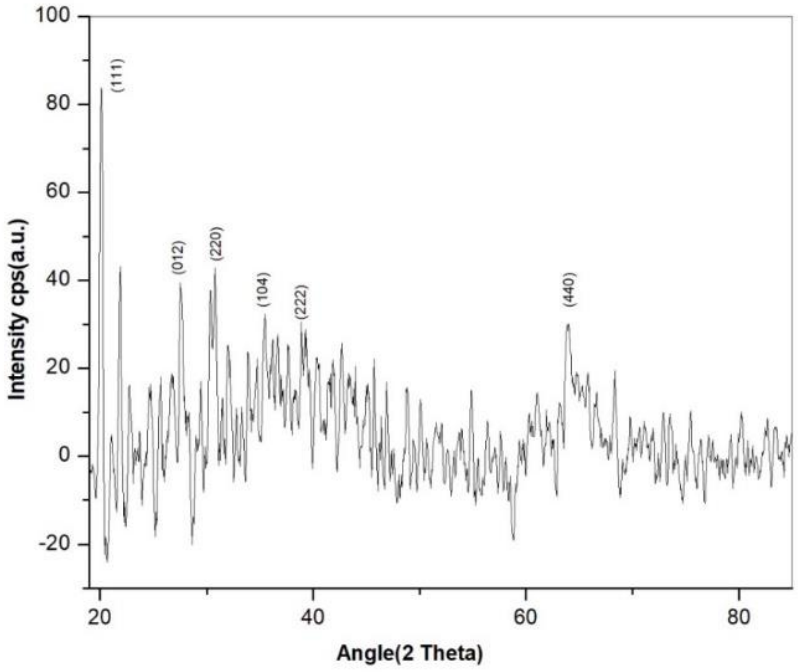

Figure 4.13: XRD Analysis of non-stoichiometric spinel with Magnesium Nitrate: Aluminium Nitrate = 1:2.25 using Fuel Urea, Heat Treated at 800°C

The analytical tool used for phase identification is standard JCPDS data sheet. The Planes at (111),(220), (222), (440) are recorded as $MgAl_2O_4$ spinel at the 2θ values of 19.99, 31.736, 38.92, 64.13 respectively obtained from the standard data. Planes (012), (104) is predicted as Alpha and Gamma powder of alumina at the 2θ values of 25.72, 34.81are obtained from the standard value. XRD patterns were recorded by an advance Bruker D8 diffractometer (with radiation of Cu Ka). The average Crystallite size of spinel powder is measured using Scherrer equation; $D = \frac{K.\lambda}{\beta.\cos\theta}$, here λ is denoted as wavelength (=0.15406 nm), θ is denoted as Bragg angle, k is denoted as constant (=0.9), and D is denoted as the crystallite size taking four diffraction peaks along (111), (220), (222), (440) planes. Average crystallite size obtained is 73.31 nm.

XRD Analysis of non-stoichiometric spinel (MagnesiumNitrate: Aluminium Nitrate = 1:1.75) with Fuel- Glycine: XRD Spectra in the figure 4.14 has given below shows the planes corresponding to the $MgAl_2O_4$ and alpha and gamma Al_2O_3 powder. The peaks have been indexed with the help of the standard JCPDS (card number: 77-1193) library. The presence of peaks of $MgAl_2O_4$ is noted at 800ºC (The angle values are specified in degrees) along with alumina phase, both yielding average crystallinity.

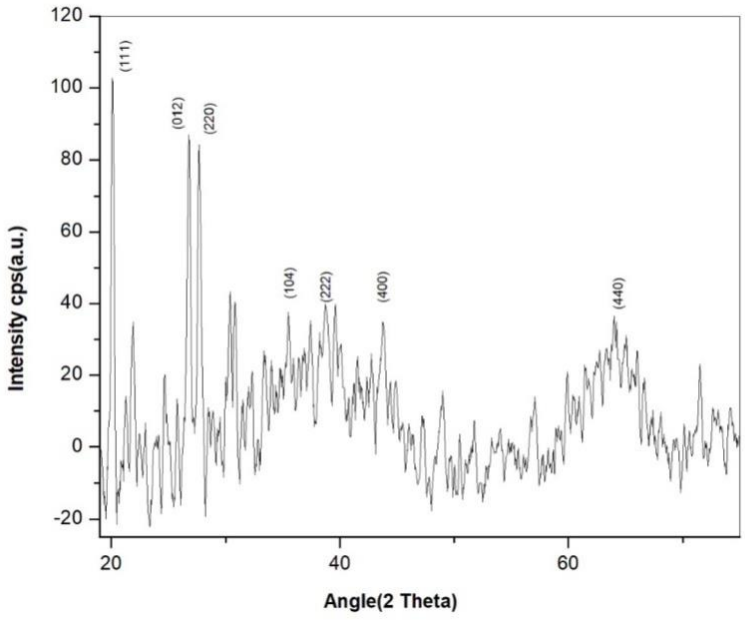

Figure 4.14: XRD Analysis of non-stoichiometric spinel with Magnesium Nitrate: Aluminium Nitrate = 1:1.75 using Fuel Glycine, Heat Treated at 800ºC

In the above diffractogram, planes (111), (220), (222), (400), (440) have been identified as $MgAl_2O_4$ spinel at the 2θ values of 19.87, 31.84, 38.91, 44.91, 64.17 respectively. Planes (012), (104) correspond to alpha, gamma phase of alumina powder at the 2θ values of 25.91 and 34.86 respectively. XRD patterns are recorded by an advance Bruker D8 diffractometer (with radiation of Cu Ka), while crystallite size of spinel powder is measured using Scherrer's equation; $D = \frac{K.\lambda}{\beta.\cos\theta}$ where λ is wavelength (0.15406 nm), θ is Bragg angle, k is constant (0.9), and D is the crystallite size. Average crystallite size is found using the Scherrer's equation to be 91.57 nm from five diffraction planes.

XRD Analysis of stoichiometric spinel (Magnesium Nitrate: Aluminium Nitrate = 1:2) with Fuel- Glycine: The result of figure 4.15 shows the planes corresponding to the $MgAl_2O_4$ spinel formation The peaks have been indexed with the help of the standard JCPDS (card number: 77-1193) library after annealing at 800ºC (The angle values are specified in degrees). The result yield major spinel phase with average crystallinity. Detailed analysis is provided below-

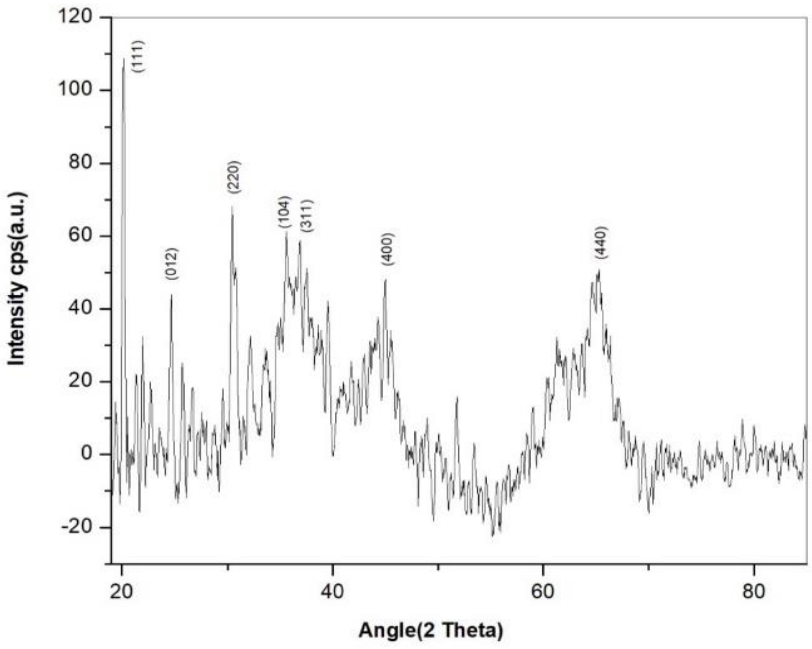

Figure 4.15: XRD Analysis of stoichiometric spinel with Magnesium Nitrate: Aluminium Nitrate = 1:2 using Fuel Glycine, Heat Treated at 800ºC

In this diffractogram major phase is spinel, corresponding to indexed matching planes of (111),(220), (311), (400), (440) at the 2θ values of 19.74, 31.72, 36.87, 44.35, 64.78 respectively. Four diffraction peaks (111), (220), (311), (400), are taken for measuring the size of crystallites which yields average crystallite size to be 89.73 nm.

XRD Analysis of non-stoichiometric spinel (Magnesium Nitrate: Aluminium Nitrate = 1:2.25) with Fuel- Glycine: In the figure 4.16 major studies is to identify crystalline behavior of various oxides. Spectra in the graph exhibits the planes obtained as peaks corresponding to the $MgAl_2O_4$ spinel, minor alpha and gamma phase of Al_2O_3. The peaks have been indexed with the help of the standard JCPDS (card number: 77-1193) library. The presence of peaks of $MgAl_2O_4$ is the sign of formation of non-stoichiometric spinel at 800ºC.

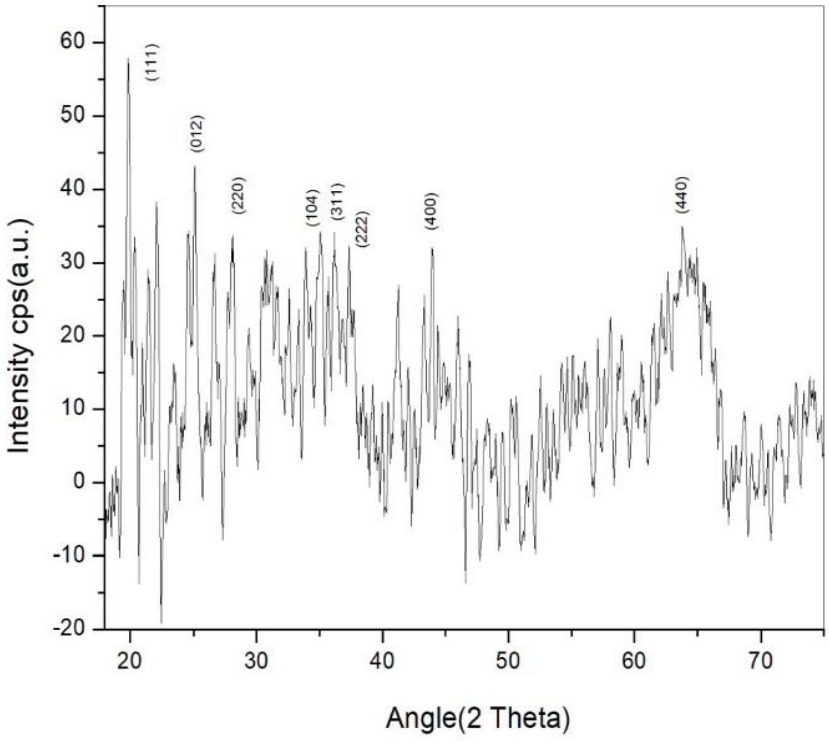

Figure 4.16: XRD Analysis of non-stoichiometric spinel with Magnesium Nitrate: Aluminium Nitrate = 1:2.25 using Fuel Glycine, Heat Treated at 800ºC

The fuel combustion process generates sufficient energy for the formation of crystalline oxides phase. It is found that planes (111),(220), (311), (222), (400), (440) are matching with $MgAl_2O_4$ spinel at the 2θ values of 19.86, 31.83, 36.14, 44.11, 64.71 respectively obtained by comparing with JCPDS standard data. Planes (012), (104) are indexed as Alpha and Gamma alumina powder at the 2θ values of 25.99, 34.59 respectively. Six diffraction peaks (111), (220), (311), (222), (400), (440) are taken for measuring the average crystallite size using Scherrer's equation to be 97.12 nm.

From the above studies of X ray Diffraction, it is observed that citric acid has produced lower range of crystallite size and formation temperature compare to use of other fuels heat treating at 800^0 C. By lowering the spinelization temperature range there is a possibility to obtain crystallite size in nano domain. All the fuels are able to form spinel as observed from the above studies. The citric acid as fuel, reducing agent is responsible for lower crystallite size with spinel phase in comparison to other fuels.

4.1.3 FTIR Spectroscopy Analysis of Different spinel alumina synthesized materials: FTIR spectra are used for assessing chemical bonding of samples along with identification of functional groups. It is an infrared absorption of spectra with interaction of molecules of synthesized materials.

Property evaluation by FTIR Analysis of non-stoichiometric as well as stoichiometric spinel (Synthesis Temperature 800ºC) with Fuel- Citric Acid:

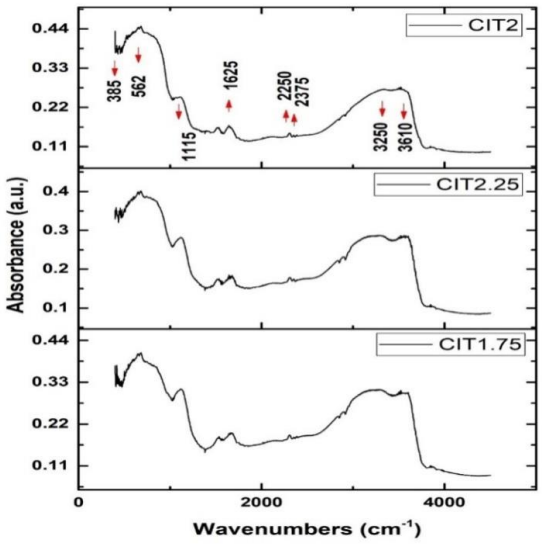

Figure 4.17: FTIR spectra of non-stoichiometric as well as stoichiometric spinel synthesized at Temperature 800ºC with Fuel Citric Acid

The infrared spectra of figure 4.17 of synthesized material of stoichometric, non-stoichometric oxides have been assessed for the bonding nature using citric acid as fuel. $MgAl_2O_4$ spinel, alpha and gamma powders of alumina is formed using Magnesium Nitrate, Aluminium Nitrate at different mole ratio followed by annealing at 800ºC. Mole ratio of 1:2 is the stoichiometric ratio for sample, which exhibits Al-O stretching bond vibration at 562 cm^{-1}, Al-Mg-O stretching bond at about 1115cm^{-1}, along with Mg-O stretching bond vibration at 385cm^{-1}. Carbonaceous based material is present in the precursor powder which can be noted at wavenumber of 1625 cm^{-1} corresponding to stretched bond vibration of carboxylate ions. Low and weak spectra at 2250 cm^{-1} is associated with N=C=O isocyanate stretching bond vibration, 2375 cm^{-1} shows O-H stretching bond, 3250 cm^{-1} H_2O stretching bond is noted while wavenumber 3610 cm^{-1} is associated with the OH anti symmetric stretching vibration in $Mg(OH)_2$. The wavenumbers corresponding to the carboxylate and nitrate ions, evaporates with increasing heating temperature of the mixture gel. **[1]**Very small deflection in the peak of the graphs for mole ratio 1:1.75 and 2.25 has been observed. These two ratios correspond to non-stoichiometric one. Annealing of non-stoichiometric ratios is also observed to exhibit Al-O bond vibration as well as Mg-Al-O bond vibrations. The present experimental findings make it clear regarding presence of $MgAl_2O_4$ spinel generated from non-stoichiometric ratio of precursors.

FTIR Analysis of non-stoichiometric as well as stoichiometric spinel (Synthesis Temperature 800ºC) with Fuel- Urea:

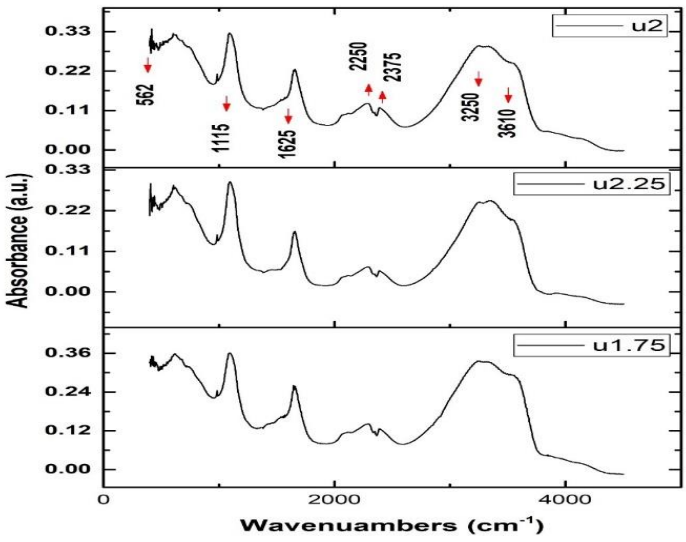

Figure 4.18: FTIR spectra of non-stoichiometric as well as stoichiometric spinel synthesized at Temperature 800ºC with Fuel Urea

Figure 4.18 reveals the IR spectra of $MgAl_2O_4$ spinel, alpha and gamma powders obtained after annealing at 800ºC using different mole ratio of Magnesium Nitrate: Aluminium Nitrate with Urea as fuel. Stoichometric spinel exhibits Al-O stretching bond vibration at 562 cm^{-1}, Al-Mg-O stretching bond vibration at 1115 cm^{-1}, stretching bond vibration of carboxylate ions at wave number 1625 cm^{-1}. At 2250 cm^{-1} Prominent stretching bond vibration of N=C=O isocyanate at 2250cm^{-1} is noted in compare to citric acid as fuel/reducing agent along with O-H stretching bond at 2375 cm^{-1}. H_2O stretching bond at 3250cm^{-1} along with OH anti symmetric stretching vibration in $Mg(OH)_2$ at c3610 cm^{-1}. Similar to the previous case, evaporation with temperature leads to suppression of carboxylate, nitrate ions in the gel mixture. [1] Non-stoichometric mole ratio of 1:1.75, 1:2.25 yields in small deflection of IR spectra while the annealing of such sample indicates presence of Al-O bond vibration as well as Mg-Al-O bond vibrations.

FTIR Analysis of non-stoichiometric as well as stoichiometric spinel (Synthesis Temperature 800ºC) with Fuel- Thiourea:

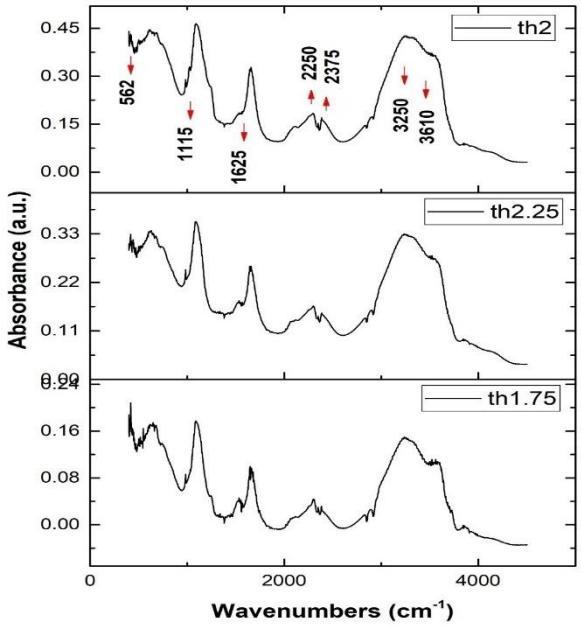

Figure 4.19: FTIR spectra of non-stoichiometric as well as stoichiometric spinel synthesized at Temperature 800ºC with Fuel Thiourea

The above figure depicts IR spectra of $MgAl_2O_4$ spinel, alpha and gamma alumina powders after annealing at 800ºC using thiourea as fuel. Mole ratio of 1:2 depicts stoichiometric ratio

which shows Al-O stretching bond vibration at 562 cm^{-1}, 1115 cm^{-1} indicates Al-Mg-O stretching bond vibration, 1625cm^{-1} corresponds to stretching bond vibration of carboxylate ions. N=C=O isocyanate bond vibration stretching is noted at about 2250cm^{-1}. The presence of wave number at 2375cm^{-1} shows O-H stretching bond, 3250 cm^{-1} corresponds to H_2O stretching bond while the wavenumber at 3610 cm^{-1} is associated with the OH anti symmetric stretching vibration in Mg(OH)2. Minor deflection in the peak behaviour has been observed for mole ratio 1:1.75 and 2.25. These two ratios are corresponding to non-stoichiometric ratio. After calcination of non-stoichiometric ratios of compound is also noticed presence of Al-O bond vibration as well as Mg-Al-O bond vibrations.

FTIR Analysis of non-stoichiometric as well as stoichiometric spinel (Synthesis Temperature 800ºC) with Fuel- Glycine:

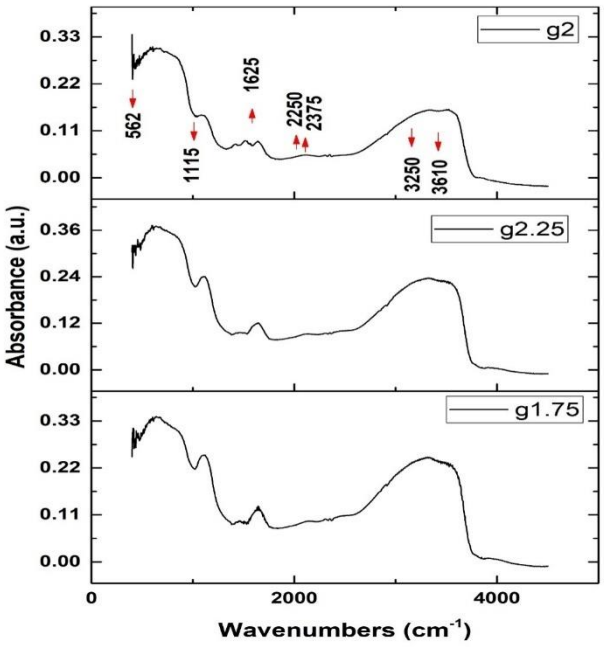

Figure 4.20: FTIR spectra of non-stoichiometric as well as stoichiometric spinel Synthesis at Temperature 800ºC with Fuel- Glycine

The Infrared spectra of $MgAl_2O_4$ spinel, alpha and gamma alumina powders at different mole ratio (Magnesium Nitrate: Aluminium Nitrate) annealed at 800^0C are shown in above figure 4.20. Mole ratio 1:2 is stoichiometric ratio which shows Al-O stretching bond vibration at 562 cm^{-1}. At 1115 cm^{-1} Al-Mg-O stretching bond vibration is present. Carbonaceous material is also present in the synthesized material which can be seen at wavenumber 1625 cm^{-1}which

is a stretching bond vibration of carboxylate ions. However, vibration at 2250 cm^{-1} is associated with N=C=O isocyanate stretching bond vibration and at 2375 cm^{-1} shows O-H stretching bond is absent in IR spectra. At 3250 cm^{-1} H_2O stretching bond can be formed with lower absorption peak compare to other fuel. Wavenumber 3610 cm-1 is associated with the OH anti symmetric stretching vibration in Mg(OH)2. Minor change of the peak in the graphs for mole ratio 1:1.75 and 2.25 has been observed. These two ratios are corresponding to non-stoichiometric ratio. After calcinations treatment of non-stoichiometric ratios presence of Al-O bond vibration as well as Mg-Al-O bond vibrations noticed. The above FTIR results indicate functional groups present in the synthesized spinel with various ratios of precursors and fuel. The variations of chemical bonding are observed with change in fuel. Some additional peaks are observed showing impurity association. This can be removed by prolong heat treatment.

4.1.4 Micro-structural studies by SEM of synthesized Alumina & Spinel:

SEM (Scanning Electron Microscope) Analysis of stoichiometric as well as non-stoichiometric spinel studied with various molar ratio synthesis at temperature 800ºC using Fuel- Citric Acid:

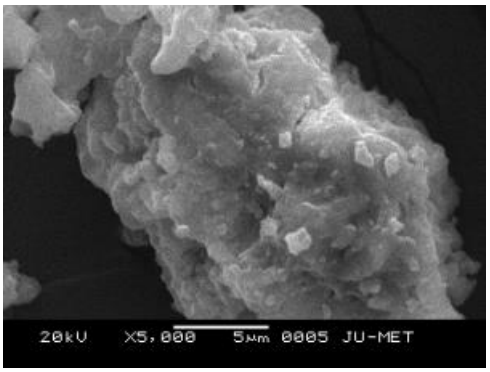

Figure 4.21: SEM image of non-stoichoimetric spinel; Mole ratio (Magnesium Nitrate: Aluminium Nitrate)Ratio= (1:1.75); Fuel- Citric

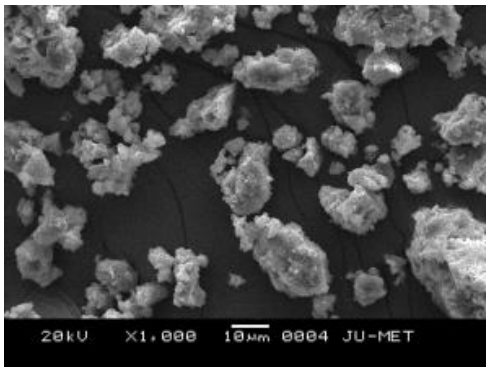

Figure 4.22: SEM image of stoichiometric spinel; Mole ratio (Magnesium Nitrate: Aluminium Nitrate)Ratio= (1:2); Fuel- Citric

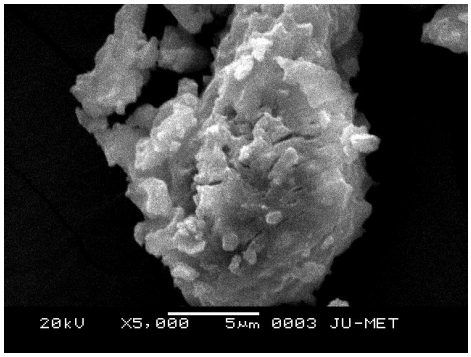

Figure 4.23: SEM image of non-stoichiometric spinel; Mole ratio (Magnesium Nitrate: Aluminium Nitrate)Ratio= (1:2.25); Fuel- Citric Acid

The figure 4.21 shows a strong spinalisation with cubic phase dispersed over the matrix. The cubic phase is fine crystalline structure particle while cloudy mass has shown of agglomeration of particles. Figure 4.22 shows strong agglomeration tendency and particles are interlocked. The particle size has shown large size due to this strong conglomeration tendency. The cubic structure formation is predominant under these experimental studies with increasing tendency of grain size. From figure 4.23 it has been observed the very fine cubic structure dispersed in the matrix. Layered cloudy mass formation enhances with larger particle size.

SEM (Scanning Electron Microscope) Analysis of non-stoichiometric as well as stoichiometric spinel (Synthesis Temperature 800ºC) with Fuel- Thiourea:

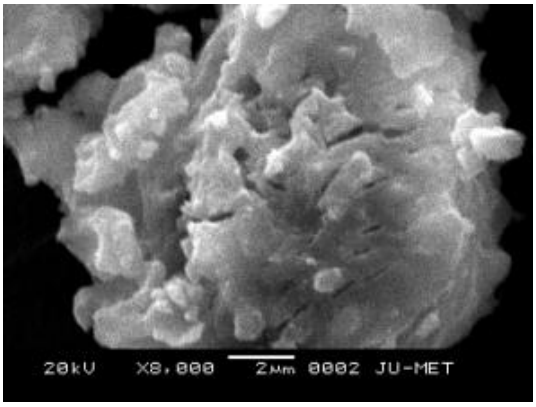

Figure 4.24: SEM image of non-stoichiometric spinel; Mole ratio (Magnesium Nitrate: Aluminium Nitrate)Ratio= (1:1.75) with Fuel- Thiourea

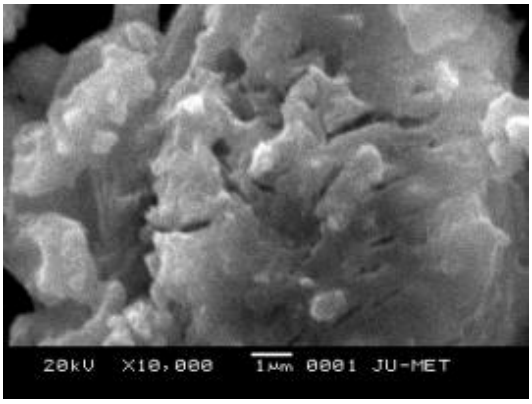

Figure 4.25: SEM image of stoichiometric spinel; Mole ratio (Magnesium Nitrate: Aluminium Nitrate)Ratio= (1:2) with Fuel-Thiourea

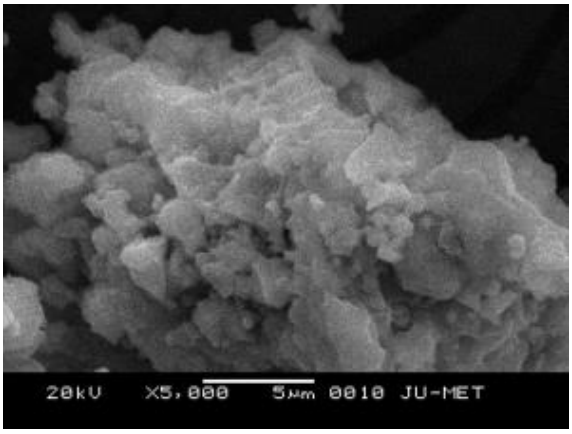

Figure 4.26: SEM image of non-stoichiometric spinel; Mole ratio (Magnesium Nitrate: Aluminium Nitrate)Ratio= (1:2.25) with Fuel-Thiourea

Figure 4.24 shows a clear agglomerated mass is observed under this experimental condition. Fine cubic crystalline phase dispersed over the matrix. The growth of particle observed in all direction. From figure 4.25 more floppy layered formation of spinel is observed. Slight flaky structure is noted. Small particulates are noted to have spherical, polygonal shape which is dispersed uniformly over the materials. On few locations preferential growth of particle is observed. Figure 4.26 shows more crystalline flaky structure is noted in agglomerated mass. Flaky mass formation is more compare to earlier micrographs. Interlocking of particles has been clearly visible showing showing strong crystalline behaviour.

SEM (Scanning Electron Microscope) Analysis of non-stoichiometric as well as stoichiometric spinel (Synthesis Temperature 800ºC) with Fuel- Urea:

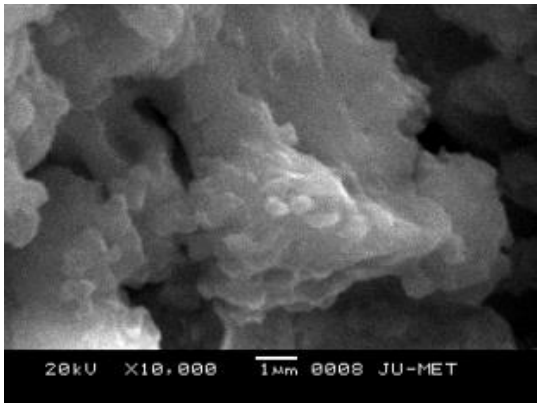

Figure 4.27: SEM image of non-stoichiometric spinel; Mole ratio (Magnesium Nitrate: Aluminium Nitrate)Ratio= (1:1.75 with); Fuel- Urea

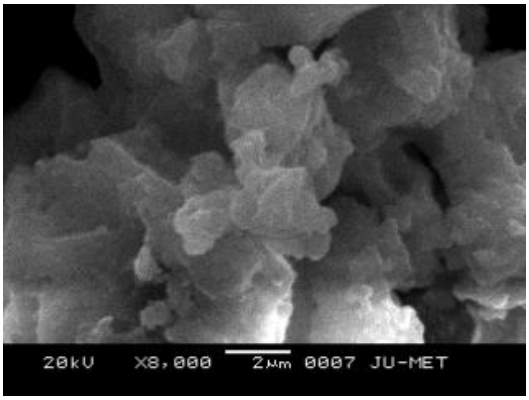

Figure4.28: SEM image of stoichiometric spinel; Mole ratio (Magnesium Nitrate: Aluminium Nitrate)Ratio= (1:2) with; Fuel- Urea

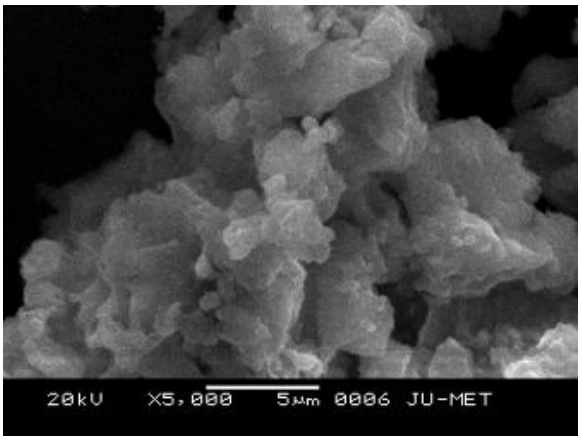

Figure4.29: SEM image of non-stoichiometric spinel; Mole ratio (Magnesium Nitrate: Aluminium Nitrate)Ratio= (1:2.25) with Fuel- Urea

In figure 4.27 layered structure is prominent over the agglomerated product. Fine particles are found to dispersed uniformly over the matrix. In figure 4.28 more flaky layered structure is formed. Overall uniform dispersions have been noticed. No secondary phase is noticeable. In figure 4.29 series of agglomerated particles are observed. Particle size has increased compare to other condition. Flaky structure with some steps is noted in some portion of the matrix. Particles are found in overlap condition.

SEM (Scanning Electron Microscope) Analysis of non-stoichiometric as well as stoichiometric spinel (Synthesis Temperature 800ºC) with Fuel- Glycine:

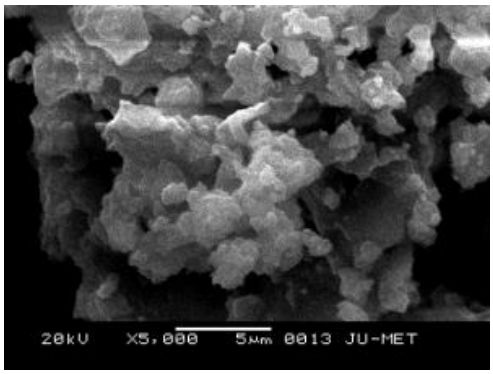

Figure 4.30: SEM image of non-stoichiometric spinel; Mole ratio (Magnesium Nitrate: Aluminium Nitrate)Ratio= (1:1.75) with Fuel- Glycine

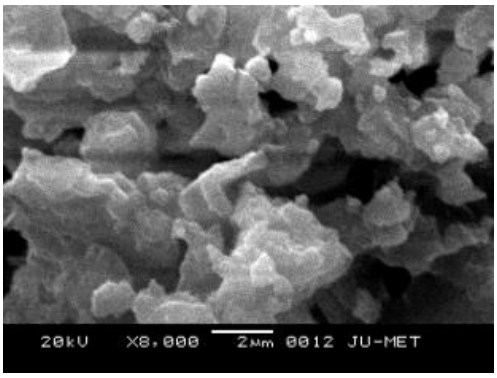

Figure 4.31: SEM image of stoichiometric spinel; Mole ratio (Magnesium Nitrate: Aluminium Nitrate)Ratio= (1:2)with Fuel- Glycine

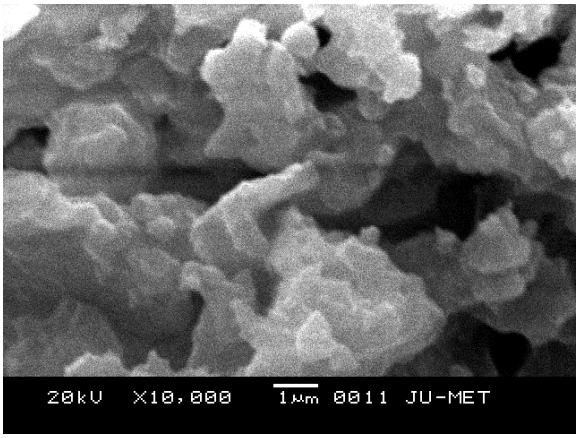

Figure 4.32: SEM image of non-stoichiometric spinel; Mole ratio (Magnesium Nitrate: Aluminium Nitrate)Ratio= (1:2.25)with Fuel- Glycine

From figure 4.30 we can say that micrograph shows agglomerated particles in various shape and size. Cubic structure is prominent. Figure 4.31 shows irregular shape agglomerates are

formed. The particles are of various size and shape. Figure 4.32 displays larger agglomerated particles are formed. Irregular shape and size are observed.

Studies on scanning electron microscope revealed micro-structural behavior of spinel and alumina. Strong agglomeration tendency is prominent from above micrograph. Cubic crystalline phase is noted to be dispersed in the matrix.

HRTEM (High Resolution Transmission Electron Microscopy) Analysis of stoichiometric spinel, heat treated at 800°C with Fuel- Citric Acid:

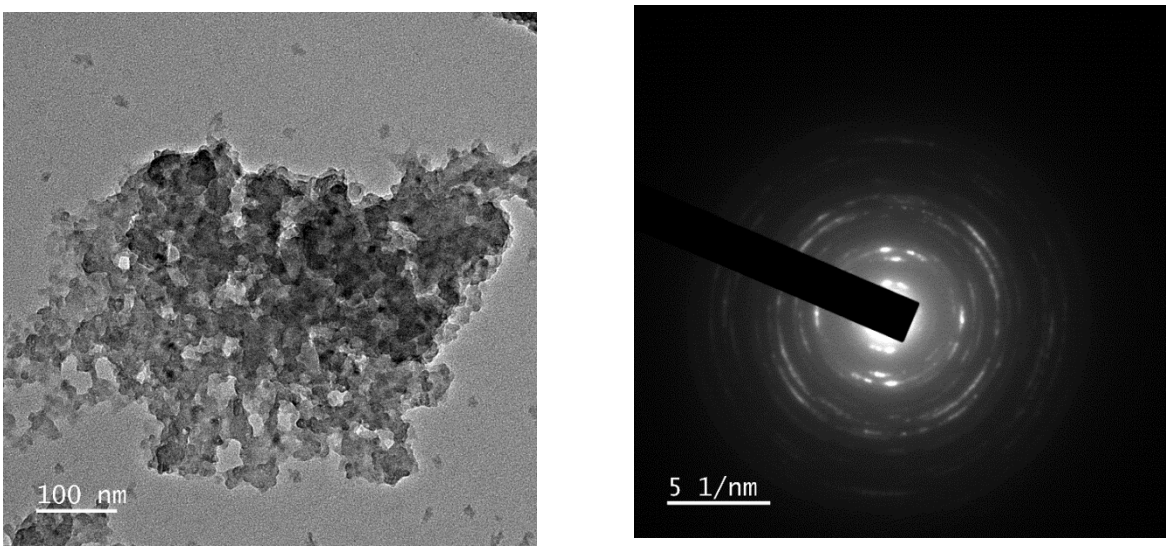

Figure 4.33 :HRTEM image of stoichiometric spinel; Mole ratio (Magnesium Nitrate : Aluminium Nitrate) = (1:2); Fuel- Citric Acid

The powder sample, heat-treated at 800°C, was analysed using High-Resolution Transmission Electron Microscopy figure 4.33 (HRTEM) confirm the formation of the nanostructure. As shown in the figure, the crystallites display a plate-like morphology with poorly defined edges. Due to the overlapping of the platelets, individual observation of each platelet was not feasible. Notably, clear growth of the nanocrystallite was observed following the annealing process at 800°C due to annular ring at SAED pattern, indicating the successful development of the nanostructure.

HRTEM (High Resolution Transmission Electron Microscopy) Analysis of stoichiometric spinel, heat treated at 800°C with **Fuel- Thiourea:**

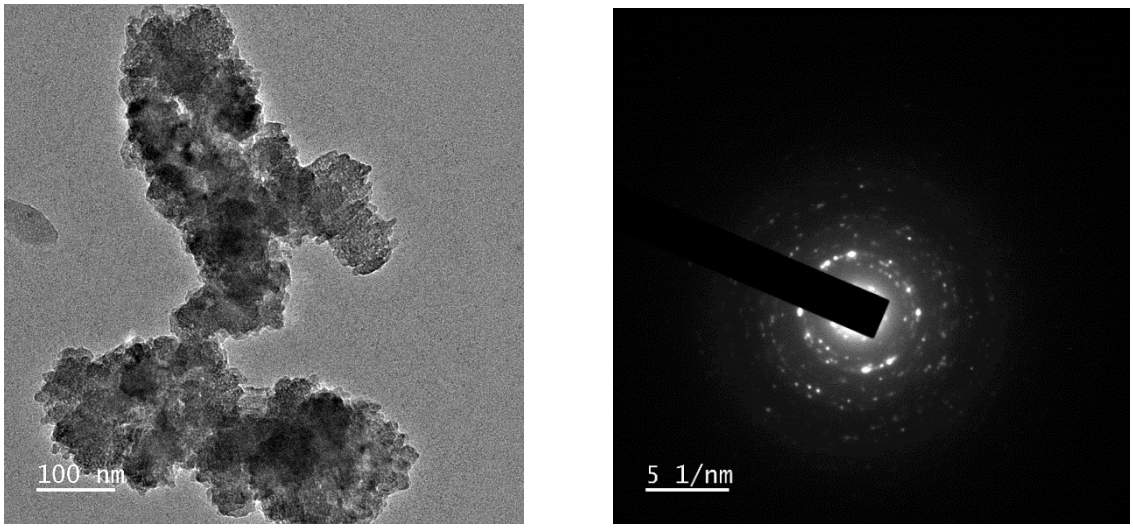

Figure 4.34: HRTEM image of stoichiometric spinel; Mole ratio (Magnesium Nitrate : Aluminium Nitrate) = (1:2) with Fuel- Thiourea

The powder sample, heat-treated at 800°C, was examined using High-Resolution Transmission Electron Microscopy (HRTEM) to verify the formation of the nanostructure. As depicted in the figure 4.34, the crystallites exhibit overlapped agglomerated plate-like morphology with indistinct edges. Due to the overlapping of these platelets, it was not possible to observe each one individually. However, the annealing process at 800°C clearly facilitated the growth of the nano-crystallites, confirming the successful development of the nanostructure with diffuse ring formation.

HRTEM (High Resolution Transmission Electron Microscopy) Analysis of stoichiometric spinel, heat treated at 800°C.; Fuel- Urea:

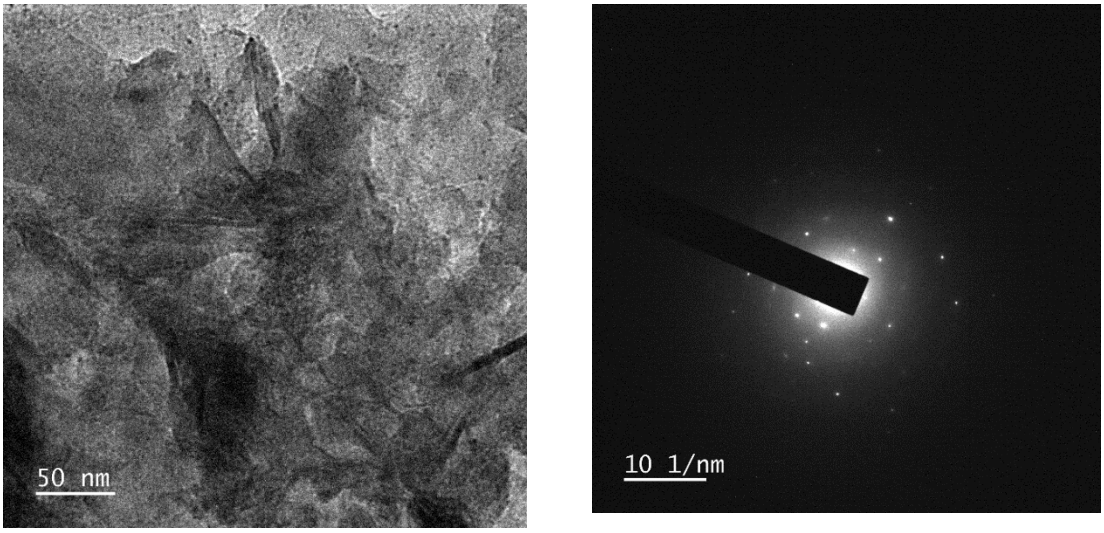

Figure 4.35: HRTEM image of stoichiometric spinel; Mole ratio (Magnesium Nitrate : Aluminium Nitrate) = (1:2); Fuel- Urea

The powder sample, subjected to heat treatment at 800°C, was analysed using High-Resolution Transmission Electron Microscopy (HRTEM) to assess the formation of the nanostructure in figure 4.35. As illustrated in the accompanying figure, the crystallites exhibit an indistinct plate-like morphology with interconnected meshing. Partial granulation of cubic crystal is visible. However, a marked growth of the crystallites was observed subsequent to the annealing process at 800°C, providing strong evidence for the successful development of the nanostructure showing diffuse ring formation.

HRTEM (High Resolution Transmission Electron Microscopy) Analysis of stoichiometric spinel, heat treated at 800°C.; Fuel- Glycine:

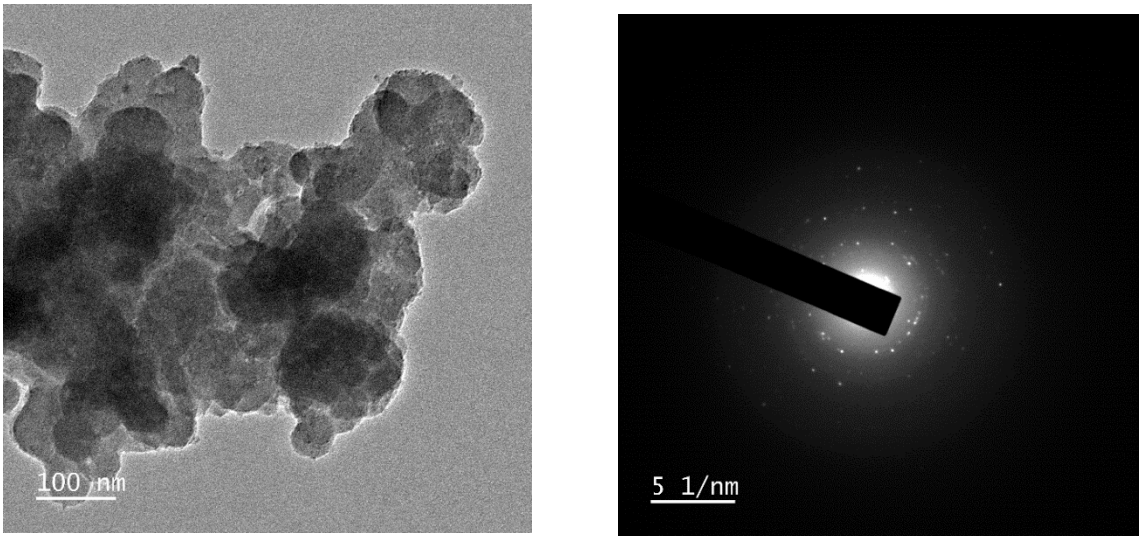

Figure 4.36: HRTEM image of stoichiometric spinel; Mole ratio (Magnesium Nitrate : Aluminium Nitrate) = (1:2) with Fuel- Glycine

The powder sample, heat-treated at 800°C, was analysed using High-Resolution Transmission Electron Microscopy (HRTEM) to verify the formation of the nanostructure in figure 4.36. As shown in the attached figure, the crystallites exhibit a plate/polygonal-like morphology with indistinct edges, diffused interconnects. Due to the overlap of the platelets, individual observation of each platelet was not possible. Notably, the annealing process at 800°C resulted in a clear growth of the crystallites, indicating the successful development of the nanostructure.

4.2 Effect of Temperature on spinel formation: Characterisation of spinel using citric acid (best fuel among four fuels used in the work) with variation of heating temperature (650°C / 700°C / 800 °C) as well as variation of mole ratio of magnesium nitrate : aluminium nitrate (1 : 1.75 / 1 : 2 / 1 : 2.25)

XRD Analysis of non-stoichiometric spinel(magnesium nitrate: aluminium nitrate = 1:1.75); Fuel- Citric Acid: Spectra shows the planes corresponding to these peaks have been indexed with the help of the standard JCPDS (card number: 77-1193) library. The presence of peaks of $MgAl_2O_4$ is the sign of formation of non-stoichiometric spinel at 650ºC (The angle values are specified in degrees). The result gives mixed phase formation of alumina and spinel with good crystallinity figure 4.37. Detailed analysis is given below-

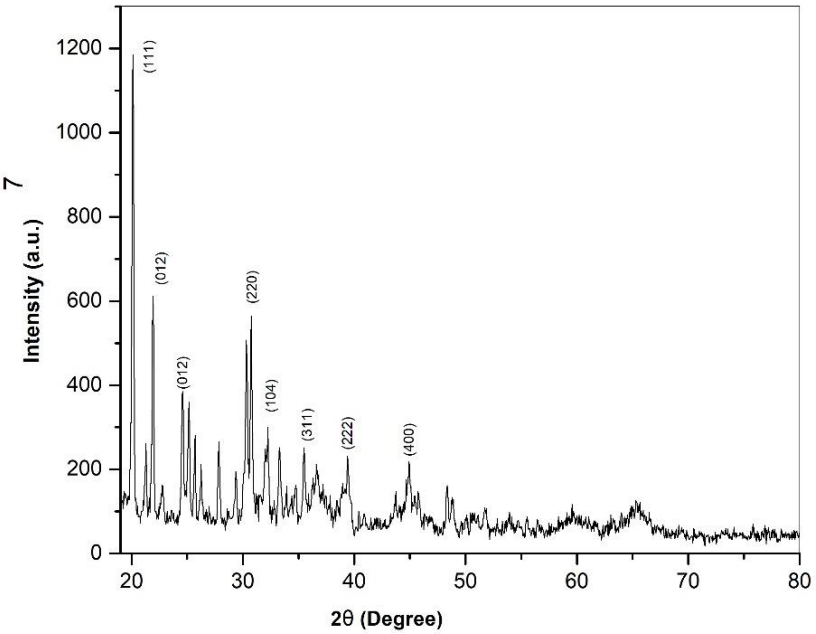

Figure 4.37: XRD Analysis of non-stoichiometric spinel(magnesium nitrate: aluminium nitrate = 1:1.75) with Fuel- Citric Acid,Heat Treated at 650ºC

Planes (111), (220), are shown as $MgAl_2O_4$ spinel at the 2θ values of 19.806, 30.850 respectively obtained from the above graph with sharp peak formation. Planes (012),(104), are shown as Alpha and Gamma powder at the 2θ values of 25.142,34.370 respectively obtained from the above graph. XRD patterns are recorded by an advance Bruker D8 diffractometer (with radiation of Cu Ka). Crystallite size of spinel powder is measured using Scherrer equation; $D = \frac{K.\lambda}{\beta.\cos\theta}$, here λ is denoted as wavelength (=0.15406 nm), θ is denoted as Bragg angle, k is denoted as constant (=0.9), and D is denoted as the crystallite size. Two diffraction peaks (111), and (220) are taken for measuring the size of crystallites. Average crystallite size is found from this Scherrer is 12.53 nm.

XRD Analysis of non-stoichiometric spinel(Mg precursors: Al precursor = 1:1.75); Fuel-Citric Acid: Figure 4.38 Spectra shows the planes corresponding to these peaks have been indexed with the help of the standard JCPDS (card number: 77-1193) library with the presence of $MgAl_2O_4$ leading to non-stoichiometric spinel at 700ºC (The angle values are specified in degrees). The result gives mixed phase formation of alumina and spinel with good crystallinity. Detailed analysis is given below-

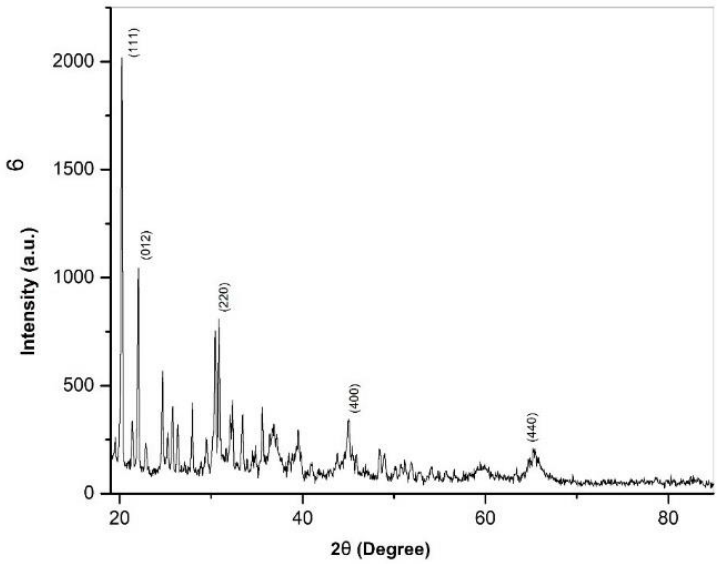

Figure 4.38: XRD Analysis of stoichiometric spinel(Magnesium Nitrate: Aluminium Nitrate = 1:1.75); Fuel- Citric Acid,Heat Treated at 700ºC

From the figure 4.38, planes (111), (220) are identified as $MgAl_2O_4$ spinel at the 2θ values of 19.806, 30.850 respectively obtained from the above graph. Planes(012),(104), are shown as Alpha and Gamma alumina powder at the 2θ values of 25.142,34.370 respectively. Crystallite size of spinel powder is measured using Scherrer's equation; $D = \frac{K.\lambda}{\beta.\cos\theta}$, here λ is denoted as wavelength (=0.15406 nm), θ is denoted as Bragg angle, k is denoted as constant (=0.9), and D is denoted as the crystallite size. It is calculated by taking mean of two diffraction peaks (111) and (220) giving average crystallite size to be 13.32 nm.

XRD Analysis of stoichiometric spinel (Mg precursors: Al precursor = 1:1.75) with Fuel- Citric Acid: Similar spectra is noted as per standard JCPDS (card number: 77-1193) library. Moreover, spinel peaks are observed leading to non-stoichometric spinel at 800ºC (The angle values are specified in degrees). The result gives mixed phase formation of alumina and spinel with good crystallinity. Detailed analysis is given below-

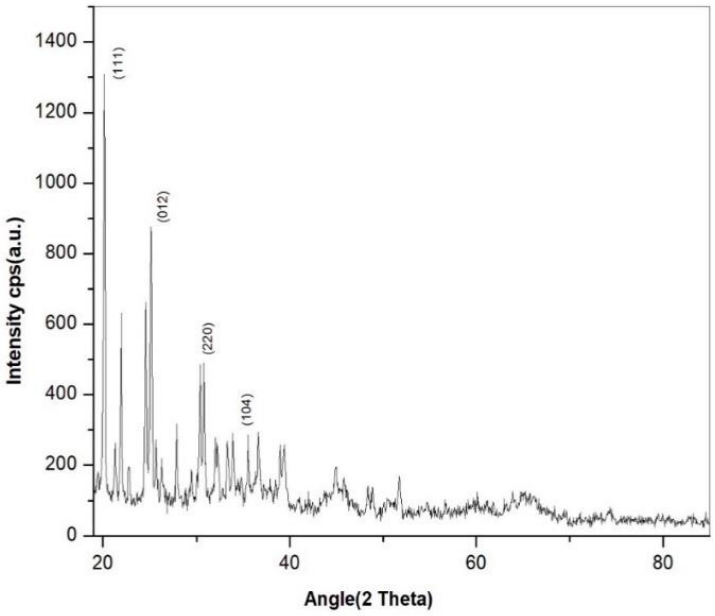

Figure 4.39: XRD Analysis of non-stoichiometric spinel (Magnesium Nitrate: Aluminium Nitrate = 1:1.75) with Fuel- Citric Acid,Heat Treated at 800ºc

The figure 4.39 reveal planes (111), (220) as $MgAl_2O_4$ spinel at the 2θ values of 19.806, 30.850 respectively obtained from the above graph while planes (012),(104), are shown as alpha and gamma alumina powder at the 2θ values of 25.142,34.370 respectively. XRD

patterns are recorded by an advance Bruker D8 diffractometer (with radiation of Cu Ka) which evaluates crystallite size. Crystallite size of spinel powder is measured using Scherrer equation; $D = \frac{K.\lambda}{\beta.\cos\theta}$, here λ is denoted as wavelength (=0.15406 nm), θ is denoted as Bragg angle, k is denoted as constant (=0.9), and D is denoted as the crystallite size based on 2 diffraction peaks on (111) and (220) planes yielding average crystallite size to be 15.92 nm.

XRD Analysis of stoichiometric spinel (Mg precursors: Al precursor = 1:2) with Fuel-Citric Acid: Spectra analysis shows the planes corresponding to these peaks as per standard JCPDS (card number: 77-1193) library. The presence of peaks of $MgAl_2O_4$ is the sign of formation of stoichiometric spinel at 650ºC (The angle values are specified in degrees). The result of figure 4.40 gives mixed phase formation of alumina and spinel with good crystallinity. Detailed analysis is given below-

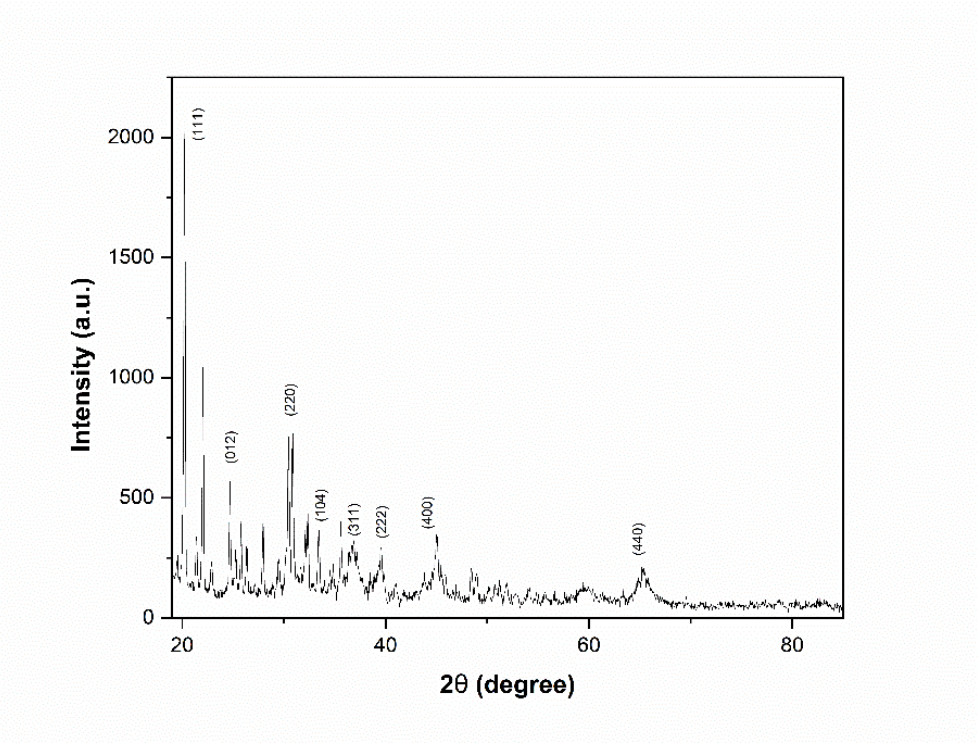

Figure 4.40: XRD Analysis of stoichiometric spinel(Magnesium Nitrate: Aluminium Nitrate = 1:2) with Fuel- Citric Acid,Heat Treated at 650ºC

Planes (111), (220) from the graph are shown as $MgAl_2O_4$ spinel at the 2θ values of 19.806, 30.850 respectively along with planes (012), (104) which correlates to Alpha and Gamma powder at the 2θ values of 25.142,34.370 respectively. XRD patterns are recorded by an advance Bruker D8 diffractometer (with radiation of Cu Ka) while crystallite size of spinel

powder is measured using Scherrer equation; $D = \frac{K.\lambda}{\beta.\cos\theta}$, here λ is denoted as wavelength (=0.15406 nm), θ is denoted as Bragg angle, k is denoted as constant (=0.9), and D is denoted as the crystallite size. Average crystallite size is found to be 16.21 nm taking average size of 2 diffraction peaks (111), (220) respectively.

XRD Analysis of stoichiometric spinel (Mg precursors: Al precursor = 1:2) with Fuel-Citric Acid: Similar spectral analysis shows the planes corresponding to these peaks with standard JCPDS (card number: 77-1193) library indicating formation of stoichiometric spinel at 700ºC (The angle values are specified in degrees) figure 4.41. The result gives mixed phase formation of alumina and spinel with good crystallinity.

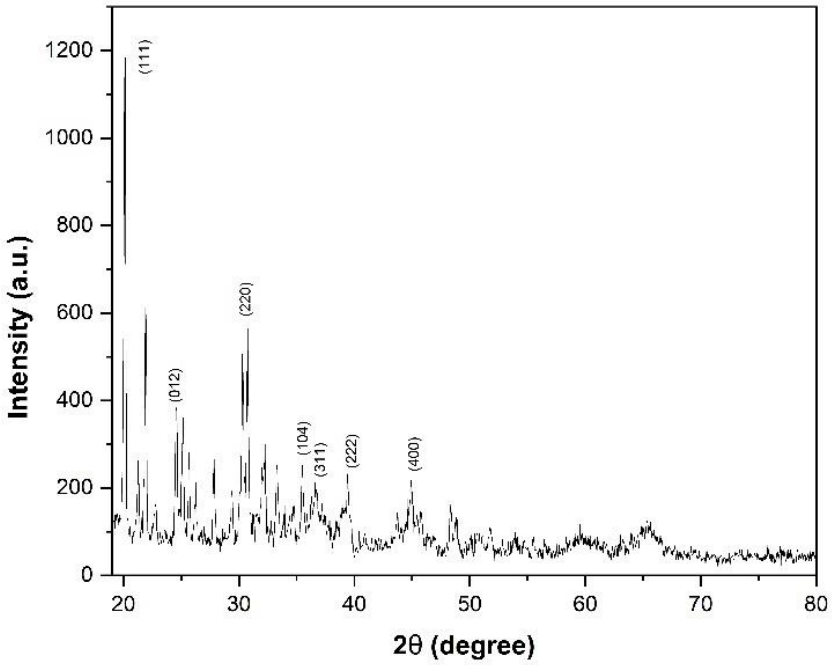

Figure 4.41: XRD Analysis of stoichiometric spinel (Magnesium Nitrate: Aluminium Nitrate = 1:2 with Fuel- Citric Acid,Heat Treated at 700ºC

Planes (111), (220), are shown as $MgAl_2O_4$ spinel at the 2θ values of 19.806, 30.850 respectively obtained from the above graph while minor alpha, gamma alumina are observed at about (012),(104) planes at the 2θ values of 25.142,34.370 respectively. XRD patterns are recorded by an advance Bruker D8 diffractometer (with radiation of Cu Ka). Crystallite size of spinel powder is measured using Scherrer equation; $D = \frac{K.\lambda}{\beta.\cos\theta}$, here λ is denoted as wavelength (=0.15406 nm), θ is denoted as Bragg angle, k is denoted as constant (=0.9), and D is denoted as the crystallite size taking average which yields to be about 17.21 nm.

XRD Analysis of stoichiometric spinel (Mg precursors: Al precursor = 1:2) with Fuel-Citric Acid: Spectra shows the similar pattern which get indexed with the help of the standard JCPDS (card number: 77-1193) library. The presence of peaks of $MgAl_2O_4$ is the sign of formation of stoichiometric spinel at 800ºC (The angle values are specified in degrees) yielding majorly spinel phase with minor alumina having good crystallinity. Detailed analysis is given below-

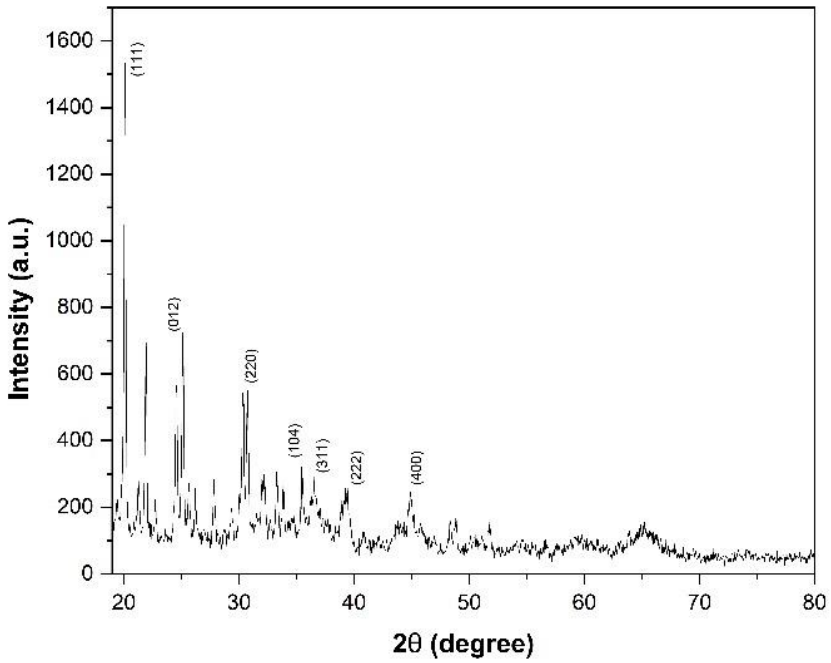

Figure 4.42: XRD graph of stoichiometric spinel (Magnesium Nitrate: Aluminium Nitrate = 1:2) with Fuel- Citric Acid,Heat Treated at 800ºC

Planes (111), (220), are shown as $MgAl_2O_4$ spinel at the 2θ values of 19.806, 30.850 respectively obtained from the figure 4.42.Planes(012),(104) are shown as Alpha and Gamma powder at the 2θ values of 25.142,34.370 respectively obtained from the above graph. XRD patterns were recorded by an advance Bruker D8 diffractometer (with radiation of Cu Ka). Crystallite size of spinel powder was measured using Scherrer equation; $D = \frac{K.\lambda}{\beta.\cos\theta}$, here λ is denoted as wavelength (=0.15406 nm), θ is denoted as Bragg angle, k is denoted as constant (=0.9), and D is denoted as the crystallite size. Two diffraction peaks (111), and

(220) were taken for measuring the size of crystallites. Average crystallite size is found from this Scherrer is 14.21 nm.

XRD Analysis of non-stoichiometric spinel (Mg precursors: Al precursor = 1:2.25) with Fuel- Citric Acid: Spectra shows the planes corresponding to these peaks have been indexed with the help of the standard JCPDS (card number: 77-1193) library. The presence of peaks of $MgAl_2O_4$ is the sign of formation of stoichiometric spinel at 650ºC (The angle values are specified in degrees). The result gives mixed phase formation of alumina and spinel with good crystallinity. Detailed analysis is given below-

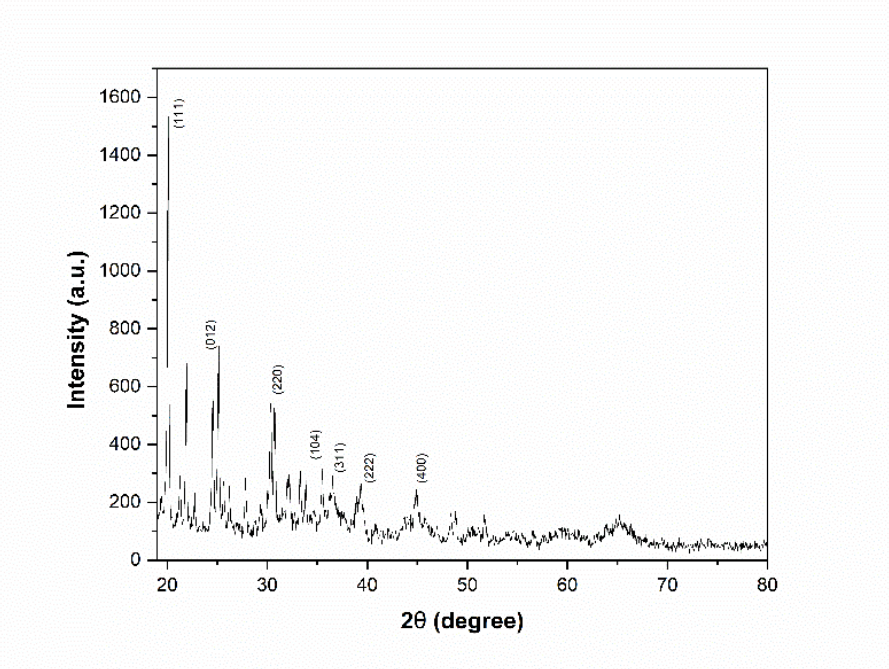

Figure 4.43: XRD graph of non-stoichiometric spinel (Magnesium Nitrate: Aluminium Nitrate = 1:2.25) with Fuel- Citric Acid,Heat Treated at 650ºC

Figure 4.43 predicts the planes (111), (220), are shown as $MgAl_2O_4$ spinel at the 2θ values of 19.806, 30.850 respectively. Further, at Planes (012) and (104) are shown as Alpha and Gamma alumina powder at the 2θ values of 25.142, 34.370 respectively obtained from the above graph. XRD patterns are recorded by an advance Bruker D8 diffractometer (with radiation of Cu Ka) which provides crystallite size of spinel powder using Scherrer equation; $D = \frac{K.\lambda}{\beta.\cos\theta}$, here λ is denoted as wavelength (=0.15406 nm), θ is denoted as Bragg angle, k is denoted as constant (=0.9), and D is denoted as the crystallite size. Average crystallite size is found from this scherrer's equation to be 19.21 nm.

XRD Analysis of non-stoichiometric spinel (Mg precursors: Al precursor = 1:2.25) with Fuel- Citric Acid: Spectra shows the planes corresponding to these peaks have been indexed with the help of the standard JCPDS (card number: 77-1193) library. The presence of peaks of $MgAl_2O_4$ correlates to non- stoichiometric spinel at 700ºC (The angle values are specified in degrees) along with alumina phase. The result is shown in figure 4.44 with good crystallinity. -

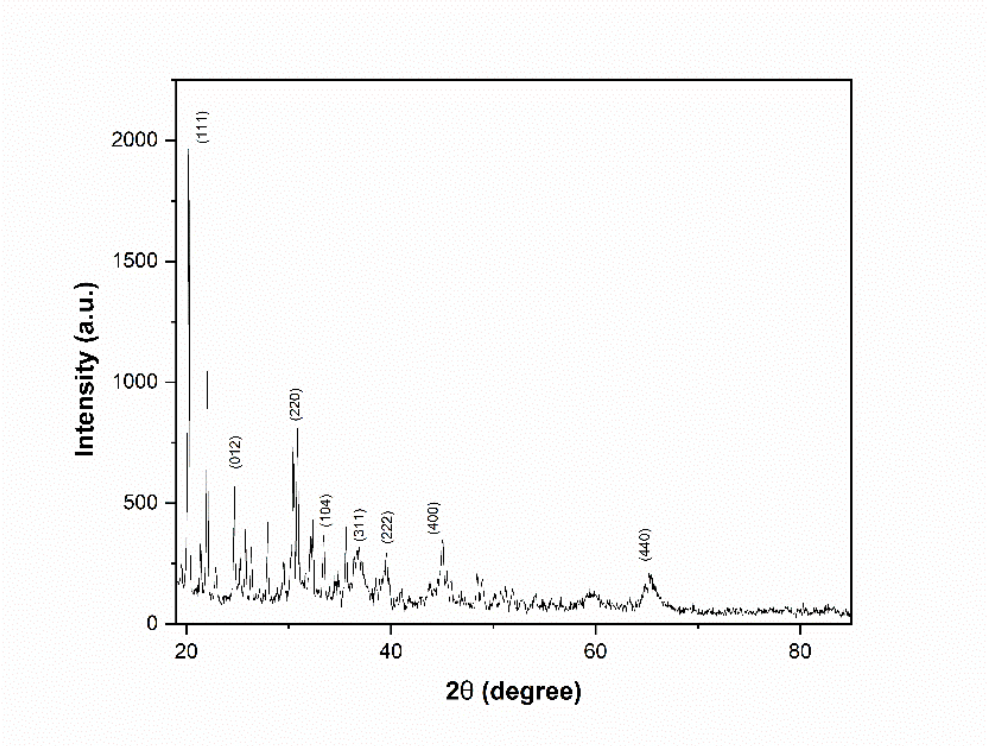

Figure 4.44: XRD graph of non-stoichiometric spinel(Magnesium Nitrate: Aluminium Nitrate = 1:2.25) with Fuel- Citric Acid,Heat Treated at 700°C

Similar planes are observed just like the previous one with presence of apha, gamma alumina phase. Planes (111), (220), are shown as $MgAl_2O_4$ spinel at the 2θ values of 19.806, 30.850 respectively obtained from the above graph figure 4.44. Planes (012), (104) are shown as Alpha and Gamma powder at the 2θ values of 25.142,34.370 respectively obtained from the above graph. Crystallite size of spinel powder is measured using Scherrer equation; $D = \frac{K.\lambda}{\beta.\cos\theta}$, here λ is denoted as wavelength (=0.15406 nm), θ is denoted as Bragg angle, k is denoted as constant (=0.9), and D is denoted as the crystallite size. Two diffraction peaks (111) and (220) are taken for measuring the average size of crystallites which yields to be 20.56 nm.

XRD Analysis of non-stoichiometric spinel (Magnesium Nitrate: Aluminium Nitrate = 1:2.25) with Fuel- Citric Acid: Spectra shows the planes corresponding to these peaks have been indexed with the help of the standard JCPDS (card number: 77-1193) library. The presence of peaks of $MgAl_2O_4$ is the sign of formation of stoichiometric spinel at 800ºC (The angle values are specified in degrees). The result in figure 4.45 gives mixed phase formation of alumina and spinel with good crystallinity.

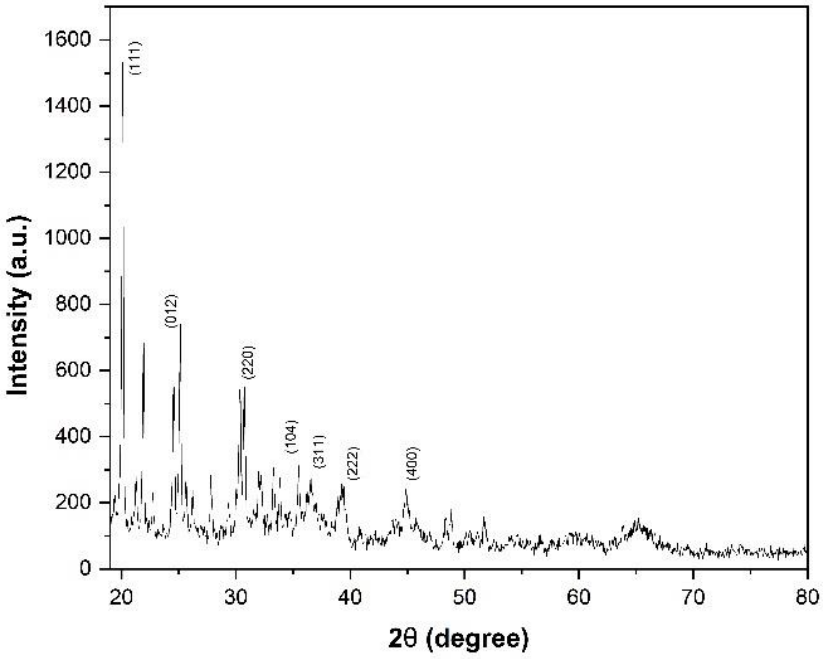

Figure 4.45: XRD graph of non-stoichiometric spinel(Magnesium Nitrate: Aluminium Nitrate = 1:2.25); Fuel- Citric Acid,Heat Treated at 800ºC

XRD figure of 4.45 gives planes (111), (220), are shown as $MgAl_2O_4$ spinel at the 2θ values of 19.806, 30.850 respectively obtained from the above graph. Planes(012),(104) are shown as Alpha and Gamma powder at the 2θ values of 25.142,34.370 respectively obtained from the above graph. XRD patterns were recorded by an advance Bruker D8 diffractometer (with radiation of Cu Ka). Crystallite size of spinel powder was measured using Scherrer equation; $D = \frac{K.\lambda}{\beta.\cos\theta}$, here λ is denoted as wavelength (=0.15406 nm), θ is denoted as Bragg angle, k is denoted as constant (=0.9), and D is denoted as the crystallite size. Two diffraction peaks (111), and (220) were taken for measuring the size of crystallites. Average crystallite size is found from this Scherrer is 21.87 nm.

Above results indicate strong influence of temperature on crystallite size as well as precursors ratio affect the structure of synthesize materials. The rise of temperature increases the crystallite size as well as increasing alumina ratio also influences growth phenomena.

FTIR Analysis of non-stoichiometric (Magnesium Nitrate: Aluminium Nitrate (1: 1.75) spinel (varying Synthesis Temperature of 650ºC / 700ºC / 800ºC); Fuel- Citric Acid:

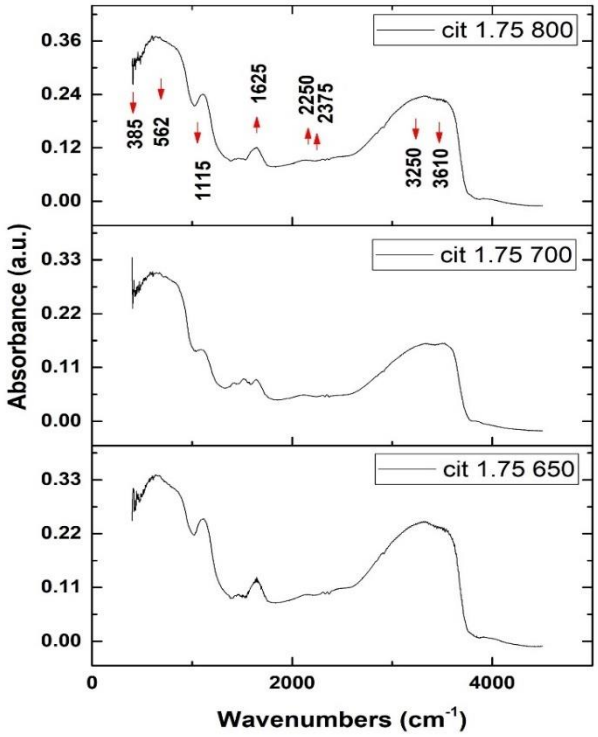

Figure 4.46: FTIR graph of non-stoichiometric (Magnesium Nitrate: Aluminium Nitrate (1: 1.75) spinel (varying Synthesis Temperature of 650ºC / 700ºC / 800ºC); Fuel- Citric Acid

The Infrared spectra of $MgAl_2O_4$ spinel and calcined alpha and gamma powders at different mole ratio (Magnesium Nitrate: Aluminium Nitrate) and calcined at 650^0C are shown in above figure 4.46. Mole ratio 1:1.75 is non-stoichiometric ratio which shows Al-O stretching bond vibration at 562 cm^{-1}. At 1115 cm^{-1} Al-Mg-O stretching bond vibration is present.385$cm^{-1}$is associated with Mg-O stretching bond vibration. Carbonaceous material is

also present in the precursor powder which can be seen at wavenumber 1625 cm^{-1}which is a stretching bond vibration of carboxylate ions. At 2250 cm^{-1} is associated with N=C=O isocyanate stretching bond vibration. 2375 cm^{-1} shows O-H stretching bond at very minor level. At 3250 cm^{-1} H_2O stretching bond can be formed. Wavenumber 3610 cm-1 is associated with the OH anti symmetric stretching vibration in Mg(OH)2. The wavenumbers corresponding to the carboxylate and nitrate ions, evaporates with increasing heating temperature of the mixture gel.**[1]** Very small deflection in the peak of the graphs for different synthesis temperature as 700**ºC** and 800 ºC has also been observed. These two ratios are corresponding to non-stoichiometric ratio. Hence, calcination of non-stoichiometric ratios are also showing presence of Al-O bond vibration as well as Mg-Al-O bond vibrations. This observation will make it clear that we will find $MgAl_2O_4$ spinel also from non-stoichiometric ratio of precursors.

FTIR Analysis of stoichiometric (Magnesium Nitrate: Aluminium Nitrate (1: 2) spinel (varying Synthesis Temperature of 650ºC / 700ºC / 800ºC); Fuel- Citric Acid:

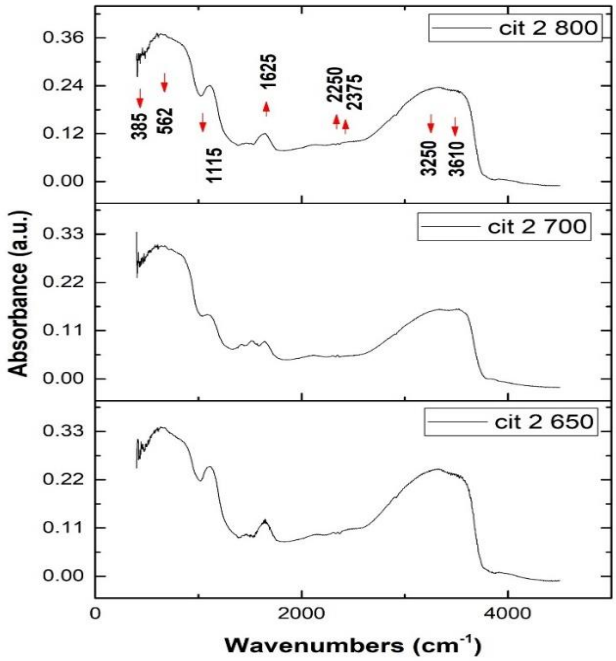

Figure 4.47: FTIR of stoichiometric (Magnesium Nitrate: Aluminium Nitrate (1: 2) spinel (varying Synthesis Temperature of 650ºC / 700ºC / 800ºC); Fuel- Citric Acid

The Infrared spectra of $MgAl_2O_4$ spinel, calcined alpha and gamma powders at stoichometric mole ratio (Magnesium Nitrate: Aluminium Nitrate, 1:2) after annealing at 650ºC are shown in above figure 4.47. Mole ratio 1:2 is stoichiometric one which shows Al-O stretching bond

vibration at 562 cm^{-1}. At 1115 cm^{-1} Al-Mg-O stretching bond vibration is present. 385$cm^{-1}$is associated with Mg-O stretching bond vibration. Carbonaceous material is also present in the precursor powder which can be seen at wavenumber 1625 cm^{-1}which is a stretching bond vibration of carboxylate ions. 2250 cm^{-1} wavenumber is associated with N=C=O isocyanate stretching bond vibration while 2375 cm^{-1} shows O-H stretching bond almost missing. At 3250 cm^{-1} H_2O stretching bond can be formed. Wavenumber 3610 cm-1 is associated with the OH anti symmetric stretching vibration in Mg(OH)2. The wavenumbers corresponding to the carboxylate and nitrate ions, evaporates with increasing heating temperature of the mixture gel. **[1]**Very small deflection in the peak of the graphs for different synthesis temperature as 700**ºC** and 800ºC has also been observed. These two ratios are corresponding to non-stoichiometric ratio. Hence, calcination of non-stoichiometric ratios are also showing presence of Al-O bond vibration as well as Mg-Al-O bond vibrations. This observation will make it clear that we will find $MgAl_2O_4$ spinel also from non-stoichiometric ratio of precursors.

FTIR Analysis of non-stoichiometric (Magnesium Nitrate: Aluminium Nitrate (1: 2.25) spinel (varying Synthesis Temperature of 650ºC / 700ºC / 800ºC) with Fuel- Citric Acid:

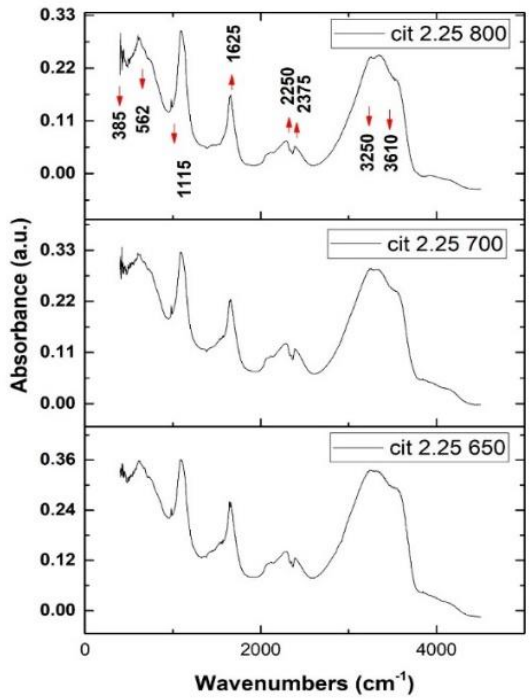

Figure 4.48: FTIR of non-stoichiometric (Magnesium Nitrate: Aluminium Nitrate (1: 2.25) spinel (varying Synthesis Temperature of 650ºC / 700ºC / 800ºC); Fuel- Citric Acid

The Infrared spectra of $MgAl_2O_4$ spinel and calcined alpha and gamma powders at non-stoichometric mole ratio (Magnesium Nitrate: Aluminium Nitrate) after annealing at 650ºC/700°C/800°C are shown in above figure 4.48. From FTIR, Al-O stretching bond vibration at 562 cm^{-1}, Al-Mg-O stretching bond vibration at 1115cm^{-1} is present. 385cm^{-1} is associated with Mg-O stretching bond vibration, while carboxylate ions are present stretching bond vibration at about 1625cm^{-1}. At 2250 cm^{-1} is associated with N=C=O isocyanate stretching bond vibration. 2375 cm^{-1} shows O-H stretching bond. At 3250 cm^{-1} H_2O stretching bond can be formed. Wavenumber 3610cm^{-1} is associated with the OH anti symmetric stretching vibration in $Mg(OH)_2$. The wavenumbers corresponding to the carboxylate and nitrate ions, evaporates with increasing heating temperature of the mixture gel. **[1]**Very small deflection in the peak of the graphs for different synthesis temperature at 700ºC and 800ºC has also been observed. Hence, annealing of non-stoichiometric ratios is also showing presence of Al-O bond vibration as well as Mg-Al-O bond vibrations like stoichometric one. This observation will make it clear that we will find $MgAl_2O_4$ spinel even having non-stoichiometric ratio of precursors.

Above FTIR spectra gives clear idea about chemical bond exist in various functional group present in the synthesize materials. With increasing temperature absorption peak shows higher value compare to low temperature value.

SEM (Scanning Electron Microscope) Analysis of non-stoichiometric spinel (1:1.75) (with various synthesis temperature); Fuel- Citric Acid:

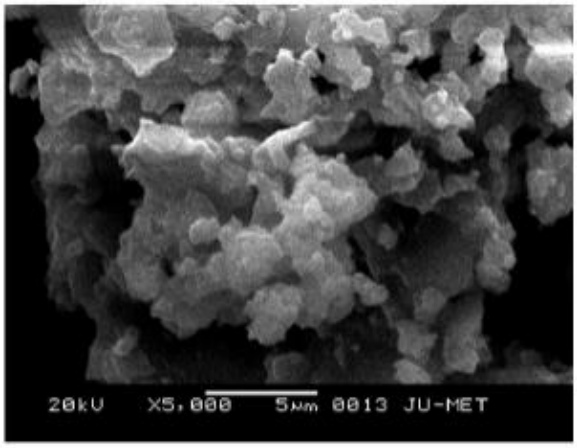

Spinel sample heat treated at 650°C

Figure 4.49: SEM image of non-stoichiometric spinel heat treated at 650°C; Mole ratio (Magnesium Nitrate: Aluminium Nitrate)Ratio= (1:1.75); Fuel- Citric Acid

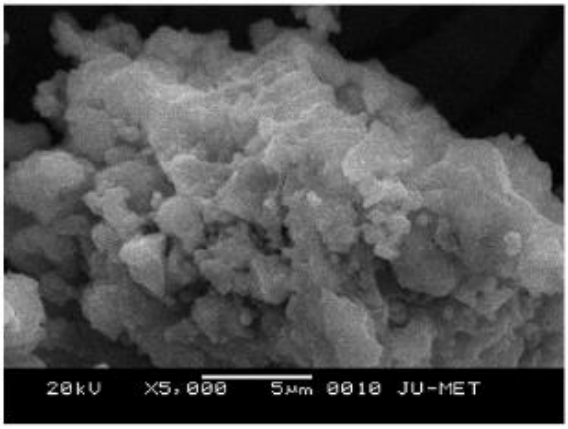

Spinel sample heat treated at 700°C

Figure 4.50: SEM image of non-stoichiometric spinel heat treated at 700°C; Mole ratio (Magnesium Nitrate: Aluminium Nitrate)Ratio= (1:1.75); Fuel- Citric Acid

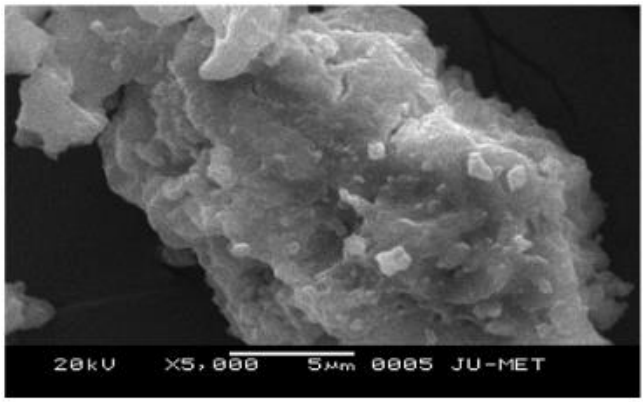

Spinel sample heat treated at 800°C

Figure 4.51: SEM image of non-stoichiometric spinel heat treated at 800°C; Mole ratio (Magnesium Nitrate: Aluminium Nitrate)Ratio= (1:1.75); Fuel- Citric Acid

The figure 4.49 shows a strong spinalisation with granulated phase dispersed over the matrix. The phases is fine structure particle while mass has shown agglomeration of particles. Figure 4.50 shows strong agglomeration tendency and particles are interlocked. The particle size has shown large size due to this strong conglomeration tendency. The cubic structure with polygonal angles formation is predominant under these experimental studies with increasing

tendency of grain size. From figure 4.51 it has been observed the very fine cubic structure dispersed in the matrix. Layered mass formation with larger particle size has shown.

EDX (Energy Dispersive X Ray) Analysis of non-stoichiometric spinel, heat treated at 650°C.; Fuel- Citric Acid:

Element	Weight%	Atomic%
O K	65.73	74.98
Mg K	24.72	18.56
Al K	9.54	6.46
Totals	100.00	

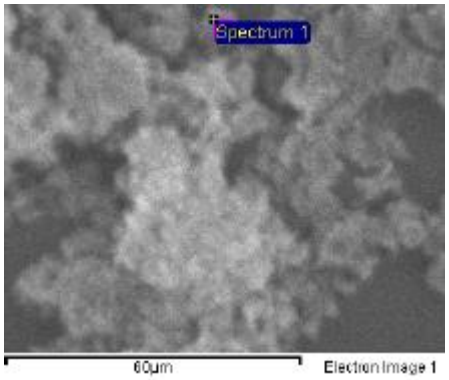

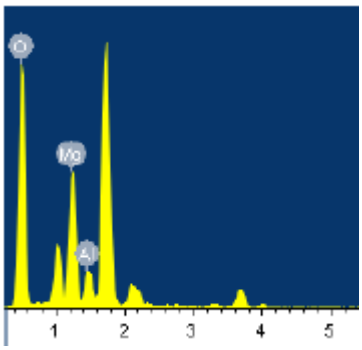

Figure 4.52:EDX of non-stoichiometric spinel, heat treated at 650°C.; Fuel- Citric Acid

In the investigations of the composition with Energy Dispersive X-ray Spectroscopy (EDX) as a pivotal tool shown in figure 4.52, decisively confirms the presence of magnesium, oxygen and aluminum constituents within the sample. Further scrutiny unveils a quantitative variation in the elemental percentages of magnesium, oxygen, and aluminum across the synthesized films. Notably, a direct correlation is observed between the number of synthesized films and the augmentation in magnesium and oxygen content. Remarkably, the

most significant concentrations of magnesium and oxygen are discerned in a specific synthesized film, suggesting an optimal coating of magnesium with oxygen on the aluminum substrate.

SEM (Scanning Electron Microscope) Analysis of stoichiometric spinel (1:2) (with various synthesis temperature); Fuel- Citric Acid:

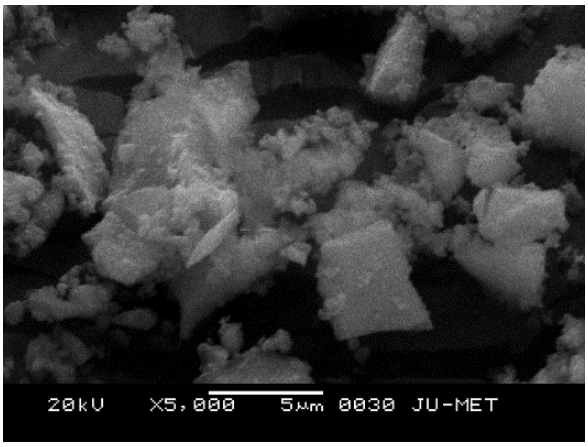

Figure 4.53: SEM image of non-stoichiometric spinel heat treated at 650°C; Mole ratio (Magnesium Nitrate: Aluminium Nitrate)Ratio= (1:2); Fuel- Citric Acid

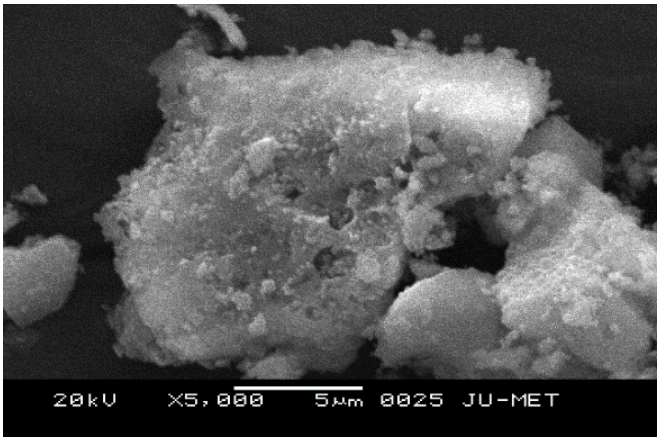

Figure4.54: SEM image of non-stoichiometric spinel heat treated at 700°C; Mole ratio (Magnesium Nitrate: Aluminium Nitrate)Ratio= (1:2); Fuel- Citric Acid

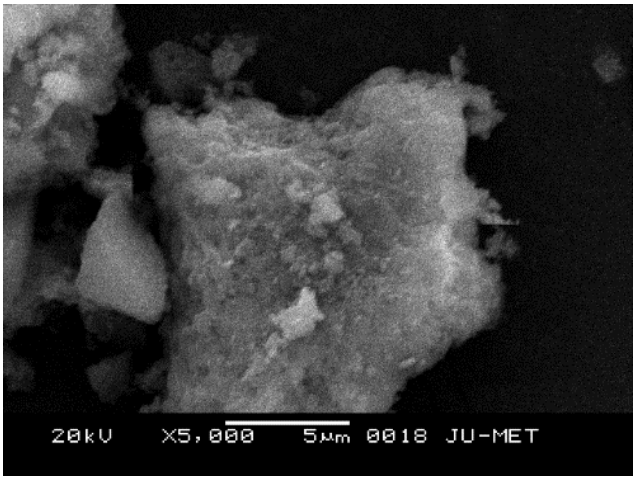

Figure 4.55: SEM image of non-stoichiometric spinel heat treated at 800°C; Mole ratio (Magnesium Nitrate: Aluminium Nitrate)Ratio= (1:2); Fuel- Citric Acid

Figure 4.53 shows a strong spinalisation with cubic phase dispersed over the matrix. The cubic phase has polygonal angles while cloudy mass has shown agglomeration of particles. Figure 4.54 shows strong agglomeration tendency and particles are interlocked. The particle size has shown very large size due to this strong conglomeration tendency. The polygonal structure formation is predominant under these experimental studies with increasing tendency of grain size. From figure 4.55 it has been observed the very fine cubic structure dispersed in the matrix. Layered cloudy mass formation enhances with larger particle size.

EDX (Energy Dispersive X Ray) Analysis of non-stoichiometric spinel, heat treated at 700°C.; Fuel- Citric Acid:

Element	Weight%	Atomic%
O K	49.60	61.51
Mg K	17.66	14.41
Al K	32.74	24.08
Totals	100.00	

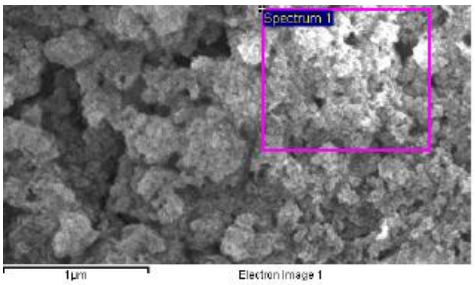

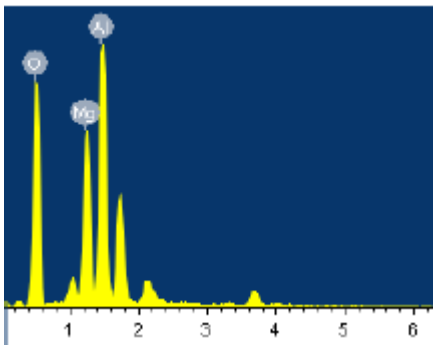

Figure 4.56: EDX of non-stoichiometric spinel, heat treated at 700°C.; Fuel- Citric Acid

EDX analysis of powder sample after annealing at 700C is shown in figure 4.56.It conclusively identifies the presence of magnesium, oxygen, and aluminum within the sample. Further examination reveals a quantitative variance in the elemental percentages of magnesium, oxygen, and aluminum within the synthesized sample verifying the composition. Interestingly, we observed a direct correlation between the development of proper sample and the growth in magnesium and oxygen content. Notably, the highest concentrations of

magnesium and oxygen are detected in the sample, indicating a maximal coating of magnesium with oxygen on the aluminum substrate.

SEM (Scanning Electron Microscope) Analysis of non-stoichiometric spinel (1:2.25) (with various synthesis temperature); Fuel- Citric Acid:

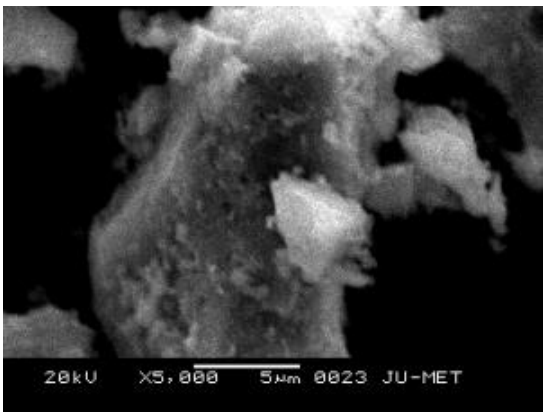

Figure 4.57: SEM image of non-stoichiometric spinel heat treated at 650°C; Mole ratio (Magnesium Nitrate: Aluminium Nitrate) Ratio= (1:2.25); Fuel- Citric Acid

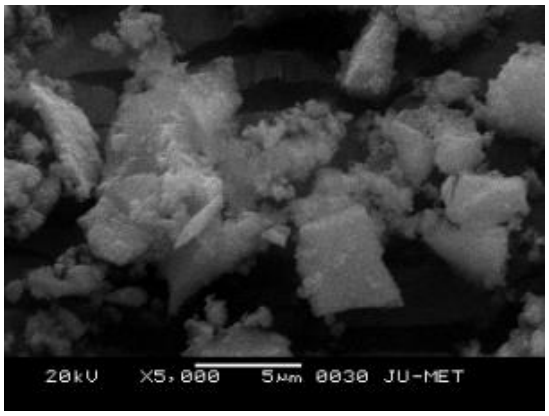

Figure 4.58: SEM image of non-stoichiometric spinel heat treated at 700°C; Mole ratio (Magnesium Nitrate: Aluminium Nitrate) Ratio= (1:2.25); Fuel- Citric Acid

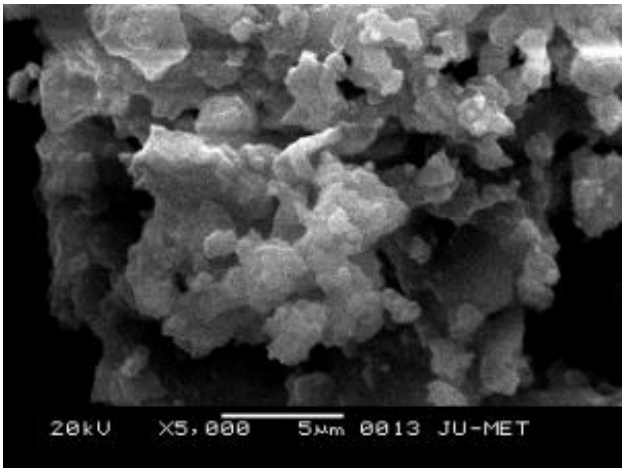

Figure 4.59: SEM image of non-stoichiometric spinel heat treated at 800°C; Mole ratio (Magnesium Nitrate: Aluminium Nitrate) Ratio= (1:2.25); Fuel- Citric Acid

The illustration in figure 4.57 illustrates a pronounced spinalization effect, characterized by the dispersion of cubic phase particles throughout the matrix. These cubic phase particles

exhibit a fine structure, while a cloudy mass demonstrates particle agglomeration. In Figure 4.58, there is a notable tendency towards particle agglomeration, with particles becoming interlocked, resulting in larger particle sizes due to this cohesive tendency. Under these experimental conditions, the formation of cubic structures predominates, accompanied by an increasing grain size trend. Figure 4.59 reveals the presence of very fine cubic structures dispersed within the matrix, alongside the formation of layered cloudy masses, which are associated with larger particle sizes.

EDX (Energy Dispersive X Ray) Analysis of non-stoichiometric spinel, heat treated at 800°C.; Fuel- Citric Acid:

Element	Weight%	Atomic%
O K	63.02	73.29
Mg K	16.00	12.24
Al K	20.98	14.46
Totals	100.00	

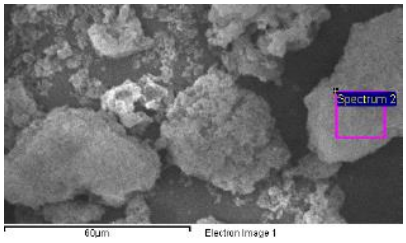

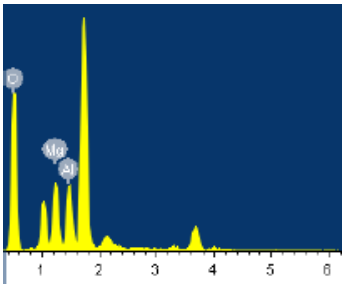

Figure 4.60: EDX of non-stoichiometric spinel, heat treated at 800°C; Fuel- Citric Acid

Investigating the composition of the sample is carried by Energy Dispersive X-ray Spectroscopy (EDX). Analysis of the EDX spectrum figure 4.60 unequivocally confirms the presence of magnesium, oxygen, and aluminum within the prepared sample. Further scrutiny reveals quantitative variations in the elemental percentages of magnesium, oxygen, and aluminum across the synthesized sample. Intriguingly, a direct relationship emerged between the number of synthesized films and the augmentation in magnesium and oxygen content. Remarkably, the highest concentrations of magnesium and oxygen are observed in the synthesized sample, indicating maximal coating of magnesium with oxygen on the aluminum substrate.

4.3 PROPERTY EVALUATION:

Sample $_{650}$ (citric acid)	
D_1	**11.6 µm**
D_2	**12.0 µm**
Load	**50 gm-f**
VHN	**661.2**
GPa	**6.484**
Dwell Time	**15 sec**

Sample$_{700}$ (citric acid)	
D_1	**12.6 µm**
D_2	**12.0 µm**
Load	**50 gm-f**
VHN	**609.6**
GPa	**5.978**
Dwell Time	**15 sec**

Sample$_{800}$ (citric acid)	
D_1	12.2 µm
D_2	11.9 µm
Load	50 gm-f
VHN	603.3
GPa	**5.917**
Dwell Time	15 sec

Table 4.3.1 :Vicker's micro-hardness analysis of spinel (1:1.75); Fuel: Citric Acid

Load and Dwell time is fixed and only hardness of various sample has been measured

The Vickers micro-hardness (MPa) assessment of $MgAl_2O_4$, subjected to various heat treatment temperatures under a 50g load, is presented in table 4.1. A consistent trend of increasing micro-hardness in the $MgAl_2O_4$ sample is observed. Notably, sample at 650 degrees treated $MgAl_2O_4$ reaches 6.484GPa much more above than untreated alumina. With the increase of synthesis temperature, hardness decreases due to coarsening of grain formation. This heightened micro-hardness is indicative of the crystallinity enhancement within the $MgAl_2O_4$ structure.

The amplification in micro-hardness is closely associated with the escalation in oxygen and magnesium contents, as revealed in the EDX analysis. Moreover, the intensified micro-hardness can be attributed to lattice distortions, vacancies, and point defects induced by the interstitial integration of oxygen ions and the incorporation of sputtered Mg into the Al matrix. These lattice distortions and point defects impede dislocation motion, thereby enhancing the micro-hardness of the $MgAl_2O_4$ sample.

Furthermore, the augmented micro-hardness values indicate the formation of compact polycrystalline $MgAl_2O_4$ samples. The comprehensive findings of this study, including crystallite size, crystallinity, surface morphology analyzed through EDX, and micro-hardness values, align well with prior research endeavors. This concurrence underscores the robustness

and reliability of the current investigation. The above findings indicate optimum mechanical property of the sample even at lower temperature of annealing.

Sample $_{650}$ (citric acid)	
D1	11.2 µm
D2	11.2 µm
Load	100 gm-f
VHN	1475.4
GPa	14.47
Dwell Time	15 sec

Sample $_{700}$ (citric acid)	
D1	10.5 µm
D2	11.9 µm
Load	100 gm-f
VHN	1471.5
GPa	14.43
Dwell Time	15 sec

Sample $_{800}$ (citric acid)	
D_1	10.4 µm
D_2	10.6 µm
Load	100 gm-f
VHN	1424.7
GPa	13.97
Dwell Time	15 sec

Table 4.3.2 :Vicker's micro-hardness analysis of spinel (1:2); Fuel: Citric Acid

Load and Dwell time is fixed and only hardness of various sample has been measured

The analysis of mechanical integrity in terms of Vickers micro-hardness (MPa) for MgAl2O4 sample under 100g load subjected to different annealing temperature with citric acid is shown in table 4.2. A consistent trend of escalating micro-hardness across the MgAl2O4 sample is noted. Particularly noteworthy is the observation that the MgAl2O4 sample treated at 650 degrees Celsius reaches 14.47 GPa, significantly surpassing the micro-hardness of untreated alumina. As the synthesis temperature increases, there is a decline in hardness due to the coarsening of grain formation. This heightened micro-hardness underscores the enhancement in crystallinity within the MgAl2O4 structure.

The increase in micro-hardness is closely linked to the rise in oxygen and magnesium contents, as revealed by EDX analysis. Additionally, the intensified micro-hardness can be attributed to lattice distortions, vacancies, and point defects resulting from the interstitial integration of oxygen ions and the incorporation of sputtered Mg into the Al matrix. These distortions and defects impede dislocation motion, thereby augmenting the micro-hardness of the MgAl2O4 sample.

Moreover, the heightened micro-hardness values suggest the formation of compact polycrystalline MgAl2O4 sample. The comprehensive analysis, including crystallite size, crystallinity, surface morphology examined through EDX, and micro-hardness values, correlates with previous research efforts. Thus the above findings is in alignment regarding the strength and reliability of the current investigation.

Sample $_{650}$ (citric acid)	
D_1	10.7 µm
D_2	10.4 µm
Load	50 gm-f
VHN	839.3
GPa	8.231
Dwell Time	15 sec

Sample $_{650}$ (citric acid)	
D_1	10.8 µm
D_2	9.5 µm
Load	50 gm-f
VHN	812.1
GPa	7.964
Dwell Time	15 sec

Sample $_{650}$ (citric acid)	
D_1	12.8 µm
D_2	12.2 µm
Load	100 gm-f
VHN	793.0
GPa	7.77
Dwell Time	15 sec

Table 4.3.3 :Vicker's micro-hardness analysis of spinel (1:2.25); Fuel: Citric Acid

Dwell time is fixed and only hardness of various sample has been measured

The present study executes an assessment on the Vickers micro-hardness (MPa) of $MgAl_2O_4$ sample subjected to various heat treatment temperatures under a 100g load. A consistent trend of increasing micro-hardness is observed across the $MgAl_2O_4$ sample. It is noted from the experimental observation, that the sample treated at 650 degrees Celsius reaches a micro-hardness of 8.231 GPa, significantly higher than untreated alumina represented in table 4.3. As the synthesis temperature increases, there is a decrease in hardness due to the coarsening of grain formation. This heightened micro-hardness suggests an enhancement in crystallinity within the $MgAl_2O_4$ structure.

The increase in micro-hardness is closely linked to the rise in oxygen and magnesium contents, as revealed by EDX analysis. The reason behind the increased microhardness is almost similar to the previous case which possibly attributes to lattice distortions, vacancies, and point defects induced by the interstitial integration of oxygen ions and the incorporation of sputtered Mg into the Al matrix. These distortions and defects impede dislocation motion, thereby enhancing the micro-hardness of the $MgAl_2O_4$ sample.

Moreover, the augmented micro-hardness values indicate the formation of compact polycrystalline $MgAl_2O_4$ spinel. The comprehensive findings of this study, including crystallite size, crystallinity, surface morphology analyzed through EDX, and micro-hardness values, are consistent with prior research endeavors. This alignment underscores the robustness and reliability of the current investigation.

Bulk Density and apparent porosity analysis of spinel (1:2) with Fuel- Citric Acid:

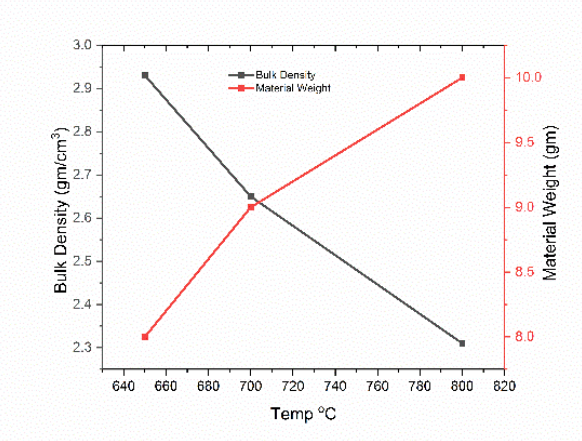

Figure 4.61: Graph of Bulk Density and Material weight vs soaking temperature of spinel (1:2); Fuel- Citric Acid

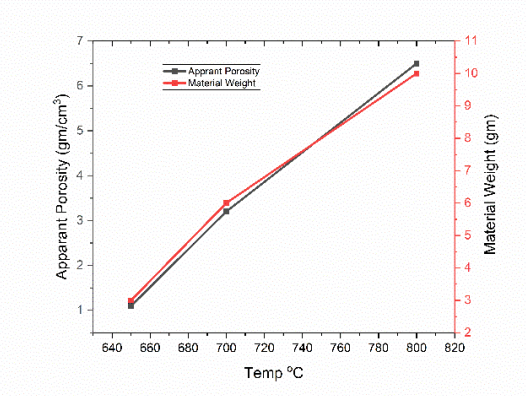

Figure 4.62: Graph of Apparent porosity and Material weight vs soaking temperature of spinel (1:2); Fuel- Citric Acid

To determine the minimum green density (GD) and maximum compact mass necessary for achieving MAS (Magnesium Aluminum Spinel) grains with a bulk density (BD) of 4.30 g/cm³ upon sintering at 1300°C for 1-hour, various masses (ranging from 2.5 to 10 grams) of the calcined precursor mixture are uniaxially compacted. These compacts underwent sintering at 1300°C for 1 hour. The accompanying figures 4.61 and 4.62 illustrate the variations in BD and apparent porosity (AP) of MAS grains in relation to the mass of powder compacts and annealing temperature. It is evident that BD decreases systematically with increasing sample mass, while AP exhibits the opposite trend. This phenomenon is primarily attributed to density gradients within the compacts, which become more pronounced with higher sample masses, although the elevated thermal mass tends to impede temperature equalization due to the low thermal conductivity of MAS. The compacts were sintered at 1300°C, with the figures depicting the BD and AP values as a function of sintering temperature and soaking time, respectively. It is observed that the soaking temperature represents the minimum temperature required to achieve a BD of 3.30 g/cm³. Furthermore, the figures demonstrate that a longer holding time (2.5 hours) at the same temperature resulted in only a slight increase in BD. The above findings on BD, AP is in correlation with microhardness variation with annealing temperature and microstructure analysis.

Chapter-5

CONCLUSIONS

Studies have been conducted on the synthesis of the Alumina &Magnesia-Alumina spinel formation at different heating temperature. The homogeneous Alumina &Magnesia-Alumina dispersion for solid-solution conversion is fabricated by solution combustion route prior to heat treatment. Also, the synthesis of phase pure Alumina & Magnesia-Alumina spinel with enhanced structural change is successfully synthesized by Molecular level mixing process and followed by Sintering. Various conclusions that can be drawn from these investigations are –

- From DSC/TGA data clear crystallization of alumina and spinel formation have been identified within the range of 650^0C temperature to 850^0C temperature.
- Thermal analysis results have identified various reactions zone during spinel formation using various fuels for combustion routes.
- Fuel combustion route supports effective Magnesia –Alumina spinel formation at lower temperature.
- From XRD data it was found that the mixture where citric acid found to be useful fuel, XRD spectra predict formation of maximum pure phase formation of magnesium aluminate spinel .
- From XRD data we can conclude that with the help of citric acid (catalyst) $MgAl_2O_4$ can be synthesized where crystallite size of the particles is measured with the help of Scherrer equation to be around 15 to 30 nm.
- Change of fuels like thiourea, urea, and glycine has increased growth of crystallites.
- FTIR analysis revealed the remarkable stability of the spinel structures even under temperature treatments up to 800°C. From FTIR spectra we can easily identify the existence of O-H group, Al-Mg-O group and other existence of functional groups.
- The alteration of heating temperature within the magnesium aluminate matrix significantly influences the evolution of particle characteristics, crystallization behavior, and morphology.
- XRD plot infers increasing temperature has positive growth of crystallites and alumina variation also influenced growth pattern

- SEM imaging revealed the formation of granular spinel with agglomerated particles, while the layered structure indicative of spinel formation demonstrated evident solid-solid interactions.

- Vicker's microhardness as well as bulk density and apparent porosity can easily represent the hardness or dense spinel particle formation at comparatively lower synthesis temperature around 650^0C with controlled size on crystallites.

- Overall results predict strong feasibility of nano order crystallite size and responsible for low temperature spinel formation.

- HRTEM results indicate support of formation nano size crystallites initially which was reported in XRD data.

Srinath Ranjan Ghosh, 18.06.25

18/06/25
HEAD OF THE DEPARTMENT
Metallurgical & Material Engineering Deptt.
Jadavpur University, Kolkata-700 032

Soumya Mukherjee
18/06/2025

Assistant Professor
Department of Metallurgical Engineering
School of Mines & Metallurgy
KAZI NAZRUL UNIVERSITY
Asansol, W.B.-713340